

# Mechanistic Insight for Improved Catalytic Conversion of Fatty Acids to Linear $\alpha$ -Olefins

A Density Functional Theory Study

---

Sondre Hilmar Hopen Eliasson

Thesis for the degree of Philosophiae Doctor (PhD)  
University of Bergen, Norway  
2020

UNIVERSITY OF BERGEN



**Mechanistic Insight for Improved  
Catalytic Conversion of Fatty Acids to  
Linear  $\alpha$ -Olefins**  
A Density Functional Theory Study

Sondre Hilmar Hopen Eliasson



Thesis for the degree of Philosophiae Doctor (PhD)  
at the University of Bergen

Date of defense: 14.02.2020

© Copyright Sondre Hilmar Hopen Eliasson

The material in this publication is covered by the provisions of the Copyright Act.

Year: 2020

Title: Mechanistic Insight for Improved Catalytic Conversion of Fatty Acids to Linear  $\alpha$ -Olefins

Name: Sondre Hilmar Hopen Eliasson

Print: Skipnes Kommunikasjon / University of Bergen

## Acknowledgements

During the work with this thesis there have been many people that deserves recognition for the help and support they have provided throughout the years. First and foremost, my deepest gratitude goes to my supervisor, Prof. Dr. Vidar R. Jensen, for giving me the opportunity to engulf myself in chemistry and try to make the world a little bit better (despite my physics background). Thank you for having provided guidance, inspiration and time for late hour deadlines; without you this thesis would never have been written. I also want to thank my co-supervisor Dr. Giovanni Occhipinti and collaborator Dr. Anamitra Chatterjee for fruitful discussions and for providing the experimental fundament from which this thesis has sprouted.

My Ph.D. position was available as a part of the Microalgae project and it has been exciting to work on such an ambitious endeavor. This multidisciplinary project has involved persons from institutions all over Norway in addition to Prof. Dr. Vidar R. Jensen and Dr. Anamitra Chatterjee at UiB; Dr. Veronika Solteszova at CMR in Bergen, Prof. Dr. Atle M. Bones and Dr. Tore Brembu at NTNU in Trondheim, Dr. Harald Throne-Holst and Dr. Gunnar Vittersø at SIFO and Cand. Scient. Line J. Barkved at NIVA in Oslo, and Prof. Dr. Tobias Boström and Dr. Anni M. Lehmuskero at UiT in Tromsø. I am glad to have met and worked with all of you. The Research Council of Norway (RCN) is acknowledged for the financial support of the project (grant number 238851), and NOTUR (NN2506K) and NORSTORE (NS2506K) for providing the computational architecture on which I could work my “magic”. Finally, I thank the University of Bergen for the doctoral fellowship.

Back in Bergen, I would like to express my gratitude to my colleagues at the institute of chemistry at UiB. A special thanks to Prof. Dr. Knut Børve who has guided me from a student to a teacher these 10 years at UiB and to Dr. Marco Foscatto who has helped me plenty of times throughout this thesis. A further thanks to Prof. Dr. Erwan le Roux, Prof. Dr. Leif J. Sæthre and my present and former accomplices Immanuel Reim, Milan Chhaganlal, Dr. Wietse Smit, Morten Tysse, Christian S. Gjermestad, Jonas B. Ekeli, Fredrik S. Nesse, Sven T. Nappen, Joakim S. Søvde, Simen P.

Følkner, Ivan F. Linares, , Hajar Nsiri, Dr. Anna Sobolewski, Vitali Koudriatsev, Anders Teigland and Emily M. MacCready, for all the good times, both business and pleasure.

At last, I am grateful for my friends and family for providing me with a life in which I could distract myself when necessary. Thanks to my girlfriend Frøya, whom with love and care (almost literally) carried me across the finish line, and to my parents, Tove and Hilmar, and my siblings, Sigrid, Frøya and Njål, for endless support and for believing in me when I could not do so myself.

## Abstract

One of the greatest challenges in our time is the replacement of fossil fuels with more sustainable alternatives for energy and chemical production. Arguably one of the most important classes of petrochemical intermediates is linear  $\alpha$ -olefins (LAOs), which are used in the production of polymers, surfactants and lubricants, and are mainly obtained through oligomerization of ethylene. Alternatively, they can be produced by ethenolysis or deoxygenation of the renewable feedstock triglycerides and their unsaturated and saturated fatty acids respectively. While there exist homogeneous, heterogeneous and biocatalysts for the deoxygenation reactions, LAOs can most selectively be produced through the homogeneous transition-metal catalyzed reaction decarbonylative dehydration. However, the reaction typically requires high temperature, excess of ligands, fatty acid activation and distillation or a toxic solvent to achieve activity and selectivity, and the development of catalysts that can compete with the fossil-based alternatives has been stifled by the lack of mechanistic insight. Only recently has the first computational investigations of the reaction arrived, and together with the first well-defined precatalyst for the transformation, Pd(cinnamyl)Cl(DPEphos) (**A1**), there is now potential for rational catalyst design. Within this thesis we have investigated, by density functional theory (DFT) calculations, how different factors of the reaction in general, and of the precatalyst **A1** in particular, affect the reaction mechanism. The reaction mechanism for a Rh catalyst is derived and compared to that of Pd, and it is found that while the rate-determining step is olefin-formation for both, the rate-determining intermediate for Rh is the starting complex,  $(\text{PPh}_3)_2\text{Rh}^{\text{I}}(\text{CO})\text{Cl}$ . The main reason for the overall higher barriers for Rh, and thus the observed higher activity of Pd, stems from the greater stability of this  $\text{Rh}^{\text{I}}\text{-CO}$  bond and the preference Rh has for a higher coordination number which leads to increased steric hindrance. For Pd a low coordinated metal center is favored for the rate-determining olefin formation, but the classic P-O-P ligand DPEphos facilitates good  $\alpha$ -olefin production and catalyst stability by hemilabile coordination. The change from bidentate  $\kappa^2$  to monodentate  $\kappa^1$ -coordination prior to decarbonylation creates a coordination site for CO deinsertion,

---

and recoordination of the phosphine arm promotes CO displacement and dissociation which is key for catalyst activity. The escaping CO is modelled using a reduced pressure in the calculation of the thermochemical corrections and the effect of this correction is that the reaction is found to be catalytic as in accordance with the experiments. The main benefit of the precatalyst **A1** beyond this hemilabile behavior of DPEphos, which ensures that the ligand does not dissociate from the complex and dismisses the requirement of ligand excess, is the faster initiation compared to *in situ* systems. A major drawback to the reaction is the fatty acid activation by a sacrificial anhydride, which forms a mixed anhydride system, and is required to cleave the strong C(=O)-O bond. However, the resulting carboxylate from the following oxidative addition is important for the reaction because it readily accepts the hydrogen transferred from the alkyl and thus prevents isomerization. Polar aprotic solvents are found to be beneficial for the reaction, even though a cationic pathway is not preferred, likely due to the destabilization of rate-determining intermediates. In conclusion the mechanism of decarbonylative dehydration has been investigated and key parameters for catalysis has been identified. Improved catalysts may be developed in the future by exploring and designing new asymmetric hemilabile ligands and faster initiating precatalysts, perhaps even automatically.

## List of Publications

### Paper I

Chatterjee, A.; Eliasson, S. H. H.; Törnroos, K. W.; Jensen, V. R.; “Palladium Precatalysts for Decarbonylative Dehydration of Fatty Acids to Linear Alpha Olefins.”, *ACS Catalysis*, **2016**, *6(11)*, 7784-7789.

### Paper II

Eliasson, S. H. H.; Chatterjee, A.; Occhipinti, G.; Jensen, V. R., “The Mechanism of Rh-catalyzed Transformation of Fatty Acids to Linear Alpha Olefins.”, *Inorganics*, **2017**, *5(4)*, 87-101.

### Paper III

Eliasson, S. H. H.; Chatterjee, A.; Occhipinti, G; Jensen, V.R., “Green Solvent for the Synthesis of Linear  $\alpha$ -Olefins from Fatty Acids.”, *ACS Sustain. Chem. Eng.*, **2019**, *7*, 4903-4911.

### Paper IV

Eliasson, S. H. H.; Jensen, V. R., “Benefit of a hemilabile ligand in deoxygenation of fatty acids to 1- alkenes.”, *Faraday Discuss.*, **2019**.

### Review article included in Appendix A:

Chatterjee, A.; Eliasson, S. H. H.; Jensen, V. R.; “Selective production of linear  $\alpha$ -olefins via catalytic deoxygenation of fatty acids and derivatives.”, *Catal. Sci. Technol.*, **2018**, *8*, 1487-1499.

The published papers are reprinted with permission from American Chemical Society (Paper I and Paper III), MDPI (Paper II) and Royal Society of Chemistry (Paper IV and Appendix A). All rights reserved.



---

# Contents

Acknowledgements.....	4
Abstract .....	6
List of Publications .....	8
Contents .....	9
<b>1. Introduction.....</b>	<b>11</b>
1.1 <i>Background</i> .....	11
1.2 <i>Aim</i> .....	15
1.3 <i>Outline</i> .....	16
<b>2. Computational Methods .....</b>	<b>17</b>
2.1 <i>Quantum Chemistry</i> .....	17
2.1.1 The Schrödinger Equation.....	17
2.1.2 The Born-Oppenheimer Approximation .....	19
2.1.3 The Variational Principle.....	20
2.1.4 The Hartree Fock Approximation.....	21
2.1.5 Density Functional Theory (DFT).....	25
2.1.6 Dispersion Corrections.....	29
2.1.7 Effective Core Potential (ECP).....	31
2.2 <i>Modelling a Chemical Reaction</i> .....	32
2.2.1 Thermodynamic Corrections.....	32
2.2.2 Treatment of Standard States.....	34
2.2.3 Solvent Calculations.....	36
2.2.4 The Conformational Issue .....	37
<b>3. Mechanistic Investigation of Decarbonylative Dehydration .....</b>	<b>39</b>
3.1 <i>Computational Details</i> .....	39
3.2 <i>General Reaction Mechanism for Decarbonylative Dehydration</i> .....	42
3.3 <i>Comparison of Rh and Pd as the Catalyst's Metal Center</i> .....	46
3.4 <i>The Advantage of a Well-Defined Precatalyst</i> .....	51
3.5 <i>The Role of the Anhydride Activation</i> .....	56

---

3.6	<i>The Benefit of a Hemi-Labile Bidentate Ligand</i> .....	59
3.7	<i>Modeling CO Removal from the Reaction Mixture</i> .....	63
3.8	<i>The Solvent Effect on 1-Alkene Formation and Isomerization</i> .....	67
3.9	<i>Additional Factors Present in Decarbonylative Dehydration Reactions</i> .....	78
4.	<b>Suggestions for Future Improvements of the Catalysis</b> .....	<b>79</b>
5.	<b>Conclusion</b> .....	<b>82</b>
6.	<b>References</b> .....	<b>84</b>

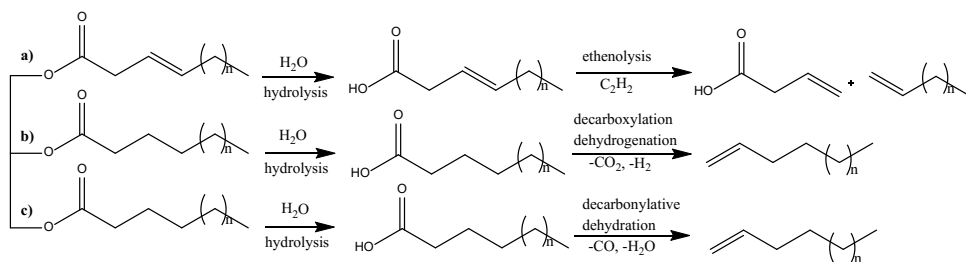
# 1. Introduction

## 1.1 Background

The world is in dire need of replacing fossil fuel-based carbon as the main energy source with more sustainable alternatives. Both because of the climate challenges related to their combustion, but also because the global storages are being depleted and the market is volatile. However, an often-forgotten point is also how dependent we are on petrochemicals as substrates for many of the products in our daily-life. If we are going to reduce our carbon footprint by stepping away from traditional fossil-resources then a development of sustainable production of large-volume chemical compounds for a greener chemical industry is needed.<sup>1-3</sup> A strategy in this regard is to use renewable, natural-based biomass like oils, lignin, cellulose and other sugars as starting point to generate platform chemicals for further valorization to more specialized derivatives.<sup>4-12</sup> One such class of platform chemicals is linear  $\alpha$ -olefins (LAOs) which from their versatile 1-alkene group allows for multiple derivatizations and are used in such applications as polyethylene production, synthesis of oxo-alcohols for the use as detergents and plasticizers, and the production of poly- $\alpha$ -olefins used in drilling fluids and synthetic lubricants.<sup>13-15</sup> The annual production of LAOs is well above one million metric tons and the global market value was estimated to 8.26 billion USD in 2018, which is expected to grow as the demand for the end-products increases.<sup>16-19</sup> It is thus likely that LAOs will defend their position as key chemical intermediates also in the foreseeable future.

LAOs are today almost exclusively produced from fossil-fuels through the process of ethylene oligomerization, which with some exceptions gives a Flory-Schultz-type distribution of even-numbered LAOs.<sup>14, 16, 20-24</sup> An alternative process is the dehydration of *n*-alkanes created through Fischer-Tropsch processing of fossil fuels, but this indirect method suffers from isomerization of the  $\alpha$ -olefins to yield the more stable internal olefins.<sup>25-27</sup> Alternatively, LOAs can be produced more sustainably and selectively from the long carbon chains of fatty oils.<sup>28-33</sup> Dependent on the source of

the oils, being animals, plants or microalgae, the composition of this carbon chain will vary, both in terms of saturation and length.<sup>34-35</sup> Unsaturated plant oil triglycerides, triacylglycerols (TAG), can be transformed directly to  $\alpha$ -olefins by olefin metathesis through selective alkene double bond ethenolysis.<sup>36-47</sup> From an unsaturated fatty acid or triglyceride this will generate an  $\alpha$ -olefin, but also an  $\alpha$ -unsaturated carboxylic acid or the triglyceride equivalent (Scheme 1a) dependent if the glyceride is hydrolyzed first.



**Scheme 1.** The possible pathways to generate  $\alpha$ -olefins from natural triglycerides and the corresponding fatty acids, a) ethenolysis, b) decarboxylation and c) decarbonylative dehydration.

An alternative to this are the deoxygenation reactions which not only yields only one olefin product but can also be performed on saturated fatty acids (Scheme 1, b and c).<sup>31</sup> This greatly increases the range of potential fatty acids available and thus the resulting linear  $\alpha$ -olefins. These reactions also remove one carbon from the even-numbered fatty acid carbon chain, yielding odd numbered linear  $\alpha$ -olefins which are not available from traditional methods or ethenolysis. Included in the deoxygenation reaction are decarboxylation, decarbonylation and dehydration. Decarboxylation transforms the fatty acids with the release of  $\text{CO}_2$  to alkanes but can be combined with dehydrogenation to yield the corresponding alkene.<sup>33, 48</sup> Decarbonylation on the other hand releases  $\text{CO}$  and combined with dehydration it produces the olefin.<sup>49</sup> While several traditional deoxygenation reactions in theory yields  $\alpha$ -olefins the selectivity is usually low or the reaction requires stoichiometric amounts of toxic reagents,<sup>50-54</sup> and a lot of research has lately been focused on developing more selective and sustainable catalysts for the transformation.

---

Recently, we published a review which covers the recent advances toward selective LAO synthesis from deoxygenation of fatty acids and derivatives within homogenous, heterogenous and bio-catalysis.<sup>55</sup> The review encompasses both experimental and computational results, and has been included here in Appendix A because it gives an overview over the current state of the research and addresses pros and cons with the various approaches. The overall picture is that biocatalysts yield excellent 1-alkene selectivity through decarboxylation at mild condition, but as the norm is with this type of catalysts, the stability and volumetric production is limited. Heterogenous catalysis on the other hand has generally higher thermal stability and can easily be separated from the reaction products. However, only a handful of results on the heterogenous conversion of fatty acids and their derivatives to LAOs have been reported and for most of them the selectivity has been low.<sup>56</sup>

The best activity and selectivity have been obtained by the homogenous catalyzed reaction decarbonylative dehydration (Scheme 1c). The process was first reported in 1966 when decarbonylation of aldehydes and carboxylic acid by ruthenium and rhodium respectively yielded olefins, albeit with low  $\alpha$ -olefin selectivity.<sup>57</sup> Only a year later also palladium catalyzed decarbonylation of aliphatic acyl chlorides was found to produce olefins along with CO and HCl.<sup>58-59</sup> In 1978, T.A Foglia and P.A. Barr investigated decarbonylative dehydration of fatty acids by phosphine coordinated rhodium and palladium complexes and reported results that are crucial for the reaction to this day.<sup>49</sup> First, it was confirmed that CO and not CO<sub>2</sub> was released, identifying the reaction to be decarbonylation in contrast to decarboxylation. Additionally, it was also found that an excess of phosphine causes the preferential loss of carbon monoxide and a purge speeds up the reaction by removal of the gas from the reaction mixture. In the absence of added phosphines, a buildup of CO around the catalyst occurs and forms catalytic inactive metal-carbonyl species. Finally, a mechanism was proposed which also assumed that the reaction was initiated by an *in situ* formation of an acid anhydride. This was many years later (1993) confirmed by J. A. Miller et al. who found that catalysis was drastically improved by the addition of acid anhydride which forms an asymmetric anhydride with the fatty acid substrate.<sup>60</sup> They also found that palladium with a large excess of

phosphines was the most active catalyst, while rhodium was able to achieve high activity with less added phosphines and without activation by anhydride. Their reported turnover number (TON) of 12 370 is the highest obtained to this date. Recently, probably due to a larger focus on green and sustainable chemistry, the reaction has regained interest and various attempts to improve the transformation of fatty acids and derivatives to 1-alkene have been published. The progress has mainly been towards improving the palladium catalyzed reaction by varying the ligand and reducing the reaction temperature and the procedure has also shown promise for application in multistep synthesis.<sup>61-68</sup> Alternative metals like iridium<sup>69-71</sup> and the more earth-abundant options iron<sup>72</sup> and nickel<sup>73-75</sup> have also been investigated. However, Pd is still the most active metal and the reaction generally requires excess phosphines, activation by a sacrificial anhydride, and continuous distillation or a toxic polar solvent to achieve good  $\alpha$ -olefin selectivity. Moreover, the activity is still not good enough to compete with the traditional fossil-fuel based processes or to reach the typical minimum TON of 50 000 for a homogenous process to be industrially viable.<sup>40, 43, 76</sup>

A problem for decarbonylative dehydration compared to for example olefin metathesis and ethenolysis,<sup>40, 77-80</sup> has been the lack of mechanistic and theoretical insight. Only during the work with this thesis, have the first computational studies of the reaction arrived.<sup>66, 74, 81-84</sup> This lack of mechanistic information has stifled the understanding of different factors of the reaction and rational design of better catalysts, and was partly the motivation for synthesizing the molecular well-defined precatalyst **A1**, Pd(cinnamyl)Cl(DPEphos).<sup>85</sup> While previous catalysts for decarbonylative dehydration have been formed *in situ*, this catalytic system was able to transform fatty acids to  $\alpha$ -olefin at relatively mild conditions (110°C) and, importantly, without excess of phosphine. It also gives high selectivity (>95% for most substrates) without continuous distillation and can handle a wide range of substrates. Most important perhaps, it provides a nice fundament for computational investigations of the reaction and facilitates improvements *via* structure-activity relationships.

## 1.2 Aim

As well as replacing fossil-fuel with renewable feedstock, a key effort for a more sustainable chemical production is the transition to more durable and active catalytic systems.<sup>86</sup> A more and more common trend, in parallel with increasing computational power and more accurate modelling methods, is that this development is guided by insight gained from investigation of the reaction mechanism, and new catalyst may even be predicted computationally before being synthesized in the lab.<sup>87-88</sup> For decarbonylative dehydration this has not been available, and thus the aim of this thesis is to investigate the mechanism of decarbonylative dehydration of fatty acids, to give a better insight of the reaction and to understand its accompanying issues.

In general, the main problems for decarbonylative dehydration have been:

- Generally low TONs combined with requirement for high temperatures.
- The use of rare-earth metals for the catalyst.
- An excess of ligands, typically phosphines, have been required to achieve activity and selectivity.
- The fatty acids need activation before catalysis starts.
- Accumulation of CO, which is produced during the reaction, poisons the catalyst and needs to be removed from the reaction mixture to ensure activity.
- Continuous distillation or a toxic polar solvent has been required to achieve high selectivity.

The molecular precatalyst **A1** has shown promise regarding many of these problems and is used as a foundation for the investigation of how factors of the catalysis affect the reaction. The overall goal of the thesis is to identify parameters that are key for catalytic activity and find potential responses for the problems to motivate and direct future development of improved catalysts for decarbonylative dehydration, both in terms of activity and overall sustainability of the reaction. This is done by combining the work presented in this thesis with other related theoretical and computational studies.

## 1.3 Outline

The thesis starts with an introductory description of the theoretical foundation of the computational methods used, which includes basic quantum chemistry and the translation from modelling a microscopical system to the macroscopic properties observed for chemical reactions (Chapter 2). We then move over to the mechanistical investigation of decarbonylative dehydration (Chapter 3) which starts with a summary of the computational tools used in the thesis (3.1), before giving a brief step-by-step overview of the general mechanism proposed for decarbonylative dehydration (3.2). The following chapters are then dedicated to the investigation of the different factors of the reaction, including different transition metals (3.3), the benefit of a well-defined precatalyst (3.4), the activation of the fatty acids (3.5), and the effect of a hemilabile bidentate ligand (3.6). A chapter is also dedicated to the computational treatment of the escaping gas CO and how this affect the reaction mechanism (3.7). Finally, the solvent effect on 1-alkene formation and isomerization is studied and a non-toxic green solvent is identified for the reaction (3.8). At the end, additional factors that are used in some setups of decarbonylative dehydration are briefly mentioned (3.9) and suggestions for further catalysis development for decarbonylative dehydration are presented (Chapter 4).



---

## 2. Computational Methods

To model the atoms and electrons that build up and constitute all matter and reactions surrounding us is a daunting task. The scale of the size and time these particles operate on are beyond observation by most instruments and thus we are relying on experimental results and theoretical studies when we try to understand what is happening in chemical reactions. Within computational theory there are various levels which are appropriate at different situations and in the following section the methods used for the molecular modelling in this thesis will be presented. The theory in this section is based on common textbooks used within the field.<sup>89-92</sup>

### 2.1 Quantum Chemistry

#### 2.1.1 The Schrödinger Equation

The basis for quantum mechanics is the wavefunction and the Schrödinger equation,

$$\hat{H}\Psi(\mathbf{x}, t) = i\hbar \frac{\partial}{\partial t} \Psi(\mathbf{x}, t). \quad (1)$$

Solving the Schrödinger equation gives the wavefunction  $\Psi(\mathbf{x}, t)$  which is a general description of a quantum mechanical system (defined by  $\mathbf{x}$  at time  $t$ ) containing all information that can be known about the system. It is unclear what the actual interpretation of the wavefunction is, but its squared modulus  $|\Psi(\mathbf{x}_1, \mathbf{x}_2, \dots, \mathbf{x}_n, t)|^2$  is a probability density, where  $|\Psi(\mathbf{x}_1, \mathbf{x}_2, \dots, \mathbf{x}_n, t)|^2 d\mathbf{x}_1 d\mathbf{x}_2 \dots d\mathbf{x}_n$  gives the probability of finding particle  $i$  at a given infinitesimal space  $d\mathbf{x}_i$ . The Hamilton operator,  $\hat{H}$ , contains the kinetic energy operator,  $\hat{T}$ , and potential energy operator,  $\hat{V}$ , and thus gives the total energy of the system,

$$\hat{H} = \hat{T} + \hat{V}, \quad (2)$$

where

$$\hat{T} = -\frac{\hbar^2}{2m} \nabla^2 \text{ and } \hat{V} = V(\mathbf{x}, t). \quad (3)$$

This gives the total form of the Schrödinger equation as,

$$\left( -\frac{\hbar^2}{2m} \nabla^2 + V(\mathbf{x}, t) \right) \Psi(\mathbf{x}, t) = i\hbar \frac{\partial}{\partial t} \Psi(\mathbf{x}, t), \quad (4)$$

where  $\nabla^2$  is the Laplacian operator,  $\nabla^2 = \left( \frac{d^2}{dx^2} + \frac{d^2}{dy^2} + \frac{d^2}{dz^2} \right)$ ,  $\hbar$  is Planck's constant divided by  $2\pi$ ,  $V(\mathbf{x}, t)$  is an external potential (e.g. the core – electron attraction) and  $i$  is the imaginary unit. By using atomic units, we can set  $\hbar$  to unity and give the mass relative to the electronic mass, simplifying the equation.

If the potential is invariable in time, that is  $V(\mathbf{x}, t) \equiv V(\mathbf{x})$ , we can do a separation of variables and split the wavefunction into a part dependent on the spatial coordinates and spin,  $\psi(\mathbf{x})$ , and a time dependent part,  $\tau(t)$ . The total wavefunction can then be written as a product of these two parts,

$$\Psi(\mathbf{x}, t) = \psi(\mathbf{x})\tau(t). \quad (5)$$

The time-independent Schrödinger equation can then be separated out as an eigenvalue equation,

$$\hat{H}\psi(\mathbf{x}) = E\psi(\mathbf{x}), \quad (6)$$

where the eigenvalue  $E$  is the total energy of the system for the state described by the stationary eigenstate  $\psi(\mathbf{x})$ .

In a typical quantum mechanical system with  $n$  electrons and  $m$  nuclei and no external potential the Hamiltonian becomes

$$\hat{H} = \hat{T}_N + \hat{T}_E + \hat{V}_{NE} + \hat{V}_{NN} + \hat{V}_{EE}, \quad (7)$$

or,

$$\hat{H} = -\frac{1}{2} \sum_{A=1}^m \frac{\nabla^2}{M_A} - \frac{1}{2} \sum_{i=1}^n \nabla_i^2 + \sum_{A=1}^m \sum_{i=1}^n \frac{Z_A}{r_{iA}} + \sum_{A=1}^m \sum_{B>A}^m \frac{Z_A Z_B}{R_{AB}} + \sum_{i=1}^n \sum_{j>i}^n \frac{1}{r_{ij}}, \quad (8)$$

where  $\hat{T}_N$  is the kinetic energy of nuclei,  $\hat{T}_E$  the equivalent for the electrons,  $\hat{V}_{NE}$  the electrostatic attraction between nuclei and electrons, and  $\hat{V}_{NN}$  and  $\hat{V}_{EE}$  is the repulsion between nuclei and the electrons respectively.  $M_A$  is the mass of nucleus  $A$  and  $Z_A$  its corresponding atomic number.  $R_{AB}$  is the distance between nuclei  $A$  and  $B$ , while  $r_{iA}$  and  $r_{ij}$  represents the distance between electron  $i$  and nucleus  $A$  and the distance between electrons  $i$  and  $j$ . This separation between nucleic coordinates and electrons will further be explored in the next section.

## 2.1.2 The Born-Oppenheimer Approximation

The Born-Oppenheimer states that since the nuclei are much heavier than the electrons their motion is usually operating at a higher time scale than the electrons. This means that one can assume that the electrons will always be able to rearrange to the new position of the nuclei which against means that within the approximation one can decouple the motion of electrons and nuclei and look at the motion of the electrons in a system with static nuclei, i.e.  $\hat{T}_N = 0$  and  $R_{AB}$  constant. The remaining terms from (8) can then be summarized as the electronic Hamiltonian which describes the motion of  $n$  electrons in the field of  $m$  point charges,

$$\hat{H}_{elec} = -\frac{1}{2} \sum_{i=1}^n \nabla_i^2 - \sum_{A=1}^m \sum_{i=1}^n \frac{Z_A}{r_{iA}} + \sum_{i=1}^n \sum_{j>i}^n \frac{1}{r_{ij}}. \quad (9)$$

The solution of the electronic Schrödinger equation,

$$\hat{H}_{elec} \psi_{elec} = E_{elec} \psi_{elec}, \quad (10)$$

is the electronic wavefunction,

$$\psi_{elec} = \psi(\mathbf{x}_1, \mathbf{x}_2, \dots, \mathbf{x}_n; \{\mathbf{R}_1, \mathbf{R}_2, \dots, \mathbf{R}_m\}), \quad (11)$$

which describes the electronic motion in a field which depends on the *parametrically* given nuclear coordinates. This means that the nuclear coordinates do not appear

explicitly in the expression, but a new arrangement of the nuclei gives a different  $\psi_{elec}$  of the electronic coordinates. The same also holds true for the electronic energy,

$$E_{elec} = E_{elec}(\{\mathbf{R}_A\}). \quad (12)$$

To obtain the total energy including the static nuclei the constant internuclear repulsion is added to the electronic energy

$$E = E_{elec} + \sum_{A=1}^m \sum_{B>A}^m \frac{Z_A Z_B}{R_{AB}}. \quad (13)$$

Furthermore, one can reversely use the electronic energy as a parameter and together with the internuclear repulsion this give a potential energy surface (PES) on which the molecule can be optimized.

### 2.1.3 The Variational Principle

Due to the complexity of the Hamiltonian, an exact solution of the Schrödinger equation cannot be found for molecular systems larger than  $\text{H}_2^+$ . Instead, restrictions and simplifications must be applied to give approximate solutions; the Born-Oppenheimer (discussed above) being one of them. The next step is to find the appropriate wavefunction and this is not trivial as there are many possible solutions for the selected Hamiltonian. Fortunately, the variational principle states that for an operator  $\hat{H}_{elec}$  any expectation value  $E_{elec}$  will be greater or equal to the expectation value of the ground state  $E_{elec}^0$ , and only equal if  $\psi_{elec}$  is the actual ground state wavefunction  $\psi_{elec}^0$ ,

$$\langle \psi_{elec} | \hat{H}_{elec} | \psi_{elec} \rangle = E_{elec} \geq E_{elec}^0. \quad (14)$$

This turns the problem into an optimization problem where the goal is to find a wavefunction that gets the expectation value as low as possible. Unfortunately, the

search space is so vast that further approximations are required to identify a proper  $\psi_{elec}$ .

### 2.1.4 The Hartree Fock Approximation

A tempting choice for a trial function for the electronic wavefunction would be a product of spin functions  $\chi_n(\mathbf{x}_n)$  called a *Hartree product*,

$$\psi_{elec} \approx \chi_1(\mathbf{x}_1)\chi_2(\mathbf{x}_2) \dots \chi_n(\mathbf{x}_n), \quad (15)$$

where the spin functions  $\chi_n(\mathbf{x}_n)$  are orthonormal one-electron wavefunctions and are made from the product of a spatial orbital  $\phi(\mathbf{r})$  and a spin component  $\sigma(s)$  (either  $\alpha(s)$  or  $\beta(s)$ ),

$$\chi(\mathbf{x}) = \phi(\mathbf{r})\sigma(s). \quad (16)$$

However, the trial function (15) does not fulfil the requirement that the electrons are *indistinguishable*. Here electron 1 occupies spin function  $\chi_1$ , electron 2 occupies  $\chi_2$  etc. This contradicts *Pauli's exclusions principle* that the wavefunction should be antisymmetric with respect the interchange of the spin functions of any two electrons, i.e.

$$\chi_1(\mathbf{x}_1)\chi_2(\mathbf{x}_2) \dots \chi_n(\mathbf{x}_n) \neq -\chi_1(\mathbf{x}_2)\chi_2(\mathbf{x}_1) \dots \chi_n(\mathbf{x}_n). \quad (17)$$

An alternative is to represent the n-electrons wavefunction as Slater determinant,

$$\psi_{elec} \approx \Phi_{SD} = \frac{1}{\sqrt{n!}} \begin{vmatrix} \chi_1(\mathbf{x}_1) & \chi_2(\mathbf{x}_1) & \dots & \chi_n(\mathbf{x}_1) \\ \chi_1(\mathbf{x}_2) & \chi_2(\mathbf{x}_2) & \dots & \chi_n(\mathbf{x}_2) \\ \vdots & \vdots & \ddots & \vdots \\ \chi_1(\mathbf{x}_n) & \chi_2(\mathbf{x}_n) & \dots & \chi_n(\mathbf{x}_n) \end{vmatrix}, \quad (18)$$

where  $(n!)^{-1/2}$  is the normalization factor. Since each row is labelled with one electron and each column is labelled with one spin function, the determinant contains all n! perturbations of the electrons and accounts for the fact that the electrons are indistinguishable. Moreover, interchanging the coordinate of two electrons

corresponds to interchanging two rows of the determinant, which changes the sign of the determinant and thus the determinant possesses the asymmetry property required for *fermions*. If two electrons occupy the same spin orbital this is equivalent to two columns of the determinant being equal, which makes the determinant zero as in accordance with Pauli's exclusion principle.

Using the variational principle (section 2.1.3) the expectation energy of  $\hat{H}_{elec}$  can now be optimized (minimized) by finding the best one-electron spin functions which are solutions to the one-electron Hartree-Fock equations,

$$\hat{f}_i \chi_i = \varepsilon_i \chi_i, \quad (19)$$

$$\hat{f}_i = -\frac{1}{2} \nabla_i^2 - \sum_A^m \frac{Z_A}{r_{iA}} + v^{HF}(i). \quad (20)$$

The first term of the fock operator  $\hat{f}_i$  is the kinetic energy of the electron, the second is the attraction to each of the nuclei and finally the Hartree-Fock potential  $v^{HF}(i)$  which is the repulsion experienced by an electron from all the other  $n-1$  electrons. This potential can be expressed as,

$$v^{HF}(\mathbf{x}_1) = \sum_j^n \left( \hat{J}_j(\mathbf{x}_1) - \hat{K}_j(\mathbf{x}_1) \right), \quad (21)$$

where

$$\hat{J}_j(\mathbf{x}_1) = \int \frac{|\chi_j(\mathbf{x}_2)|^2}{r_{12}} d\mathbf{x}_2, \quad (22)$$

and

$$\hat{K}_j(\mathbf{x}_1) \chi_i(\mathbf{x}_1) = \int \chi_j^*(\mathbf{x}_2) \frac{1}{r_{12}} \chi_i(\mathbf{x}_2) d\mathbf{x}_2 \chi_j(\mathbf{x}_1). \quad (23)$$

The  $\hat{J}_j(\mathbf{x}_1)$  operator is the Coulomb repulsion between an electron in  $\mathbf{x}_1$  and the average charge of an electron in spin function  $\chi_j$  and  $\hat{K}_j(\mathbf{x}_1)$  is the exchange operator resulting from the asymmetry of the Slater determinant. While the Coulomb repulsion

is easy to rationalize, there exist no classical equivalent to the exchange operator which only give contributions from electrons of equal spin (alpha or beta).

As seen from the equations, the operators  $\hat{f}_j(\mathbf{x}_1)$  and  $\hat{K}_j(\mathbf{x}_1)$  both depend on the spin orbitals  $\chi_j$  themselves, thus the eigenvalue equation (19) can only be solved iteratively. An initial guess of spin orbitals is provided for the first iteration and after solving the  $n$  Hartree-Fock equations the resulting new spins orbitals are used as an updated basis for the next iteration. This iterative process is continued until convergence, i.e. that the updated set  $\chi_j$  is sufficiently close to the set that was used as input for that iteration. This process is referred to as the *self-consistent field* (SCF).

The spin functions themselves were defined in (16) as a product of a spatial part and a spin part. The spatial part can further be constructed as a linear combination of a set of  $l$  basis functions  $\{\varphi\}_l$ ,

$$\phi_i = \sum_{\mu=1}^l c_{\mu i} \varphi_{\mu}, \quad (24)$$

where  $c_{ik}$  are coefficients and each  $\varphi_k$  is usually either a single or a combination of atom centered Slater or Gaussian type orbitals (STOs and GTOs). Slater type orbitals have the correct shape but cannot calculate exactly more than two-center integrals. Gaussian type orbitals on the other hand can do these calculations, but do not behave properly. Thus, usually a linear combinations of Gaussian type orbital are used to form a single basis function of the correct shape (contraction).

Due to this new expansion of the spin orbitals, the Hartree-Fock equations can be rewritten as,

$$\sum_{\mu=1}^l c_{\mu i} \int \varphi_{\nu}^*(\mathbf{r}) \hat{f}_i(\mathbf{r}) \varphi_{\mu}(\mathbf{r}) d\mathbf{r} = \varepsilon_i \sum_{\mu=1}^l c_{\mu i} \int \varphi_{\nu}^*(\mathbf{r}) \varphi_{\mu}(\mathbf{r}) d\mathbf{r} \quad \text{for } \nu \in \{1, l\}. \quad (25)$$

This system of  $l$  equations can be rewritten as a single matrix equation

$$\mathbf{FC} = \mathbf{SCe}, \quad (26)$$

$$F_{\nu\mu} = \int \varphi_{\nu}^*(\mathbf{r}) \hat{f}_i(\mathbf{r}) \varphi_{\mu}(\mathbf{r}) d\mathbf{r}, \quad (27)$$

$$S_{\nu\mu} = \int \varphi_{\nu}^*(\mathbf{r}) \varphi_{\mu}(\mathbf{r}) d\mathbf{r}, \quad (28)$$

$$\mathbf{C} = \begin{bmatrix} c_{11} & \cdots & c_{1l} \\ \vdots & \ddots & \vdots \\ c_{l1} & \cdots & c_{ll} \end{bmatrix}, \quad (29)$$

$$\mathbf{e} = \begin{bmatrix} \varepsilon_1 & \cdots & 0 \\ \vdots & \ddots & \vdots \\ 0 & \cdots & \varepsilon_l \end{bmatrix}. \quad (30)$$

Where  $\mathbf{F}$  is the Fock matrix,  $\mathbf{S}$  is the overlap matrix,  $\mathbf{C}$  the matrix of linear expansion coefficients, and  $\mathbf{e}$  the diagonal matrix of the orbital energies. This formulation turns solving the non-linear optimization problem into a linear algebra problem that can be solved more easily by computers.

Due to the way the Hartree-Fock approximation is constructed there are some systematic errors introduced in the results. Firstly, the electron-electron interaction is calculated as the repulsion experienced by an electron from the average of all the other electrons. This means that instantaneous interactions are not considered, i.e. the electrons do not “see” each other, resulting in electrons being too close to each other and an artificially high repulsion (dynamic correlation). While the dynamic correlation is not considered, the exchange operator (21) gives a lowering of the repulsion, but only for electrons with parallel spin. Also, due to the way the electron-electron interaction is calculated, the sum of the orbital energies  $\varepsilon_i$  is not equal to the total energy because this would double count the repulsion from pairwise electrons. However according to the *Koopmans’ theorem*, the orbital energy can be approximated to the ionization potential, which is rationalized by cancellation of missing correlation and relaxation effects. Secondly, a single Slater determinant as used in Hartree-Fock cannot describe all systems accurately, and some (especially nearly degenerate configuration) require a combination of multiple Slater determinants.



Alas, due to the intrinsic “problems” with the Hartree-Fock procedure, the variational principle, with even the largest and most complete basis set  $\{\varphi\}_L$ , can only give a best estimate, the Hartree-Fock limit, that is higher than the exact ground state energy calculated in the unrelativistic Born-Oppenheimer approximation. The difference between the Hartree-Fock energy,  $E_{HF}$ , and the exact energy,  $E_{exact}$  is called correlation energy,  $E_{corr}$ ,

$$E_{corr} = E_{exact} - E_{HF}. \quad (31)$$

### 2.1.5 Density Functional Theory (DFT)

The basis for the Hartree-Fock approach was the electronic wavefunction, but as already stated the wavefunction has no physical representation. The electron density on the other hand can both be understood and observed through experiments. What more, while the wavefunction depends on the three spatial coordinates and spin for each electron, the density only depends on the three spatial coordinates regardless of the number of nuclei and electrons in the system, reducing the computational costs. Going from our previously defined probability density, we can give the electron density as

$$\rho(\mathbf{r}_1) = n \int \dots \int |\psi_{elec}(\mathbf{x}_1, \mathbf{x}_2, \dots, \mathbf{x}_n)|^2 d\mathbf{x}_1 d\mathbf{x}_2 \dots d\mathbf{x}_n, \quad (32)$$

which determines the probability of finding any of the  $N$  electrons within the volume element  $d\mathbf{r}_1$  with an arbitrary spin while all other electrons have arbitrary positions and spin. From the density,  $\rho(\mathbf{r})$ , we can derive the total number of electrons,

$$\int \rho(\mathbf{r}) d\mathbf{r} = n, \quad (33)$$

and the position and type of the atoms from the position and the derivative of the cusp of  $\rho(\mathbf{r})$ .

Since the density can provide us with the number of electrons,  $n$ , the position,  $R_A$ , and charge,  $Z_A$ , of the nuclei we do in fact have all the components necessary to construct a system-specific Hamiltonian. Thus, from the ground state density we get

$$\rho_0 \Rightarrow \{n, R_A, Z_A\} \Rightarrow \hat{H} \Rightarrow \psi_0 \Rightarrow E_0, \quad (34)$$

which means that the energy is a functional of the electron density (the first Hohnberg-Kohn theorem):

$$E_0[\rho_0] = T[\rho_0] + E_{ee}[\rho_0] + E_{Ne}[\rho_0]. \quad (35)$$

It is important to note here that the term  $E_{Ne}[\rho_0]$ , the electron-nuclei potential energy, is the only term that is dependent on the system parameters,  $n, R_A$  and  $Z_A$ . Unfortunately, this is also the only term that is explicitly known,

$$E_{Ne}[\rho_0] = \int \rho_0(\mathbf{r}) V_{Ne} d\mathbf{r}. \quad (36)$$

The remaining parts; the kinetic energy,  $T[\rho_0]$ , and the electron-electron interaction,  $E_{ee}[\rho_0]$ , collected to the *Hohnberg-Kohn* functional

$$F^{HK}[\rho] = T[\rho] + E_{ee}[\rho], \quad (37)$$

are system independent and thus, if known, would be universally applicable to all molecular systems. Instead we must contain ourselves to approximations to this functional. Moreover, according to the second Hohnberg-Kohn theorem, only the electron density corresponding to the ground state electron density,  $\rho_0$ , gives the ground state energy,  $E_0$ , which is the DFT equivalent of the variational principle.

$$E[\rho] \geq E[\rho_0] \quad (38)$$

This mean, as for *Hartree-Fock*, that an iterative procedure is required to identify  $\rho_0$ .

Early attempts at using the density as the “fundamental quantity”, i.e. the Thomas-Fermi Model, demonstrated that a major problem was to recover the kinetic energy of the system, as there is no trivial relationship between the spatial density and

velocities. A solution provided by Kohn and Sham was to instead try to recover as much of the true kinetic energy by returning to an orbital approach like *Hartree-Fock*. A non-interacting reference system of  $n$  electrons with an introduced local potential,  $V_s(\mathbf{r})$ , is used to mimic the real system,

$$\hat{H}_S = -\frac{1}{2} \sum_{i=1}^n \nabla^2 + \sum_{i=1}^n V_s(\mathbf{r}_i). \quad (39)$$

The solution to the ground state of such a system is, as previously, a Slater determinant

$$\Theta_S = \frac{1}{\sqrt{n!}} \begin{vmatrix} \vartheta_1(\mathbf{x}_1) & \cdots & \vartheta_n(\mathbf{x}_1) \\ \vdots & \ddots & \vdots \\ \vartheta_1(\mathbf{x}_n) & \cdots & \vartheta_n(\mathbf{x}_n) \end{vmatrix} \quad (40)$$

The so-called Kohn-Sham (KS) orbitals  $\vartheta_i$  are determined as solutions of,

$$\hat{f}^{KS} \vartheta_i = \varepsilon_i \vartheta_i, \quad (41)$$

$$\hat{f}^{KS} = -\frac{1}{2} \nabla^2 + V_s(\mathbf{r}), \quad (42)$$

where  $\hat{f}^{KS}$  is the Kohn-Sham operator. The requirement to this reference system is that the resulting density from the KS orbitals is equal to the ground state density of the real interacting system. From the KS orbitals the kinetic energy to the non-interacting system can be calculated as

$$T_s = -\frac{1}{2} \sum_{i=1}^n \langle \vartheta_i | \nabla^2 | \vartheta_i \rangle, \quad (43)$$

which is used as an approximation to the real kinetic energy,  $T[\rho_0]$ , differing only in a relatively small correction,  $T_c[\rho_0]$ . The expression for the classical Coulomb repulsion between electrons,  $J[\rho]$ , is also known, leaving the nonclassical portion of the missing electron-electron interaction,  $E_{ee}[\rho_0]$ , to be determined. With this new information, the Hohnberg-Kohn functional can be rewritten as

$$F^{HK}[\rho] = T_S[\rho] + T_C[\rho] + J[\rho] + E_{ncee}. \quad (44)$$

Moreover, the unknown terms,  $T_C[\rho]$  and  $E_{ncee}$  can be collected to the exchange-correlation functional,  $E_{XC}$ , which represents the connection between the reference system and the real interacting one,

$$F^{HK}[\rho] = T_S[\rho] + J[\rho] + E_{XC}[\rho]. \quad (45)$$

The related exchange-correlation potential is simply defined as the functional derivative

$$V_{XC} \equiv \frac{\partial E_{XC}}{\partial \rho}, \quad (46)$$

which allows that the fictional potential in the Kohn-Sham operator (39) to be rewritten as

$$V_S(\mathbf{r}) = \int \frac{\rho(\mathbf{r})}{r_{12}} d\mathbf{r}_2 - \sum_A^m \frac{Z_A}{r_{1A}} + V_{XC}(\mathbf{r}_1). \quad (47)$$

As for *Hartree-Fock*, the potential is dependent on the solution,  $\rho(\mathbf{r})$ , which again means an iterative scheme is needed to identify the coefficients of the linear combinations of the basis set functions used to construct the density that fulfil the self-consistent field condition. However, an explicit term for  $E_{XC}[\rho]$  is still required and there are different strategies used to define this missing functional.

The simple approximation that is the background for the most basic calculations of  $E_{XC}[\rho]$  is the idea of a uniform electron gas and is called *local density approximation* (LDA). In this approximation the electron density,  $\rho(\mathbf{r})$ , is assumed to have a constant value everywhere in the system, even though this is not at all the case. This can further be split into individual densities for  $\alpha$  and  $\beta$  spin electrons, the so-called *local spin density approximation*.

A more sophisticated approach is to also include the gradient of the density together with constraints that fulfil physical demands of the system, and functionals that take

---

this into consideration are collectively known as *generalized gradient approximation* (GGA). These functionals have an advantage over the LDA functionals because the gradient somewhat reflects the non-homogeneity of the true density of the system. In this regard, GGA functionals are sometimes said to be non-local, because they also contain information about the surrounding density. This strategy can be further extended to include the second derivative of the electron density and the meta-GGA family of functionals. A feature of these families of functionals is that the exchange-correlation contribution,  $E_{XC}$ , is often split into its two components,  $E_X$  and  $E_C$ , and approximations sought for each individually. Moreover, approximations for these terms are typically not based on any physical model, but only constructed to give satisfactory results, reflecting the pragmatic nature of density functional theory in general.

One way to define the exchange-part of  $E_{XC}$ , is to introduce the true non-local Hartree-Fock exact exchange into the functionals. However, it has been shown that giving  $E_X$  as only the exact Hartree-Fock exchange is unsound both in concept and results, and thus it is often only given as a portion that is empirically parameterized. As this approximation of  $E_{XC}$  gives a mixture of DFT and Hartree-Fock, this class of functionals is called hybrid functionals. An example of this type of functional that helped DFT rise to prominence is B3LYP which is somewhat a standard now when modelling organic molecules.

### 2.1.6 Dispersion Corrections

A major shortcoming of DFT with regards to modelling molecules is the lack of dispersion interaction. Dispersion is an intermolecular interaction that results from instantaneously induced dipoles in the electron density from other nearby, but not directly bonded densities, i.e. a molecule in proximity or not directly bonded portions of the same molecule. Since this interaction derives from two separate points in space, the local character of  $V_{XC}(\mathbf{r})$ , which is dependent on the density and perhaps gradient at a single point  $\mathbf{r}$  cannot account for dispersion. While the dispersion forces

are weak, compared to bonds and permanent dipole interactions, they are far reaching and multiple. Thus, neglect of dispersion can seriously hamper accuracy, especially in cases where it is the governing forces, as between noble gases or in association/dissociation reactions.<sup>93</sup> Many of the earlier developed functionals suffered due to this, as they were typically not parameterized against training sets involving dispersion-bonded complexes, but in recent years strategies have been developed to introduce dispersion. There are mainly two approaches that are considered when dispersion is included in DFT-calculations. One is the parameterization of the functionals to fit dispersion. The Minnesota functionals e.g. are heavily parameterized to fit high quality benchmark databases and the M06L<sup>94-96</sup> functional is used in this thesis. Another is the use of empirical dispersion correction (DFT-D) where an empirical  $C_6/R^6$  term running across atom pairs is added to the conventional DFT energy,

$$E_{DFT-D} = E_{KS-DFT} + E_{disp}. \quad (48)$$

In the DFT-D method devised by Grimme<sup>97-99</sup>  $E_{disp}$  is typically defined as

$$E_{disp} = -s_6 \sum_{i=1}^M \sum_{j=i+1}^M \frac{C_6^{ij}}{R_{ij}^6} f_{amp}(R_{ij}), \quad (49)$$

where  $s_6$  is a scaling parameter dependent on the functional used,  $C_6^{ij}$  is a dispersion coefficient for the two atoms with an internuclear distance  $R_{ij}$ , and  $f_{amp}(R_{ij})$  is a dampening factor to ensure that the dispersion term drops when  $R_{ij}$  gets small to avoid double counting of electronic correlation.<sup>100-101</sup> In Paper II, this type of empirical dispersion correction with different types of dampening were employed.

### **2.1.7 Effective Core Potential (ECP)**

When modelling heavy transition metals (as in this thesis) there are two issues that emerges. First, these metals have many electrons, meaning that the effort associated with the calculations, which typically scales as  $N^4$  with the,  $N$ , number of electrons, drastically increases as we move down the periodic table. Second, as the charge of the nucleus increases, so will the velocity of the inner electrons, meaning that relativistic effects cannot be neglected anymore, as was done in the un-relativistic Schrödinger equation (1) in the very beginning. The introduction of an effective core potential (ECP) offers a solution to both these problems. In ECP, as given in the name, the core electrons are gathered into a pseudopotential that includes the interaction between the valence electrons and the core electrons, and interactions among the core electrons themselves. This leaves only the valence electrons to be explicitly modelled when interacting with other atoms. Moreover, the ECP is derived from very accurate atomic calculations which may also include any potential relativistic effects. The physical rationale for the use of ECP is, analogously to semi-empirical methods, that the core electrons, while energetically important, does not really contribute or change during chemical reactions and can thus be simplified to potentials. Practically this allows a more accurate treatment of the valence electrons, and often leads to reduced basis set superposition error than when the core-electrons are explicitly included.

## 2.2 Modelling a Chemical Reaction

### 2.2.1 Thermodynamic Corrections

We have so far considered the calculations of individual (or few) molecular species. However, to relate the properties we find in the calculations to the experimental observations, there must be a translation to the macroscopic world. In general, chemistry deals in fundamental functions of thermodynamics, such as internal energy (U), enthalpy (H), entropy (S), and Gibbs free energy (G), and these can be obtained from the microscopic system through statistical thermodynamics.

The fundamental quantity of statistical thermodynamic is the partition function,  $Q$ . For an interacting system of N particles, Q is defined as a sum over all possible energy states,  $E_i$ , for all the particles,

$$Q = \sum_{i=1}^{\infty} e_i^{-\frac{E_i}{k_b T}}. \quad (50)$$

Where T is the temperature and  $k_b$  is Boltzmann's constant. From Q, all thermodynamic functions get accessible and can be expressed as

$$U = k_b T^2 \left( \frac{\partial \ln Q}{\partial T} \right)_V, \quad (51)$$

$$H = U + PV = k_b T^2 \left( \frac{\partial \ln Q}{\partial T} \right)_V + k_b TV \left( \frac{\partial \ln Q}{\partial V} \right)_T, \quad (52)$$

$$S = k_b \ln Q + k_b T \left( \frac{\partial \ln Q}{\partial T} \right)_V, \quad (53)$$

$$G = H - TS = k_b TV \left( \frac{\partial \ln Q}{\partial V} \right)_T - k_b T \ln Q. \quad (54)$$

Where P is the pressure and V is the volume. However, it is not possible to obtain the partition function for an interactive system exactly and some approximations are introduced. First, if we assume that the system is non-interacting, i.e. an ideal gas, the energy levels for each conformation can be calculated exactly within the *rigid-rotor*-



*harmonic-oscillator* approximation. In this approximation it is assumed that the energy levels can be separated into different contributions and the partition function for a single molecule can be written as a product of its electronic, translational, rotational and vibrational parts,

$$q = q_{el}q_{tr}q_{rot}q_{vib}. \quad (55)$$

For the electronic part we assume that all excited states are inaccessible, and that the ground state energy is set to zero. This gives

$$q_{el} = \omega_0, \quad (56)$$

where  $\omega_0$  is the multiplicity of the ground state. The translational part computed with the ideal gas approximation becomes

$$q_{tr} = \left( \frac{2\pi mk_b T}{h^2} \right)^{\frac{3}{2}} \frac{k_b T}{P}. \quad (57)$$

The rotational part computed within the rigid rotor approximation is

$$q_{rot} = \frac{\sqrt{\pi I_1 I_2 I_3}}{\sigma} \left( \frac{8\pi^2 k_b T}{h^2} \right)^{\frac{3}{2}}, \quad (58)$$

where  $I_i$  are the three moments of inertia and  $\sigma$  is the symmetry number calculated from the molecular symmetry group.

Finally, the vibration contributions are computed within harmonic oscillator approximation and written as

$$q_{vib} = \prod_k^{3N-6(5)} \frac{e^{-\frac{h\nu_k}{2k_b T}}}{1 - e^{-\frac{h\nu_k}{k_b T}}}, \quad (59)$$

where  $\nu_k$  are the harmonic frequencies and  $3N - 6(5)$  is the difference between non-linear (6) and linear (5) molecules. The harmonic frequencies are obtained as the second derivative of the electronic energy with respect to the displacement of the

nuclei in Cartesian coordinates. The resulting cartesian force constants are then transferred into mass-weighted ones, and the matrix yields a set of  $3N$  eigenvectors and  $3N$  eigenvalues which are the frequencies. The first 6 (5) frequencies corresponding to rotational and rotational motions, are close to zero and not used further. Note that while the translational and rotational contributions to the partition function are quite trivial to calculate, the vibrational frequencies require all energy second derivatives which may come at a significant computational cost.

When all the parts of the molecular partition function have been collected the partition function of the non-interacting ensemble can be calculated as

$$Q = q^N. \quad (60)$$

From the partition functions one can calculate the contributions to entropy and enthalpy from the different terms using the equations above (51-54). A point here is that while the enthalpy for low frequencies converges to a constant factor  $RT$ , the entropy goes towards infinity. Thus, the harmonic oscillator model for the free energies vibrational modes break down at low frequencies and care must be taken. In the papers this has been considered by up-shifting the lower frequencies.<sup>102</sup>

## 2.2.2 Treatment of Standard States

When calculating the thermochemical corrections, as in the previous section, the usual assumption is that every compound is calculated separately from the other in gas phase and the amount of each is typically taken to be 1 mol at 1 atm (101325 Pa) pressure. For 1 mol of compound  $A_1$ , a correction to the free energy can be given as,

$$G(A_i) = G^0(A_i) + RT \ln \left( \frac{P(A_i)}{P^0} \right), \quad (61)$$

and for a partial pressure of  $P(A_i)$  of 1 atm this results in  $G(A_i) = G^0$ . However, if the reaction occurs in a liquid medium, as in this case, a standard state corresponding

---

to a concentration of 1 M is typically used. The effect this will have on the free energy can be calculated by using Mendeleev-Clapeyron equation for an ideal gas,

$$P(A_i) = \frac{n(A_i)}{V(A_i)}RT. \quad (62)$$

By combining equation (62) and (63), the correction for the standard state of 1 M (1000 mol/m<sup>3</sup>) can be written as,

$$G(A_i) = G^0(A_i) + RT \ln \left( \frac{1000RT}{P^0} \right). \quad (63)$$

E.g. at room temperature this corresponds to a correction of  $0.592 \left( \frac{\text{kcal}}{\text{mol}} \right) \ln(24.464) = 1.89 \left( \frac{\text{kcal}}{\text{mol}} \right)$  for each compound in liquid phase.<sup>103</sup>

A challenge when modelling chemical reactions is how to treat potential gaseous species. As seen, the molecular species which are involved in the reaction can be corrected to change from 1 atm to 1M, which is appropriate for homogenous catalysis. This correction is not done for obvious gas compounds and they are typically still modelled with a partial pressure set to 1 atm (and  $G(A) = G^0$ ). However, in an open system with good mixing and venting any produced gas will typically escape from the reaction mixture and thus give a deficiency in the concentration compared to the other species. This deficiency will in turn, in accordance with Le Chatalier's principle, change the equilibrium towards the product and may affect the overall free energy of the reaction (e.g. if it is catalytic or not) and may change which reaction step is the rate-determining.<sup>104</sup> However, it is not straightforward to model this as it depends on the experimental setup and diffusion rates, and would require a detailed chemical engineering model. Instead a very simple approach, which has been applied in this work, is to calculate the free energy of gaseous species (CO) using a reduced pressure in equation (61).<sup>81</sup> This is, as in accordance with Henry's law, equivalent to a change in the concentration of the gaseous specie and can be estimated by the solubility of the gas in the solvent.

### 2.2.3 Solvent Calculations

Since the chemical reaction investigated in this thesis is homogenous catalysis, with the catalyst solvated in a medium, it is important to consider the effect the solvent has on the reaction. The possible treatments of solvents are to either include the solvent molecules explicitly in the calculation or to treat the solvent as a continuous medium.<sup>105-107</sup> The first method will require the inclusion of several solvent molecules in the surrounding of the solute before the quantum calculations, and with increasing accuracy, i.e. more solvent molecules, this methodology become extremely expensive, especially when considering all the possible conformations (see below) that would be available. Thus, this method is seldom feasible when modelling a chemical reaction.

While some explicit solvent molecules were included in Paper III, the work in thesis has mainly used the second approach based on the polarizable continuum model (PCM).<sup>108-110</sup> There the solvent is modelled as a continuous dielectric with a relative permittivity  $\epsilon_r$  and the solute placed in a suitable hole in the medium. The energy contribution in this model can be summarized as

$$\Delta G_{solvation} = \Delta G_{cavity} + \Delta G_{disp} + \Delta G_{elec}, \quad (64)$$

where  $\Delta G_{cavity}$  is the destabilization associated with creating a cavity in the medium,  $\Delta G_{disp}$  is the dispersion interaction between the solvent and the solute, while  $\Delta G_{elec}$  is the stabilizing effect arising from the solute polarizing the solvent, which in turn will act back on the electron density of the molecule.

The shape of the cavity is usually made by superimposing spheres on the nuclei with radii typically related to the Van der Waals radius of the atom. The resulting surface can then be related to  $\Delta G_{cavity}$  and  $\Delta G_{disp}$  through parametrization. The main difficulty is to determine  $\Delta G_{elec}$  due to the back and forth interaction between the solvent and the solute, i.e. the molecule polarizing the solvent which again affects the molecule. The Poisson's equation gives a connection between the charge distribution of the solute  $\rho$  and the dielectric constant  $\epsilon_r$ ,

$$\nabla \cdot (\epsilon_r \nabla \Phi(\mathbf{r})) = -4\pi\rho(\mathbf{r}). \quad (65)$$

This equation can be coupled to quantum calculations to give the electrostatic potential resulting from the iteratively updated polarization,  $\phi_\sigma$ , at the surface boundary between the cavity and the solvent, called the reaction field. This updated potential is then added to the gas-phase Hamiltonian operator to give

$$\hat{H} = \hat{H}_0 + \phi_\sigma(\mathbf{r}). \quad (66)$$

This permutation to the Hamiltonian will result in a new wavefunction, which again will give a new value of  $\phi_\sigma(\mathbf{r})$ , which is used in the next iteration until the solute wavefunction  $\Psi$  and the surface charges are self-consistent. The electrostatic contribution to the free energy of solvation can finally be given as

$$\Delta G_{elec} = \langle \Psi | \hat{H}_0 - \frac{e}{2} \phi_\sigma(\mathbf{r}) | \Psi \rangle + \frac{e}{2} \sum_k Z_k \phi_\sigma(\mathbf{r}_k) - \langle \Psi_0 | \hat{H}_0 | \Psi_0 \rangle, \quad (67)$$

where  $Z_k$  is the atomic number of atom  $k$ ,  $\phi_\sigma(\mathbf{r}_k)$  is the field potential evaluated at atom  $k$ ,  $\hat{H}_0$  and  $\Psi_0$  are the solute original gas phase electronic Hamiltonian and wavefunction, and  $\Psi$  is the self-consistent wavefunction of the solute in solution. There are different options regarding how the PCM is set up and parameterized, and in this thesis the SMD model has been applied.<sup>111</sup>

## 2.2.4 The Conformational Issue

One of the greater challenges when modelling chemical reactions and molecules is the conformational issue, or the multiple minima and combinatorial explosion problem as it is also known. Any polyatomic molecule, as treated here, has many possible conformations, i.e. multiple minima on the potential energy surface. When doing geometry optimizing on a molecule, regardless of the level of the theory (MM, HF, DFT), the algorithms used typically only finds the local minimum at the potential energy surface. This is dependent on the input structure and may not be close to the actual global minimum, furthermore the different conformations may separate by soft

rotations i.e. low barriers that are traversable at the reaction temperature. Therefore, a randomly generated conformation used to compute reaction energies may lead to incorrect results and conclusions.<sup>112</sup> To avoid potential issues there are different methods to find the most stable conformations, including molecular dynamics and Monte Carlo simulations as well as genetic algorithms. In the work presented here a systematic conformational search has been used. This involves a 360° scan over rotational bonds in fixed increments and a minimization of the generated conformation to derive the associated minimum energy conformation. However, this quickly evolves into a massive task since the number of generated structures grows in exponential fashion,

$$\text{Number of conformations} = \prod_{i=1}^N \frac{360}{\theta_i}, \quad (68)$$

where  $\theta_i$  is the dihedral increment chosen for bond  $i$ . This means that some considerations must be made to make this a feasible approach. First, instead of using a computational costly method like HF and DFT, a more reasonable choice is to use molecular mechanics (MM) or semi-empirical methods to optimize the generated conformations. These methods are much more efficient, and while they are not necessarily giving an accurate zero-point energy, a qualitative relative stability between the conformers (which we are interested in) can be estimated with some precision. Second, the number of rotatable bonds can be limited by freezing or removing irrelevant or less important rotations. This is for example applied in this thesis by using a model substrate which has a minimum of rotatable bonds. Finally, stable conformers that can be used as starting points may be identified by finding similar structures in other computational studies or databases, like the Cambridge Structural Database<sup>113</sup> which collects crystal structures of organic and organometallic molecules.

---

## 3. Mechanistic Investigation of Decarbonylative Dehydration

### 3.1 Computational Details

The computational explorations of the mechanisms in this thesis has been performed using the following programs and settings. The DFT-calculations were done using the Gaussian09 package.<sup>114</sup>

#### *Geometry Optimization*

The geometry optimizations were done assuming gas phase using the hybrid range-separated functional  $\omega$ B97XD (Paper I and Paper II), which includes empirical atom-atom dispersion terms,<sup>99, 115-116</sup> and the local density functional M06-L which is parameterized to account for dispersion (Papers III and IV).<sup>94-96</sup> The  $\omega$ B97XD functional has been shown to reproduce X-ray geometries of transition metal based homogenous catalysts with high accuracy, while the M06-L also has performed well for transition metal chemistry, including PPh<sub>3</sub> binding energies, and is at the same time relatively fast due the fact that it is a LDA functional.<sup>117-118</sup> The switch from  $\omega$ B97XD to M06-L was mainly motivated by the fact that other computational studies of decarbonylative dehydration had been performed using this functional.<sup>66, 74, 81</sup> The input geometries for the Pd and Rh complexes were constructed in the Spartan08 software<sup>119</sup> by modifying available X-ray-structures or DFT-optimized geometries from the other previously mentioned computational studies.<sup>66, 81, 85, 120</sup> Systematic conformational searches were performed by using the MMFF force-field<sup>121</sup> and competitive conformations were preoptimized using the semi-empirical method PM3.<sup>122-125</sup> The geometries were then DFT-optimized to a maximum force of  $1.5 \cdot 10^{-5}$  a.u. (keyword opt=tight) and numerical integrations were performed using the ultrafine grid (keyword int=ultrafine) due to the sensitivity of the M06L functional.<sup>126-128</sup> The SCF density-based convergence was tightened to  $10^{-10}$  (keyword SCF(conver=10)). For Pd and Rh, the Stuttgart 28-electron relativistic effective core potential (ECP28MDF) was used in conjugation with the accompanying correlation-consistent valence double- $\zeta$  plus polarization (cc-pVDZ-PP) basis set.<sup>129-131</sup> All the

other atoms were described by standard correlation-consistent valence double- $\zeta$  plus polarization (cc-pVDZ) basis sets. The potential energy surface (PES) curvature at stationary points was determined by the analytic Hessian calculation, and the PES between minima was often scanned using the linear transit (keyword `opt=scan`) method implemented in Gaussian09. Potential transition states found by the scan were optimized, sometimes by the QST3 method (keyword `opt=qst3`) which uses the product and reactant together with the preliminary TS structure. The optimized TSs were finally connected to their respective reactants and products by intrinsic reaction coordinate (IRC) calculations.<sup>132-134</sup> NBO6.0<sup>135</sup> as implemented in Gaussian09 was used to analyze the Pd–Cl bonds in Paper I.

### *Thermochemistry*

The thermal corrections to give the Gibbs free energies were calculated using the ideal gas, rigid-rotor and harmonic oscillator approximations (Chapter 2.2.1) with the temperature used in the experiments (523.15 K Paper II and 373.15 K Paper III and IV). The frequencies below a certain threshold (100  $\text{cm}^{-1}$  Paper II and 50  $\text{cm}^{-1}$  Paper III and IV) were shifted to the threshold to reduce the errors caused by soft harmonic modes when calculating entropy.<sup>102</sup>

### *Single-Point Calculations (SP)*

Accurate energies were obtained through SP calculation on the optimized geometries by improving the basis sets: ECP and the accompanying correlation-consistent quadruple- $\zeta$  basis set (cc-pVQZ-PP) for Pd and Rh, and correlation-consistent quadruple- $\zeta$  plus polarization (cc-pVQZ) for all other atoms obtained from the ESML basis set exchange website.<sup>136</sup> Diffuse functions from the “aug-cc-pVQZ Diffuse” set<sup>137</sup> were added to all atoms except Pd, C and H.

In Paper II, different functionals in addition to M06-L were tested to monitor the effect on the results: (1) the gradient-corrected Perdew-Burke-Ernzerhof (PBE) functional<sup>138-139</sup>, and (2) the hybrid B3LYP functional.<sup>140</sup> Both were treated with Grimme’s empirical dispersion term D3, and PBE was investigated in combination with both the original Becke-Johnson dampening<sup>100</sup> (giving PBE-D3BJ) and the



---

recently modified dampening parameters<sup>101</sup> (giving PBE-D3(M)BJ). B3LYP on the other hand was used only in combination with the modified parameters (giving B3LYP-D3(M)BJ). The conclusion was that the functionals reproduced similar trends with some differences. Overall M06-L gave the lowest barrier for the rate-determining step, and together with the fact that it has proved to correlate well with coupled cluster computations in benchmark studies of the reaction,<sup>81</sup> it was the functional of choice for SP calculations in this thesis.

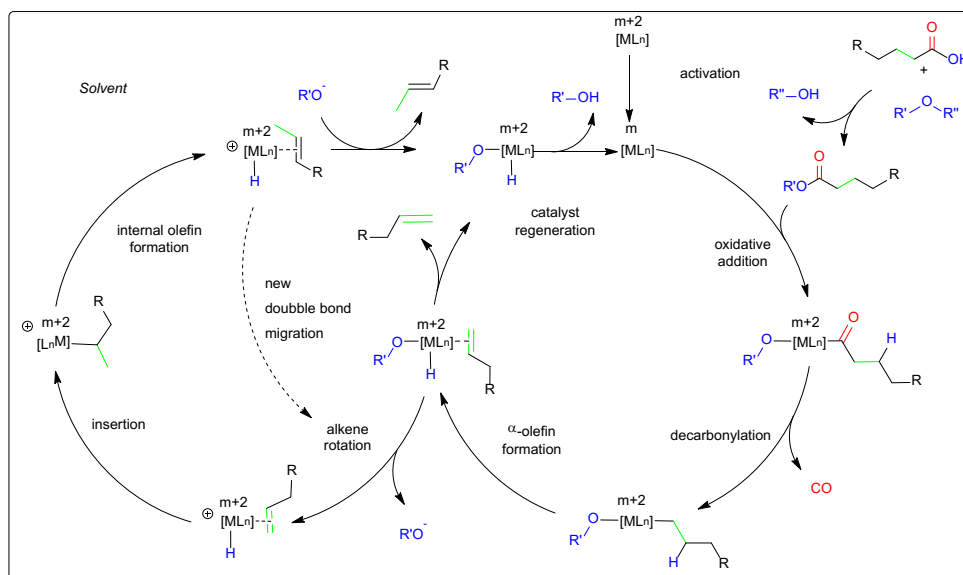
To model the solvent effects, the continuum solvation model (SMD) as implemented in Gaussian09 was applied in the SP calculations.<sup>141</sup> However, not all the solvents applied in the experiments are parameterized in Gaussian09 and thus approximations were made. N,N-dimethylacetamide (DMA,  $\epsilon_r = 37.8$ ) was used to mimic highly polar aprotic solvents like N,N'-dimethylpropyleneurea (DMPU,  $\epsilon_r = 36.1$ ), N-Methyl-2-pyrrolidone (NMP,  $\epsilon_r = 32.2$ ) and  $\gamma$ -valerolactone (GVL,  $\epsilon_r = 36.5$ ) which are favorable for the reaction, while butanoic acid (BA,  $\epsilon_r = 2.85$ ) was used as an approximation to the solvent free reaction mixture formed by the substrate (stearic acid,  $\epsilon_r = 2.3$ ), the mixed anhydride (butyric anhydride,  $\epsilon_r = 12.0$ ) and the two equivalents of acid formed in the reaction (acidic acid,  $\epsilon_r = 6.25$ ).

### *Free Energies*

The free energies were obtained by using a standard state of 1 M solution for all species except CO (see chapter 2.2.2). Accordingly, a factor of  $RT \ln\left(\frac{1000RT}{p^0}\right)$  was added to change from 1 atm as reported in Gaussian09 to 1 M. To accommodate the fact that CO escapes the reaction mixture, a reduced pressure ( $10^{-5}$  atm) was used when calculating the thermal corrections for this gas. The rationale for selecting this pressure is discussed in chapter 3.7. With the above-mentioned corrections, the total free energy becomes  $G_{tot} = G_{gas} + \Delta G_{solv} + \Delta G^{1 atm \rightarrow 1 M}$ , where  $G_{gas}$  is the gas phase Gibbs free energy resulting from the SCF SP energy,  $\Delta G_{solv}$  is the solvent correction due to the difference between the gas-phase SCF energies and the SMD calculation and  $\Delta G^{1 atm \rightarrow 1 M}$  is the standard state correction from 1 atm to 1 M. All the reported energies are Gibbs free energies in kcal/mol unless otherwise stated.

## 3.2 General Reaction Mechanism for Decarbonylative Dehydration

As seen in the introduction there has been different setups for decarbonylative dehydration. However, in general the reaction can be summarized in five steps; *activation*, *oxidative addition*, *decarbonylation*, *alkene formation* and *catalyst regeneration*. In addition, there is the undesired *isomerization* side-reaction, which transforms the produced target  $\alpha$ -olefins to internal olefins (Scheme 2).



**Scheme 2.** The general reaction scheme for decarbonylative dehydration of carboxylic acids to 1-alkene, as well as the subsequent, unwanted isomerization to internal olefins. The subscript  $m$  signifies the oxidation number of the transition metal, i.e.  $m = 0$  for Pd and  $m = 1$  for Rh, for the active catalytic specie, while  $n$  is the number of (neutral)ligands attached to the catalyst which may change throughout the reaction. Note that, due to carboxylate dissociation, the catalyst is cationic in the isomerization pathway. Altered and reprinted with permission from ref.[82]. Copyright 2019 Royal Society of Chemistry.

---

Below, the different steps will be summarized as identified by the different computational studies done for homogenous decarbonylative dehydration of fatty acid substrates.<sup>66, 74, 81-82, 142</sup>

### *Catalyst Activation*

One of the major issues regarding decarbonylative dehydration of fatty acids is the need for activation, both for the fatty acid substrate and the catalyst. A typical activation of the catalyst involves dissociation of one or more ligand(s) to give a lower coordinated metal complex with the correct ligands attached. This has generally been done *in situ* where either  $n$  L ligand(s) dissociate to give a  $[\text{ML}_n]^m \xrightarrow{-n\text{L}} [\text{ML}_{n-n}]^m$  activation, or a dissociation of two X ligands to reduce the metal complex before the catalytic cycle,  $[\text{ML}_n]^{m+2} \xrightarrow{-2\text{X}} [\text{ML}_n]^m$ . The activation usually requires energy and may need an excess of the desired ligand to ensure coordination to the metal, e.g. phosphines to  $\text{PdCl}_2$ .

### *Substrate Activation and Oxidative Addition*

Following the activation of the catalyst, the first step of the reaction is the oxidative addition of the substrate to metal center, increasing the oxidation state  $m$  to  $m+2$ . This involves the cleavage of a  $\text{C}(=\text{O})\text{-O}$  bond in the substrate before subsequent binding to the metal. Since the  $\text{C}(=\text{O})\text{-OH}$  bond in fatty acids is strong, this typically requires an activation by another substrate, e.g. anhydrides, to form a  $\text{-C}(=\text{O})\text{-O-R'}$  bond where the C-O bond is weakened. Oxidative addition is usually favored by electron rich complexes and thus usually there is no further dissociation of ligands before this step unless it is necessary to make space, both electronically and sterically, for the incoming substrate.

### *Decarbonylation*

After oxidative addition, CO is deinserted from the acyl chain, to form a carbonyl ligand and the resulting alkyl chain. This step is promoted by a dissociation of a ligand to give a free coordination site on the metal. Which ligand that dissociates is very system dependent and can be a neutral ligand like phosphine or CO, or the -OR (carboxylate) group formed in the oxidative addition, especially in a polar solvent.

The decarbonylating step is typically found to be the second highest barrier, and the relatively high reaction barrier is consistent with other decarbonylating reactions. The formed CO may dissociate directly following this step, but this is dependent on the experimental conditions.

### *Alkene Formation*

The step that is usually found to be rate-determining for decarbonylative dehydration is the alkene formation, which happens through reductive elimination. In this step a  $\beta$ -hydrogen is transferred from the alkyl chain to the -OR group to form the corresponding acid, either in a direct transfer stabilized by an agostic bond to the metal, or through a stepwise process where the hydrogen is first transferred to the metal by  $\beta$ -hydride elimination to form the proper metal hydride prior to the transfer to the -OR group. As for the decarbonylation, space must be made on the metal center as the direct outer sphere hydrogen transfer is highly unlikely. Again, this space may be created by dissociation of a neutral L ligand (CO, phosphine), or switching of coordination mode or complete dissociation of the accepting molecule (e.g. carboxylate). Dissociation is also beneficial as the reductive elimination, which reduces the catalyst back to its original oxidation number  $m$ , is favored by electron poor complexes.

### *Catalyst Regeneration*

Following the formation of the desired  $\alpha$ -olefin, the catalyst must be reformed to the initial active catalytic species. This involves dissociation of the olefin or any remaining formed carbon monoxide and acid, and reassociation of the necessary L ligands (phosphines). This step is crucial because CO typically forms a strong bond with the metal complexes, which gives a thermodynamic sink in the reaction and makes subsequent cycles difficult. Furthermore, reassociation of ligands and dissociation of the olefin and the hydrogen acceptor (acid) is critical because they all play a role in the unwanted isomerization of the  $\alpha$ -olefin to internal olefins.

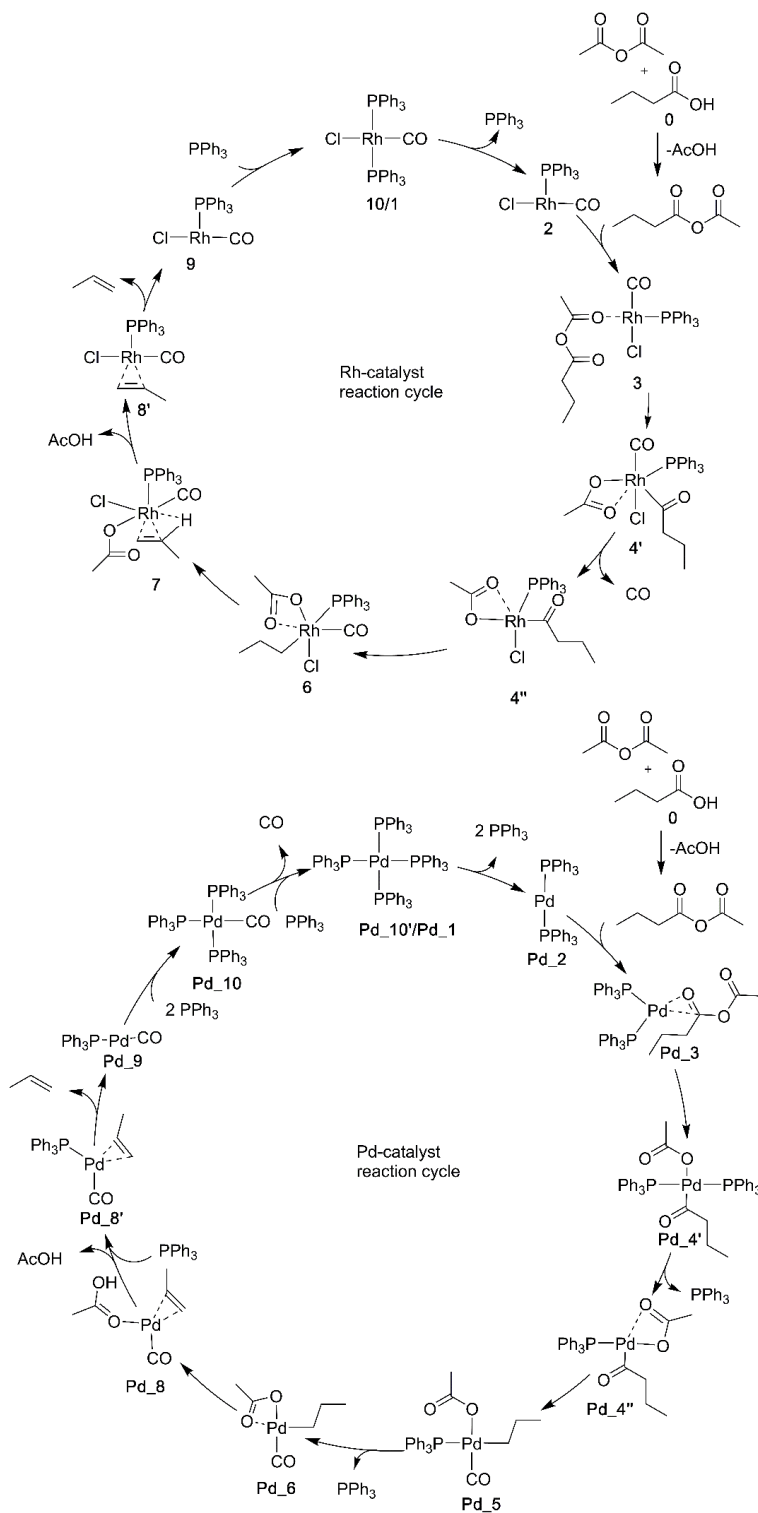
### *Isomerization*

The main side-reaction of decarbonylative dehydration is the isomerization of the  $\alpha$ -olefin to the more thermodynamically stable internal olefins. Isomerization happens *via* reinsertion of the eliminated hydride (or another hydrogen) to the  $\alpha$ -carbon following an olefin rotation. This is promoted by the formation of cationic hydride complexes, where the hydrogen has not been transferred to a dissociated -OR group, and by olefin retention i.e. that the desired  $\alpha$ -olefin is not removed from the active catalyst. Following the formation of the internal olefin the process may repeat itself for further double bond migration.

---

### 3.3 Comparison of Rh and Pd as the Catalyst's Metal Center

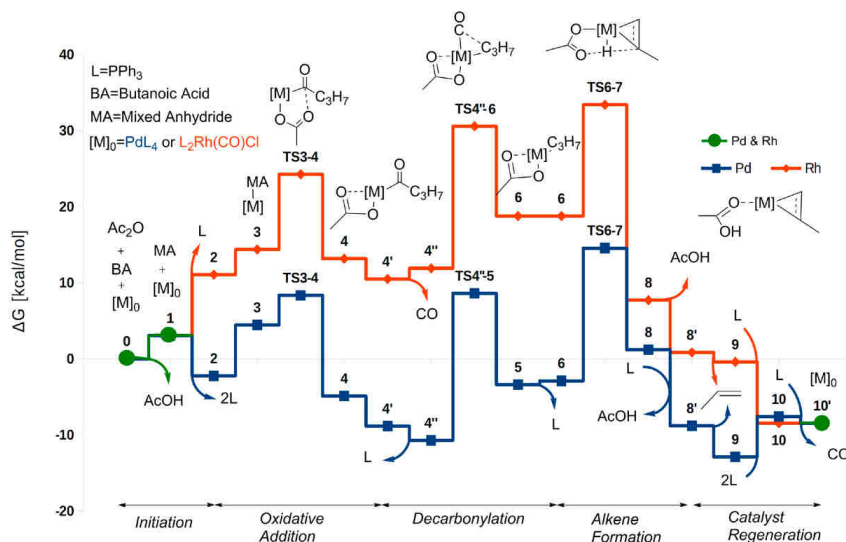
While there have been experimental studies of decarbonylation dehydration using a range of different metals, including Ir<sup>69-71</sup> and the more abundant Fe<sup>72</sup> and Ni<sup>73-75</sup>, the highest catalytic activity has been observed by using Pd and Rh.<sup>49, 60, 62-63</sup> Pd has shown higher activity, but Rh on the other hand has not required a large excess of ligand to ensure activity and selectivity and is thus attractive from an atom-economic point of view.<sup>49, 57, 60</sup> Rh has also been used in dehydroformylation and other similar decarbonylation reactions,<sup>49, 142-145</sup> and it is therefore surprising that few have further explored this metal for use in deoxygenation of fatty acids.<sup>75</sup> As mentioned before, this development may have been stifled because no computational investigation of Rh as catalyst for decarbonylative dehydration, in comparison to Pd and Ni, has been present. This, in this thesis the Rh catalyzed mechanism was calculated and compared to the Pd mechanism proposed by Ortuño, M. et al.<sup>81, 84</sup> Both of the systems investigated use the triphenylphosphine (PPh<sub>3</sub>) ligand, and butanoic acid (BA), activated by acetic anhydride to form a mixed anhydride, was used as substrate. The reaction temperature was set to 250°C in *neat* (apolar) conditions as in the comparable experiment.<sup>60</sup> (PPh<sub>3</sub>)<sub>2</sub>Rh(CO)Cl has been demonstrated to be the active catalytic complex for Rh in decarbonylative dehydration, while PdCl<sub>2</sub> in excess of phosphine is reduced to Pd<sup>0</sup> and coordinates four phosphines to form the complex Pd(PPh<sub>3</sub>)<sub>4</sub>.<sup>49, 60, 68</sup> While the two metals differ in oxidation and preferred coordination number, the reaction follows the same steps and the different parts can be recognized and compared. The reaction cycles found for the two metals are shown in Scheme 3 and the comparison of the calculated energy profiles can be seen in Scheme 4 and is discussed below.



**Scheme 3.** Top: The calculated reaction cycle for Rh-catalyzed decarbonylative dehydration of butanoic acid. Bottom: The calculated reaction cycle of Pd-catalyzed decarbonylative dehydration of butanoic acid. The starting Pd-structures were taken from ref. [81] and modified to the present substrates (butanoic acid and acidic anhydride) before reoptimization. Modified and reprinted with permission from ref. [84]. Copyright 2017 MDPI.

The reaction for both metals starts by dissociating phosphine ligands from the starting complexes to make space for the oxidative addition. One phosphine dissociates from  $(\text{PPh}_3)_2\text{Rh}(\text{CO})\text{Cl}$  and two from  $\text{Pd}(\text{PPh}_3)_4$  which is in accordance with experimental observations.<sup>146</sup> Already here a significant difference appears, as this is favorable for the Pd catalyst while it requires energy for Rh. The energy difference is 13.2 kcal/mol and this difference sticks around in the reaction, for example the following oxidative addition barrier (**TS3-4**) relative to the active catalyst **2** is comparable for both but compared to the starting point the difference becomes large. The oxidative addition oxidizes  $\text{Rh}^{\text{I}}$  to  $\text{Rh}^{\text{III}}$  and  $\text{Pd}^0$  to  $\text{Pd}^{\text{II}}$  respectively, which for Rh goes from the square planar  $d^8$ -complex, to an octahedral complex, while  $\text{Pd}^{\text{II}}$  retains a square planer orientation with a relatively low coordination sphere. Pd may also rearrange the phosphines to be trans to each other, which is the more stable conformation (**4'**). In both cases the acetate switches back and forth between monodentate and bidentate coordination to facilitate the catalytic cycle and maintain the preferred orientation. catalytic cycle and maintain the preferred orientation. This is seen before decarbonylation, where CO and  $\text{PPh}_3$  dissociates from Rh and Pd respectively to make space for decarbonylation and the acetate compensates by  $\kappa^1$  to  $\kappa^2$  coordination.





**Scheme 4.** Reaction profile for both decarbonylative dehydration of butanoic acid by Pd (blue) and Rh (red) using reduced CO pressure ( $10^{-5}$  atm, see Computational Details). The steps that have the same energy along the reaction pathway are indicated by green color. Free energies are given relative to the starting complex for both catalysts. Reprinted with permission from ref. [84]. Copyright 2017 MDPI.

The decarbonylation barrier is also much higher for Rh (**TS4''-6**) than Pd (**TS4''-5**) compared to the rate-determining intermediates (**0** and **4''** for Rh and Pd respectively), with a difference of 11.3 kcal/mol. The higher barrier is also paralleled by a marked difference in the thermodynamic stability of the products. This is consistent with the fact that the metal-CO bond formed in the decarbonylation is expected to be stronger in Pd<sup>II</sup> than in Rh<sup>III</sup> because CO prefers lower oxidation states. Indeed, in the following step, Rh keeps the formed CO while Pd instead dissociates a phosphine, leaving both metals with a bis-coordinated acetate and one CO attached to stabilize the next reductive step.

The alkene formation (**TS6-7**) is found to be the rate-determining step for both Rh and Pd. The barrier is once again higher for Rh ( $\Delta G^\ddagger = 33.4$  kcal/mol) and agrees with the experimental observations that Pd ( $\Delta G^\ddagger = 25.3$  kcal/mol) is the more active catalyst. However, an important thing to note at this stage is that Pd dissociates both

PPh<sub>3</sub> ligands before the β-hydrogen transfer while keeping the CO. This makes space for an agostic carbon-metal bond and the steric hinderance is probably a reason for the higher barrier for Rh. However, as seen in experiments, the phosphine dissociation comes at a cost for Pd. For this metal, as opposed to Rh, an excess of phosphine is required to ensure catalytic activity, which is consistent with the fact that two phosphines, must bind again to before a new catalytic cycle can start. A lack of phosphine will lead to isomerization at the phosphine-free and coordinatively available Pd sites as well as catalyst decomposition via formation of Pd<sup>0</sup> clusters. By comparison an excess of phosphine for Rh, slows down the reaction because it ensures the formation of the very stable starting complex **0**.

After the alkene formation, both metals form very stable metal-CO complexes with a low oxidation state ((PPh<sub>3</sub>)<sub>2</sub>Rh<sup>I</sup>(CO)Cl, **10'**<sup>0</sup>, and Pd<sup>0</sup>(CO)PPh<sub>3</sub>, **9**) which actually are the rate-determining intermediates. However, while Pd<sup>0</sup>(CO)PPh<sub>3</sub> can mediate the oxidative addition, this complex instead sheds the CO before starting a subsequent preferred pathway. In contrast (PPh<sub>3</sub>)<sub>2</sub>Rh<sup>I</sup>(CO)Cl is a very stable thermodynamic sink and lower the activity for the Rh-catalyzed reaction. This is also found for Ni catalysts where a stable Ni<sup>0</sup>-CO complex hinders new reaction cycles.<sup>74</sup> The Wilkinson's catalyst, Rh(PPh<sub>3</sub>)<sub>3</sub>Cl, could thus be an attractive alternative starting point, due to the missing CO, but will after decarbonylation form the stable Rh-CO complex and enter into the same pathway in subsequent catalytic cycles, as seen from the calculations.<sup>75, 84</sup>

The overall conclusion is that Pd yields the higher activity due to lower barriers from less steric hinderance and a less stable Pd<sup>0</sup>-CO complex and is thus the transition metal of choice so-far. However, care must be taken to ensure catalyst regeneration and hinder isomerization. This has traditionally been handled using excess phosphine ligands, but this may in turn hinder activity as a low coordinated complex is preferred for the rate-determining alkene formation step. It is also problematic in terms of the atom economy and overall greenness of the reaction. In the next sections we will see how the use of a well-defined precatalyst and bidentate hemilabile ligands can solve these problems.

### 3.4 The Advantage of a Well-Defined Precatalyst

The usual approach for Pd catalyzed decarbonylative dehydration is an *in situ* formation of the active Pd<sup>0</sup>L<sub>2</sub> complex. This is done by mixing a Pd<sup>II</sup>X<sub>2</sub> precursor (X = Cl, Br, OAc) with an excess of the L ligand (L<sub>2</sub> = 2·PPh<sub>3</sub>, DPEphos, 2·NHC etc.) in solution. The Pd<sup>II</sup> dissociates the two X ligands and is reduced to Pd<sup>0</sup> before coordinating the necessary ligands to form the active Pd<sup>0</sup>L<sub>2</sub> complex. A seemingly logical proposal would be to instead start from a Pd<sup>0</sup>L<sub>n</sub> precursor e.g. Pd(PPh<sub>3</sub>)<sub>4</sub> or Pd(dba)<sub>2</sub>, but these have actually been found to be less active than the Pd<sup>II</sup> alternatives.<sup>60-62, 85</sup> It has been suggested that the X ligand facilitates the reaction by forming anionic [Pd<sup>0</sup>X]<sup>-</sup> complexes,<sup>147</sup> but another reason, when used with excess of the ligand, is that the formation of stable Pd<sup>0</sup>L<sub>4</sub> species could act as a thermodynamic sink. As seen from the previous chapter, the preferred pathway for the Pd(PPh<sub>3</sub>)<sub>4</sub> catalyst requires that all the PPh<sub>3</sub> ligands dissociates before the rate-determining alkene formation step. This means that when starting from the inactive complex Pd(PPh<sub>3</sub>)<sub>4</sub>, more ligands must dissociate and, in excess of the ligand, the tetra coordinated complex is always available. In contrast, when starting from a Pd<sup>II</sup>X<sub>2</sub> precursor, the formation of PdL<sub>4</sub> is not given, although still available in an excess of L ligands. However, in this case, the ligands need to attach to form the active catalyst Pd<sup>0</sup>L<sub>2</sub> before catalysis starts.

This realization of this contradiction of requiring an excess of ligands, but favoring a low coordinated complex for the rate-determining step, was the motivation for trying to identify more well-defined precatalyst for the reaction in the style of (PPh<sub>3</sub>)<sub>2</sub>PdCl<sub>2</sub> which had been employed successfully for the reaction previously.<sup>63</sup> Experimental screening, see Table 1 and Figure 1, found the best precatalytic system to be **A1** (Figure 2),<sup>85</sup> which combines a bidentate DPEphos (oxydi-2,1 phenylene)bis(diphenylphosphine) ligand, that has been used successfully for decarbonylative dehydration,<sup>61, 63-64, 74</sup> with an allyl ligand (cinnamyl) which is prone for reductive elimination. This type of Palladium-allyl system has been used in Pd catalyzed cross-coupling reactions and been found to be activate even at room temperature.<sup>148-152</sup>

**Table 1.** Comparison of *in situ* catalytic system with precatalysts<sup>a</sup> Modified and reprinted with permission from ref.[85]. Copyright 2016 American Chemical Society.

$\text{C}_{17}\text{H}_{35}\text{COOH} \xrightarrow[\text{-CO, -AcOH}]{\text{Pd-catalyst, 200 mol\% Ac}_2\text{O, 9 mol\% NEt}_3, \text{DMPU, 110 }^\circ\text{C, 15 h}}$ 
 $\text{C}_{15}\text{H}_{31}\text{CH=CH}_2 + \text{internal olefins}$

entry	Pd precursor (mol%)	ligand (mol%)	yield [%] <sup>b</sup>	$\alpha$ -olefin [%] <sup>c</sup>
1	PdCl <sub>2</sub> (3)	DPEPhos (9)	100	97
2	PdCl <sub>2</sub> (1)	DPEPhos (1)	35	97
3	PdCl <sub>2</sub> (0.5)	DPEphos (0.5)	10	97
4	Pd(OAc) <sub>2</sub> (1)	DPEphos (1)		
5	Pd(dba) <sub>2</sub> (1)	DPEphos (1)	3	ND <sup>d</sup>
6	Pd(PPh <sub>3</sub> ) <sub>4</sub> (1)	DPEphos (1)	5	ND
7	PdCl <sub>2</sub> (PPh <sub>3</sub> ) <sub>2</sub> (1)	DPEphos (1)	42	97
8	[Pd(cinnamyl)Cl] <sub>2</sub> (0.25)	DPEphos (0.5)	65	96
9	[Pd(cinnamyl)Cl] <sub>2</sub> (0.25)	Xantphos <sup>e</sup> (0.5)	22	96
10	<b>A1</b> (0.5)		88	99
11	<b>B1</b> (0.5)		30	97
12	<b>C1</b> (0.5)		40	96
13	<b>D1</b> (0.5)		5	ND
14	<b>E1</b> (0.5)		14	64
15	<b>A1</b> (0.5)		70	96 <sup>f</sup>

<sup>a</sup>Conditions: 1mmol substrate, 2 mmol Ac<sub>2</sub>O, 2 mL DMPU, 15 h. <sup>b</sup>Determined as the average of two experiments by <sup>1</sup>H NMR using methyl benzoate as an internal standard, with a maximum  $\Delta$ yield =  $\pm$  5%.

<sup>c</sup>Determined as the average of two experiments by <sup>1</sup>H NMR, with a maximum  $\Delta$ selectivity =  $\pm$  1%. <sup>d</sup>ND: not determined. <sup>e</sup>Xantphos: 4,5-Bis(diphenylphosphino)-9,9-dimethylxanthene. <sup>f</sup>In absence of base.

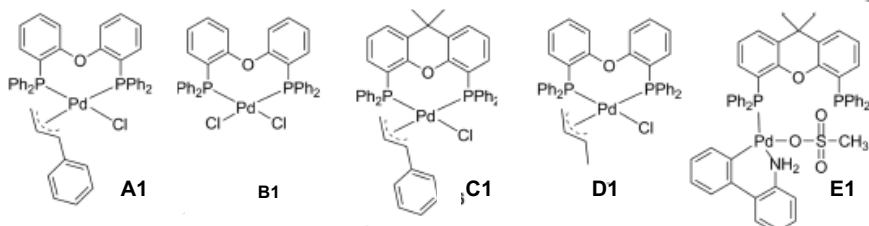


**Figure 1.** Precatalysts screened for decarbonylative dehydration. Modified and reprinted with permission from ref.[85]. Copyright 2016 American Chemical Society.

Investigation of the X-ray structure found that the geometry was as expected for a  $\text{Pd}(\eta^3\text{-allyl})(\text{bis-phosphine})$  complex<sup>153</sup> with the chloride in an axial position and cinnamyl and phosphine ligands occupying the equatorial plane. The Pd-C distances was found to be dissimilar and is believed to facilitate the activation, while the Pd-Cl bond was longer than in the symmetric planar  $(\text{DPEphos})\text{PdCl}_2$  case. Further computational investigation found that this lone chloride is almost completely ionic ( $\text{NI} = -0.92$  and covalent bond order of 0.37) in contrast to the covalent polar Pd-Cl bonds of  $(\text{DPEphos})\text{PdCl}_2$  ( $\text{NI} = -0.5$ , covalent bond order of 0.88) which may also explain the higher activity observed.

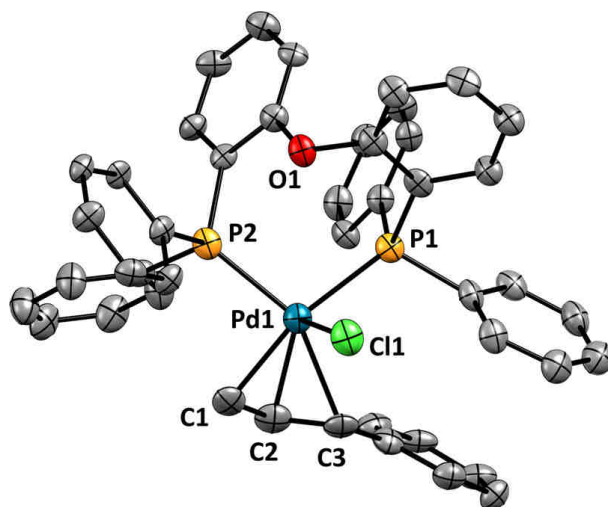
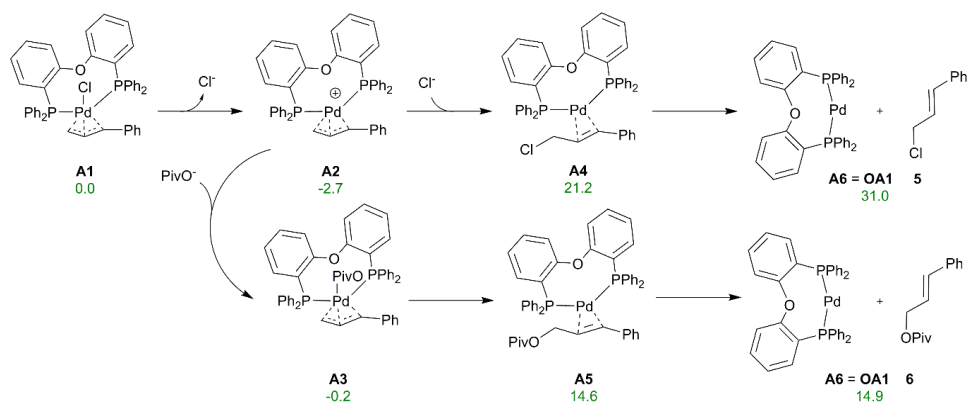


**Figure 2.** X-ray structure of A1 (hydrogens omitted for clarity). Selected bond lengths. Pd1–C1 2.133(4) Å; Pd1–C2 2.200(4) Å; Pd1–C3 2.373(4) Å; Pd1–P1

2.3370(10) Å; Pd1–P2 2.2978(10) Å; Pd1–Cl1 2.7216(10) Å. Bite angle P2–Pd1–P1 102.19(4)°. Reprinted with permission from ref. [85]. Copyright 2016 American Chemical society.

Indeed, the mechanistic investigation of the reaction found that the dissociation of the chloride is facile in a polar solvent, such as DMA; see Scheme 5. At the same time, the stability of the chloride makes the reductive elimination of the allyl chloride very costly (31.0 kcal/mol). A more reasonable alternative was the reductive elimination by a present base (here: pivalate) which comes at less than half the price (14.6 kcal/mol). The carboxylate should be in excess in the reaction as the corresponding acid is formed both in the activation of the fatty acid (see Chapter 3.5) and at the end of the reaction (see Chapter 3.7 and 3.8) and could be deprotonated by an added base, i.e. pyridine or ethyl amine. The stabilization of the Pd<sup>II</sup> to Pd<sup>0</sup> activation by bases and similar activation by base and nucleophilic attack has also been previously suggested.<sup>148, 154-155</sup> The final dissociation of the internal olefin from the active catalyst **A6** is almost ergoneutral and the cost of the activation by base is found to be 14.9 kcal/mol. The *in situ* generation of **A6** on the other hand is costlier and less efficient. For example, dissociating DPEphos from the tetra-coordinated complex Pd<sup>0</sup>(DPEphos)<sub>2</sub> is calculated to cost 16.8 kcal/mol and the excess DPEphos used (e.g. 3 equivalents) means that it may be formed and act as a thermodynamic sink at any time of the catalysis.



---

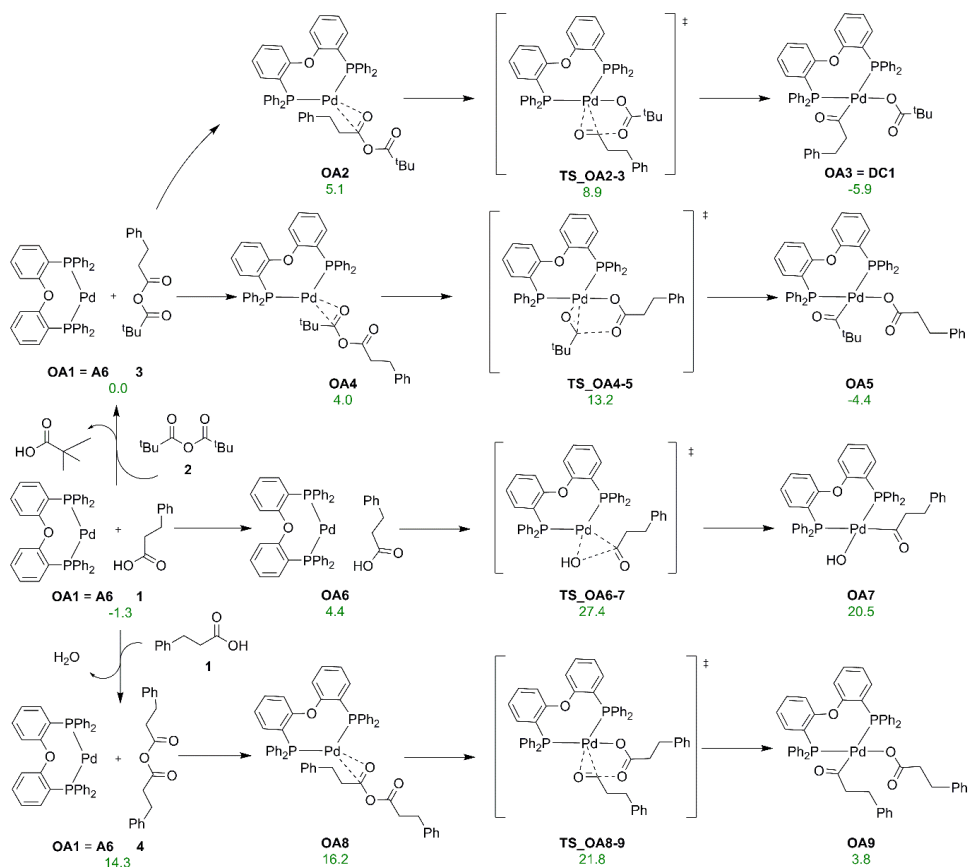
**Scheme 5.** Activation of precatalyst. Numbers are calculated free energies (kcal/mol) at 100 °C using DMA as solvent; see the Computational details section. Reprinted with permission from ref. [82]. Copyright 2019 Royal Society of Chemistry.

In contrast, for a well-defined catalyst, such as **A1**, the base and substrate, but not the ligand are present in large excess compared to the catalyst. This means that the base-triggered dissociation of the cinnamyl coupling product is likely to be irreversible. Of course, this also means that any dissociation of ligand from the catalyst is probably irreversible as well. Indeed, attempts at using the precatalyst  $(\text{PPh}_3)_2\text{PdCl}_2$  have also required an excess of ligands.<sup>60, 62-63</sup> This means that the ligand plays a crucial role in the reaction as DPEphos, as opposed to  $\text{PPh}_3$ , sticks around for the entirety of the reaction. This role of the bidentate ligand will be explored later (Section 3.6).

### 3.5 The Role of the Anhydride Activation

In principle, decarbonylative dehydration could happen directly from the inactivated fatty acids (Scheme 1c). Unfortunately, the C-O bond in carboxylic acids are not easily broken due to hydroxide (-OH) being a poor leaving group which makes the oxidative addition of the fatty acid unfavorable, see Scheme 6. For example, the barrier for oxidative addition of hydrocinnamic acid to Pd(DPEphos), **TS\_OA6-7**, requires 28.7 kcal/mol relative to the sum of the free energy of the separated molecules. To make this rupture easier, the fatty acids are activated by an electron withdrawing group. This is typically done by an acid anhydride (as in this thesis) to form asymmetric anhydrides, but there have also been procedures involving activation by *p*-nitrophenylchloroformate to form *p*-nitrophenyl esters,<sup>66-67</sup> and setups where PPh<sub>3</sub> act as a reductant.<sup>73</sup> The formation of the asymmetric anhydride can be done both before catalysis and *in situ* and is typically a nearly ergoneutral process (1.0-3.0 kcal/mol) further promoted by an excess of acid anhydride in the reaction mixture. The following oxidative addition of the anhydride is much more facile compared to the fatty acid, i.e. the mixed anhydride formed by activating the hydrocinnamic acid by a pivalic anhydride, **TS\_OA2-3**, only has a barrier of 9.2 kcal/mol compared to the same zero-point as before. The resulting complex from an oxidative addition of the anhydride results in an acyl group and a carboxylate which can bind in both monodentate and bidentate fashion dependent on the metal complex. Alternatively, an acyl group will not be formed if the wrong (O=C)-O bond is cleaved during the addition of the substrate, **TS\_OA4-5**, and will not lead to the desired olefin product. This pathway has however been found to be higher in energy<sup>81-82</sup> and, while the type of anhydride seems to be of less importance, the use of a bulky anhydride (e.g. pivalic anhydride) may further disfavor this side reaction.<sup>61, 64, 81, 83</sup>





**Scheme 6.** Investigated pathways of substrate activation and oxidative addition. Numbers are calculated free energies (kcal/mol) at 100 °C using DMA as solvent; see the Computational details section. Reprinted with permission from ref. [82]. Copyright 2019 Royal Chemistry Society.

The need of a sacrificial activator for the fatty acid is an issue that yet needs to be answered, and alternative methods involving photocatalysis have recently been investigated.<sup>156-157</sup> There the fatty acids are activated by a photocatalyst which turns the fatty acid into a radical which binds more easily to the alkene forming catalyst. In this thesis we have not explored alternative ways to activate the fatty acid, however an interesting possibility is the formation of symmetric anhydride *in situ* by dehydration of two fatty acids. This reaction has been assumed to take place at high temperatures (250 °C) and, using the same substrates as before, is calculated to

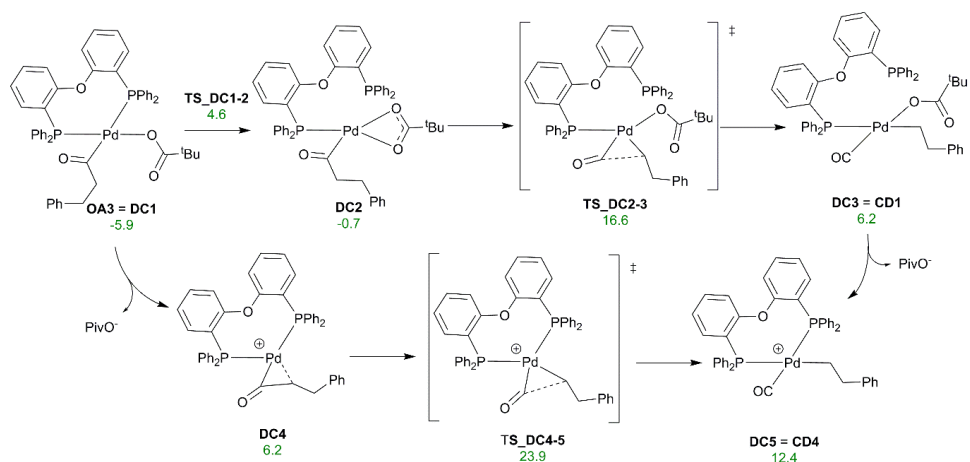
involve a reaction free energy of 15.6 kcal/mol. Still, once formed the symmetric anhydride readily undergoes oxidative addition, **TS\_OA8-9**, with a low barrier (5.6 kcal/mol) compared to the weakly coordinated complex **OA8**. This is consistent with the high yields of  $\alpha$ -olefins obtained when starting from preformed symmetric anhydrides (however, addition of acid is required) and naturally removes the possibility of cleaving the wrong C-O bond.<sup>63</sup> While the anhydride activation seems like a necessary evil for starting the catalysis, the resulting carboxylate from the oxidative addition is also key regarding alkene formation and isomerization as it acts as the proton acceptor for the eliminated  $\beta$ -hydrogen from the alkyl chain (see chapter 3.8).

### 3.6 The Benefit of a Hemi-Labile Bidentate Ligand

As discussed previously one of the major problems regarding the experimental setup of decarbonylative dehydration has been the need of an excess of the neutral ligand L to achieve activity and selectivity for the  $\alpha$ -olefins. An explanation was that computational studies found that complete dissociation of PPh<sub>3</sub> from the catalyst was beneficial for activity, and an excess is needed to ensure the reformation of the active catalytic specie and hinder isomerization.<sup>81</sup> However, when employing the well-defined precatalyst with a DPEphos ligand, **A1**, activity and selectivity was obtained without the need for excess of ligand, implying that DPEphos does not dissociate from the complex. It is important to note that the reaction modelled here was done at 110°C, meaning that the entropic benefit of dissociating the ligand is less compared to the 190°C degrees used in many of the PPh<sub>3</sub> experiments. In fact, in all the experiments performed at relative low temperatures (110-130) in a polar solvent, a strongly coordinating chelating ligand (Xantphos and DPEphos) was optimal. This indicates that a different reaction pathway is preferred at these conditions.

Following oxidative addition, the formed tetra coordinated square planar Pd<sup>II</sup> complex is often the most stable intermediate of the reaction. To retain this orientation a dissociation should occur, to open a coordination site for the CO formed in the following decarbonylation step. With a monodentate ligand like PPh<sub>3</sub> it is plausible that the ligand quite simply dissociates, but for strongly coordinating bidentate ligand this is less likely. The mechanistic study of decarbonylation of *p*-nitrophenol esters by a Pd-Xantphos catalyst in a polar solvent (DMA) for instance found that the decoordination of the anion was preferred, yielding a cationic Pd<sup>+</sup> bis coordinated Xantphos complex.<sup>66</sup> This was also suggested as a possible pathway for the Pd(PPh<sub>3</sub>)<sub>2</sub> catalyst in a polar medium (see later solvent discussion, chapter 3.8).<sup>81</sup> However, for the precatalytic **A1** system in the same polar solvent (DMA) it was instead found that decarbonylation following DPEphos switching coordination mode from  $\kappa^2$  to  $\kappa^1$  and dissociating one phosphine group, **TS\_DC2-3** via **TS\_DC1-2**, was less costly than decarbonylation after carboxylate dissociation, **TS\_DC4-5** (Scheme 7). This can be supported by two factors. First, DPEphos has a more flexible backbone than

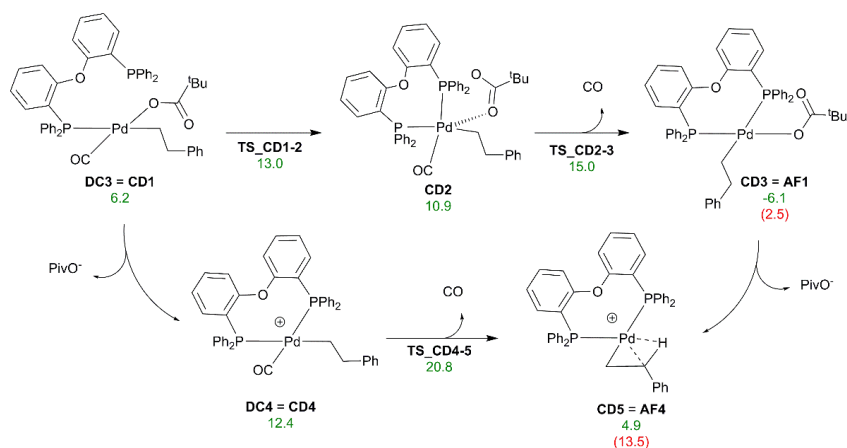
Xantphos and can presumably more easily rotate away from the metal center.<sup>81, 158-160</sup> This may explain the higher yield obtained with DPEphos, compared to Xantphos, as a ligand for **A1** (88 % and 40% respectively). Second, the carboxylate, compared to the ester-anion, can also change between mono and bidentate coordination and is thus less likely to dissociate from the metal and may instead stabilize the coordination switch of DPEphos. In contrast, decarbonylation directly from the fully coordinated complex **DC1** was found to be even less favorable and, in fact, without the partial decooordination of DPEphos, decarbonylation through **TS\_DC4-5** would be the rate-determining step of the reaction.



**Scheme 7.** Investigated pathways of decarbonylation. Numbers are calculated free energies (kcal/mol) at 100 °C using DMA as solvent; see the Computational details section. Reprinted with permission from ref. [82]. Copyright 2019 Royal Chemistry Society.

The benefit of this hemi-labile behavior of DPEphos is that, even though one arm dissociates, it remains close to the metal and available for recoordination later in the catalytic cycle (Scheme 8), in contrast to monodentate ligands which are less likely to recoordinate when not in excess. In fact, following decarbonylation, partial (or full) dissociation of the DPEphos ligand was not found to be favorable in later stages of the reaction. This makes decomposition of the DPEphos-catalyst less likely and hinders isomerization. Furthermore, the dangling arm can recoordinate and displace

the formed CO which is key for activity as CO poisons the catalyst. Such behavior has also been suggested for the heterogenized Pd/C based version of the precatalyst **A1**.<sup>161</sup> In fact, the computational study found that CO was favored to dissociate directly following decarbonylation and recoordination of the dangling DPEphos arm, see Scheme 8, in contrast to previous studies.<sup>66, 81</sup> Not dissociating CO at this point of the cycle lead to overall higher barriers for the following rate-determining alkene formation step and the potential formation of stable M-CO complexes which retards the reaction (see chapter 3.7). While DPEphos in principle could be a tridentate ligand with the bridging oxygen weakly coordinated, this was never found to be favored in the calculations, even for lowly coordinated complexes.



**Scheme 8.** Investigated pathways of CO dissociation. Numbers are calculated free energies (kcal/mol) at 100 °C using DMA as solvent. Thermochemical corrections for CO have been calculated using a reduced ( $10^{-5}$  atm, numbers rendered in green) or standard (1 atm, numbers rendered in red and in parenthesis) pressure. See the Computational details and the next section (3.7) for more information. Reprinted with permission from ref. [82]. Copyright 2019 Royal Chemistry Society.

The L ligand (here: DPEphos) is probably the moiety of the for decarbonylative dehydration catalyst which has the greatest potential for optimization. Mostly different phosphine based ligands, both monodentate and bidentate, have yielded the overall best results, but activity have also been found with amine ligands<sup>69</sup> and N-

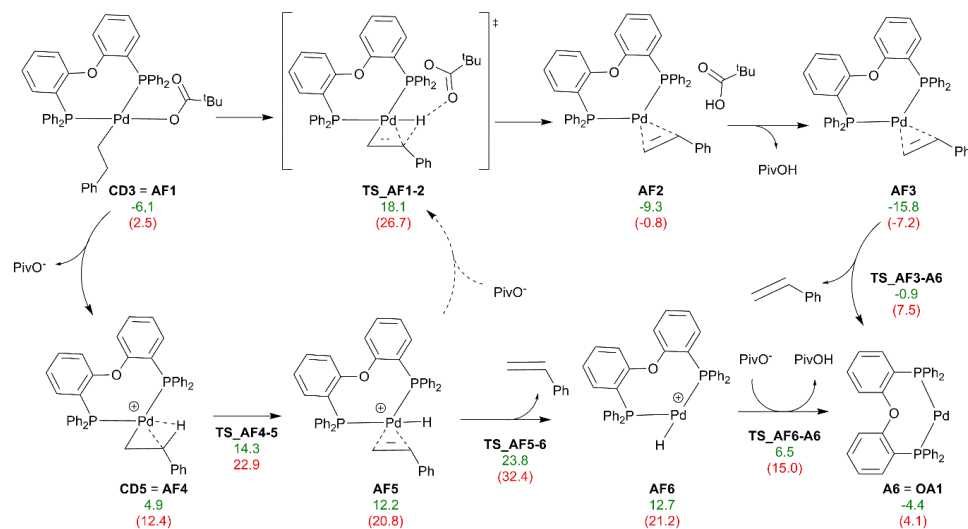
heterocyclic carbenes (NHCs)<sup>66</sup>. Interestingly, decarbonylation and alkene formation barriers were found to be lower for the NHC-catalyst, 1,3-bis(2,6-diisopropylphenyl)imidazole-2-ylidene (IPr) than for the corresponding catalyst with a bidentate phosphine (Xantphos) coordinated.<sup>66</sup> In this work we have presented the benefit that having a ligand which can switch coordination mode has on decarbonylative dehydration. It looks like having one arm that is strongly bound to the metal and one arm that can easily dissociate and associate is favorable for combined high activity and low isomerization and decomposition. This opens interesting channels for further design and optimization of asymmetric hemilabile ligands.

### 3.7 Modeling CO Removal from the Reaction Mixture

During the decarbonylation step of decarbonylative dehydration a CO molecule is produced. What happens to this molecule is of utter importance for the reactions since all investigations, experimental and theoretical, points toward CO accumulation as one of the main factors that kills the reaction. An exception being FeCl<sub>2</sub> catalyzed decarbonylative dehydration which interestingly requires a CO overpressure of 5 bar for activity, presumably because an iron-carbonyl is the active specie.<sup>83</sup> Indeed, all the computational studies have found that if CO is retained at the metal very stable M(CO) complexes, that act as thermodynamic sinks for the reaction, are formed.<sup>74, 81, 84</sup> To account for this the experiments facilitate dissociation of CO from the reaction mixture by combining high temperature, stirring and open systems or even vacuum purges. The eventual loss of CO is then verified by the observed vigorous bubbling.

In computational studies the effect of this removal of CO from the mixture has been modelled by using a reduced partial CO pressure of 10<sup>-5</sup> atm (see the computational details and standard state corrections).<sup>66, 82, 84-85</sup> The immediate effect of this is that all steps following CO dissociation is lowered in free energy (e.g. by -8.5 kcal/mol at 100°C as used in Paper III). Crucially, this has meant that the overall decarbonylative dehydration reaction has been modelled to be exergonic (in contrast to endergonic without), i.e. that the reaction is indeed catalytic as in accordance with experiments. For mechanisms where CO is assumed to dissociate at the end just before a new catalytic cycle, e.g. as for Pd(PPh<sub>3</sub>)<sub>2</sub>, the benefit of the low pressure is only observed at the final overall calculated reaction free energy.<sup>66, 74, 81</sup> In contrast, for (PPh<sub>3</sub>)<sub>2</sub>Rh(CO)Cl (Paper II) and the Pd(DPEphos) catalyzed system (Paper IV), CO was found to dissociate straight before and after decarbonylation respectively, with the result that the following intermediates and transition states also get lower in energies as seen in Scheme 9 (Free energies calculated using a reduced pressure (10<sup>-5</sup> atm) in green and at standard state (1 atm) in red). For example, the free energy of the rate-determining transition state, **TS\_AF1-2**, is reduced from 26.7 kcal/mol to 18.1 kcal/mol. Still, it is important to note that the overall preferred pathway (Scheme 10) was not altered due to this reduced pressure, and neither was the rate-determining

step different. Symptomatic, also here the overall reaction went from endergonic ( $\Delta G = 4.1$  kcal/mol at 1 atm) to exergonic ( $\Delta G = -4.4$  kcal/mol at  $10^{-5}$  atm) emphasizing the need for a reduced pressure treatment.



**Scheme 9.** Investigated pathways of alkene formation and catalyst regeneration. Numbers are calculated free energies (kcal/mol) at 100 °C using DMA as solvent. Thermochemical corrections for CO have been calculated using a reduced ( $10^{-5}$  atm, numbers rendered in green) or standard (1 atm, numbers rendered in red and in parenthesis) pressure. See the Computational details section for more information. Reprinted with permission from ref. [82]. Copyright 2019 Royal Chemistry Society.

Regarding the choice of partial pressure ( $10^{-5}$  atm), this has been somewhat arbitrarily chosen. A potential more sensible choice could be to use the partial pressure in the atmosphere (ca.  $10^{-7}$  atm) which amounts to assuming negligible solubility, efficient diffusion of CO in the solvent (DMA here), and efficient exchange with the gas phase above the solvent. This lower limit for partial pressure gives an overall free energy of  $\Delta G = -7.8$  kcal/mol (see Table 2), which is 3.4 kcal/mol lower than with the assumed pressure of  $10^{-5}$  atm, and the same activation barriers since the rate-determining intermediate is equally stabilized by the lower pressure. An alternative is to look at a completely CO saturated solution. CO is an

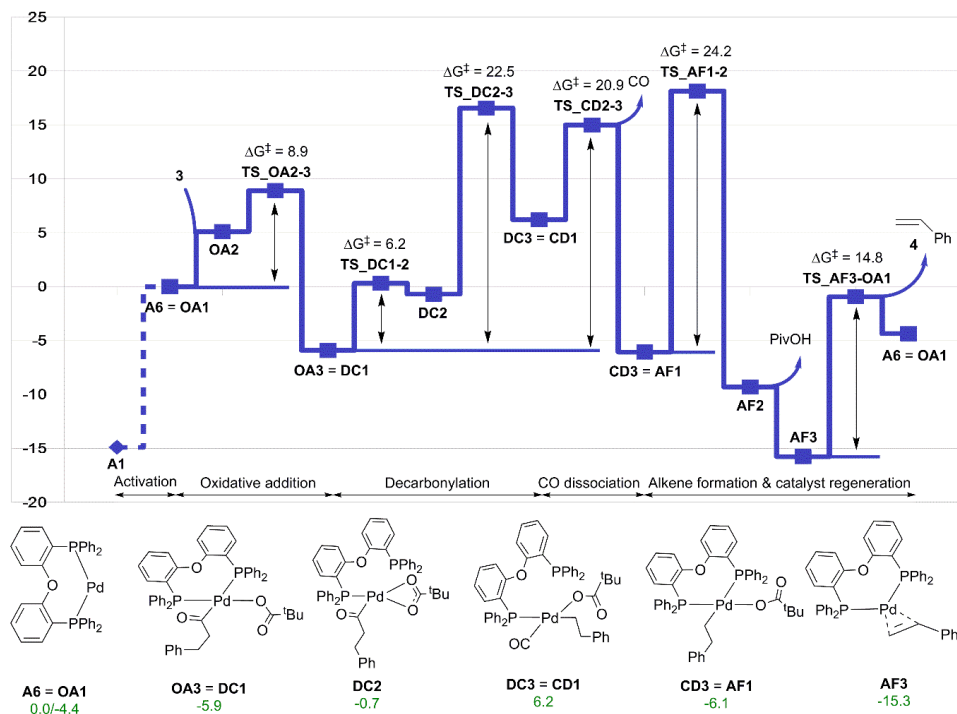


apolar molecule and the solubility in polar solvents (as used here) is low. The solubility of CO in the solvent of choice DMA ( $\epsilon_r = 37.8$ ) was not obtained, but in DMSO ( $\epsilon_r = 46.7$ ) the solubility is lower than 0.01 g/100g (or 0.004) at 20 °C.<sup>162</sup> This concentration, which is artificially high at 100 °C, corresponds to a closed system in equilibrium with the saturated CO solution. The corresponding partial pressure (0.12 atm) may thus be taken as an upper limit of the CO pressure in the reaction and gives a positive reaction free energy of 2.5 kcal/mol, i.e. not catalytic. These two partial pressures represent the boundaries for the actual CO concentration. The lower pressure ( $10^{-7}$ ) does correspond to a catalytic reaction and is probably closer to reality, however it does not take into effect any dissolved CO and probably overestimates the exergonicity somewhat. An increase in the partial pressure from  $10^{-7}$  to  $10^{-5}$  atm only has a moderate effect on the calculated relative energies (Table 1), but is used to reflect an expected weak leftward displacement of the equilibrium due to residing dissolved CO.

**Table 2.** Relative free energies, reaction free energy ( $\Delta G$ ), and free energy of activation ( $\Delta G^\ddagger$ ), calculated for different CO pressures.

Free Energies (kcal/mol)	1 atm	0.12 atm	$10^{-5}$ atm	$10^{-7}$ atm
$\Delta G(\text{TS\_AF1-2})$	26.7	25.1	18.1	14.8
$\Delta G(\text{OA3} = \text{DC1})$	-5.9	-5.9	-5.9	-5.9
$\Delta G(\text{DC3} = \text{AF1})$	2.5	0.9	-6.1	-9.4
$\Delta G(\text{reaction})$	4.1	2.5	-4.4	-7.8
$\Delta G^\ddagger(\text{G}(\text{TS\_AF1-2})-\text{G}(\text{OA3} = \text{C1}))$	32.6	31.0		
$\Delta G^\ddagger(\text{G}(\text{TS\_AF1-2})-\text{G}(\text{DC3} = \text{AF1}))$			24.2	24.2

In general, it looks like a reduced pressure is a simple, but efficient way to estimate the effect of a gaseous specie escaping from the reaction mixture, and it should be employed both in decarbonylative dehydration and for other reactions involving gases.<sup>104</sup>



**Scheme 10.** The calculated free energies (kcal/mol) of the preferred pathway of decarbonylative dehydration to  $\alpha$ -olefin **4** by the catalyst **A1**. Temperature: 100 °C. Solvent: DMA via SMD model. CO pressure:  $10^{-5}$  atm to model escaping CO. See the Computational details section for more information. Reprinted with permission from ref. [82]. Copyright 2019 Royal Chemistry Society.

---

### 3.8 The Solvent Effect on 1-Alkene Formation and Isomerization

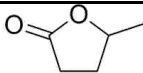
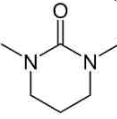
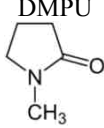
In general, decarbonylative dehydration can be performed in neat conditions without a solvent. However, this has typically required high temperatures and distillation is necessary to achieve good selectivity. Instead, at lower temperatures and when employing a bidentate ligand, a polar solvent has been most effective and eliminates the requirement of distillation for  $\alpha$ -olefin selectivity.<sup>85</sup> Unfortunately these solvents are typically toxic and should be replaced by greener alternatives.

A screening of solvents for the precatalyst **A1** found that not using a solvent at all, but doing the reaction in the combined medium formed by the substrates fatty acid (stearic acid,  $\epsilon_r=2.3$ ) and anhydride (pivalic anhydride,  $\epsilon_r= 12.0$ ), and the resulting mixed anhydride and pivalic acid ( $\epsilon_r=3.0$ ), yielded lackluster results (yield/selectivity = 45%/65%). This was in accordance with poor results using other apolar solvents like toluene ( $\epsilon_r=2.4$ ) and xylene ( $\epsilon_r=2.3$ ) (16-23% yield).<sup>85</sup> The best results were once again obtained using the toxic highly polar solvents DMPU ( $\epsilon_r=36.1$ )<sup>163</sup> and NMP ( $\epsilon_r=32.2$ ),<sup>164</sup> but also the green solvent  $\gamma$ -valerolactone (GVL)<sup>165</sup> with similar dielectric constant ( $\epsilon_r= 36.6$ )<sup>166</sup> was promising (Table 2). Protic polar solvents on the other hand did not work at all. Other green aprotic polar solvents screened, such as EtOAc, 2-methyltetrahydrofuran, acetone and methyl ketone did not yield positive results due to either having a boiling point below the reaction temperature (110°C), decomposition in the reaction medium, or strong palladium-solvent coordination blocking access for the target substrate.

GVL also showed indication of strong Pd-solvent coordination and since it contains the same (CO)-O fragment (Table 2) as in mixed anhydride it prompted investigation of potential oxidative addition which would form a stable metallacycle that could hamper further catalysis. Such metallacycles have been observed for different transition metals including palladium.<sup>167-170</sup> This is also the case for the solvent propylene carbonate (PC) which looked tempting on paper ( $\epsilon_r= 64.9$ , boiling point = 241.7 °C), but performed poorly (<5% yield). However, in both cases the oxidative

addition was found to be much more costly for the solvents than for the mixed anhydride, and the resulting metallacycle was not particularly stable. This indicates that oxidative addition of the GVL is not likely, but the strong coordination to the metal might explain the lower activity for GVL compared to DMPU and NMP which do not have the (CO)-O moiety (Table 3). An explanation for the low observed activity in PC is that this solvent is known to react with carboxylic acids.<sup>171</sup> In the modelled case, PC may react with the substrate fatty acid or the pivalic acid formed in the reaction. The calculated reaction free energy for these two possibilities indeed showed that, while the formation of the mixed anhydride is endergonic, the competing reactions with PC and substrate fatty acid is exergonic and irreversible and will erode yields by removing the substrate.

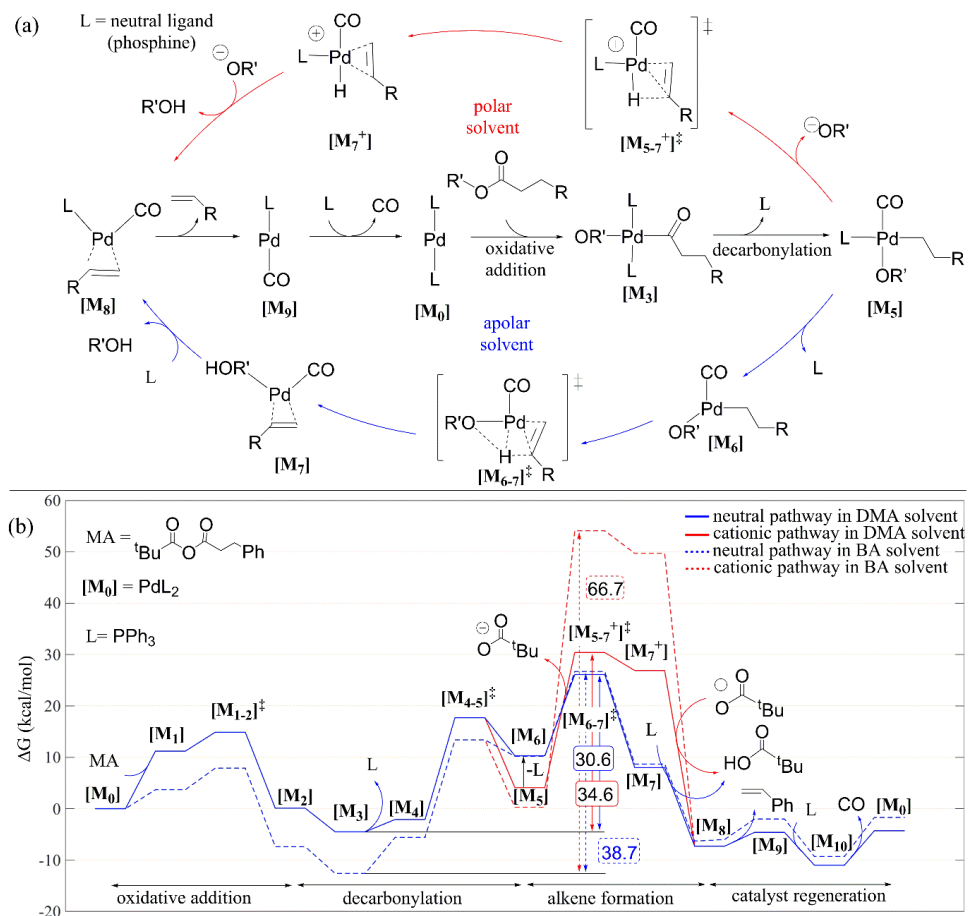
**Table 3.** Comparison of GVL with traditional, non-green solvents, and *neat* conditions. Modified and reprinted with permission from ref. [83]. Copyright 2019 American Chemical Society.

entry	solvent	boiling point (C°)	$\epsilon^a$	yield [%]	$\alpha$ -olefin [%]
1	 $\gamma$ -valerolactone (GVL)	207.0	36.5 <sup>165</sup>	70	90
2	 DMPU	246.5	36.1	84	94
3	 NMP	202	32.0	74	89
4	<sub>-b</sub>	-	3.0 <sup>b</sup>	45	65

<sup>a</sup>Relative permittivity (dielectric constant) of the liquid at 25°C,<sup>163</sup> unless otherwise stated. <sup>b</sup>In the case of no added solvent, the substrates (stearic acid ( $\epsilon = 2.3$ ) and pivalic anhydride ( $\epsilon = 12.0$ )) will still form a medium and during the reaction two equivalents of pivalic acid is formed ( $\epsilon = 3.0$ ). Pivalic acid is thus used as model.

The results from the solvent screening affirm that polar solvents are superior, and the question that follows is how they affect the overall reaction mechanism. As seen in the previous sections, at certain parts of the reaction a ligand must dissociate to make space for the CO and alkene formation. A potential candidate has been proposed to be the carboxylate (or equivalent anion) by other computational studies, both with monodentate ( $\text{PPh}_3$ ) and bidentate (Xantphos) ligand, when using a polar solvent.<sup>66, 81</sup> In these cases, the rate-determining  $\beta$ -hydrogen transfer from the alkyl chain, is assumed to be a proper  $\beta$ -hydride elimination, followed by a transfer of the proton from the cationic catalyst to the  $\text{OR}^-$  anion (Scheme 11).<sup>66</sup> This is consistent with the theory that solvents stabilize transition states reflecting their polarity, that is, a polar solvent stabilizes an activated complex with higher charge density than its reactants.<sup>172</sup> Aprotic dipolar solvent also drastically increases the reactivity of anions which should benefit hydrogen transfer from the hydride. In contrast, dipolar *protic* solvents inhibit activity of anion by forming strong hydrogen bonds between the solvent and the anion, which means that the basicity of the anion is lowered. For the protic dipolar solvents screened (water, MeOH,  $i$ PrOH, ethanol and 1-propanol) it is thus likely that the carboxylate dissociates from the complex due to the polarity of the solvent but is a much less efficient Brønsted base and hampers the important olefin-forming hydrogen transfer-step.

Indeed, when investigating the SMD solvent effect on the  $\text{Pd}(\text{PPh}_3)_2$  catalyzed mechanism<sup>81</sup> by changing from the apolar protic solvent (butanoic acid,  $\epsilon_r=2,9$ ) to a aprotic polar solvent (DMA,  $\epsilon_r=37,8$ ), it was found that the cationic  $\beta$ -hydride elimination via  $[\mathbf{M}_{6-7}^+]^\ddagger$  experiences a massive decrease in energy (from 66.7 kcal/mol to 34.6 kcal/mol) (Scheme 11).<sup>83</sup> The preferred pathway however was still found to be the neutral low-coordinated Pd complex via  $[\mathbf{M}_{5-7}^+]^\ddagger$ , which barrier was reduced from 38.7 kcal/mol to 30.6 kcal/mol, mainly due to the destabilization of the rate-determining intermediate  $[\mathbf{M}_3]$ .



**Scheme 11.** (a) The proposed general reaction mechanisms for Pd-catalyzed decarbonylative dehydration in polar and apolar solvent. (b) The free energy profile re-calculated (at 373 K) for two different solvents, DMA (complete lines) and BA (dashed lines), starting from geometries reported for Pd(PPh<sub>3</sub>)<sub>2</sub>-catalyzed decarbonylative dehydration.<sup>81, 84</sup> The red lines show the pathway of the charge-separated  $\beta$ -hydride elimination in contrast to the neutral alkene formation (blue). Reprinted with permission from ref. [83]. Copyright 2019 American Chemical Society

In contrast, it was expected that in reactions using bidentate ligands and polar solvents, the increased binding strength, combined with the increased activity of the anions, would facilitate an anion leaving over the neutral phosphine.<sup>66</sup> Indeed, for the

---

computational investigation of the mechanism of Pd(DPEphos) in a polar solvent (DMA), a cationic  $\beta$ -hydride elimination via **TS\_AF4-5** was found to be lower in energy ( $\Delta G = 14.3$  kcal/mol) than the neutral direct hydrogen transfer from the alkyl chain to the carboxylate via **TS\_AF1-2** ( $\Delta G = 18.1$  kcal/mol) (Scheme 9). However, the subsequent  $\alpha$ -olefin dissociation involves a barrier (via **TS\_AF5-6**) that is more than 6 kcal/mol higher than that of the intramolecular direct transfer, while the latter neutral pathway also provides a facile 1-alkene dissociation. This is surprising seeing, as observed, that polar solvents give better activity and the rate-determining step is assumed to be alkene formation.<sup>66, 74, 81, 83-84</sup> An alternate pathway, where the hydride hydrogen is transferred to the carboxylate prior to olefin dissociation, was also explored computationally, but whenever the pivalate approached the hydride in **AF5**-like complexes, the pivalate associated with Pd to complexes similar to **AF1** and subsequent hydrogen transfer following the neutral pathway. Finally, the preferred TS, **TS\_AF1-2** (Figure 3), is overall neutral, but also zwitterionic, and the pivalate-Pd distance is relatively long ( $L(\text{Pd-O}) = 2.6685$  Å), indicating that the polar solvent may stabilize this structure. However, the SMD solvent model does not stabilize **TS\_AF1-2**. In fact, the activation energy of this TS is lower without the solvent corrections ( $\Delta G_{\text{gas}}^{\ddagger} = G^{\ddagger}(\text{TS\_AF1-2}) - G(\text{CD3=AF1}) = 20.9$  kcal/mol). In contrast, SMD calculations substantially stabilize the cationic complexes **AF4 – AF6** in polar solvents (e.g.  $\Delta G_{\text{gas}}^{\ddagger} = G^{\ddagger}(\text{TS\_AF4-AF5}) - G(\text{CD3=AF1}) = 97.0$  kcal/mol). Still, this SMD-calculated solvent stabilization is not enough to make the cationic pathway preferred.

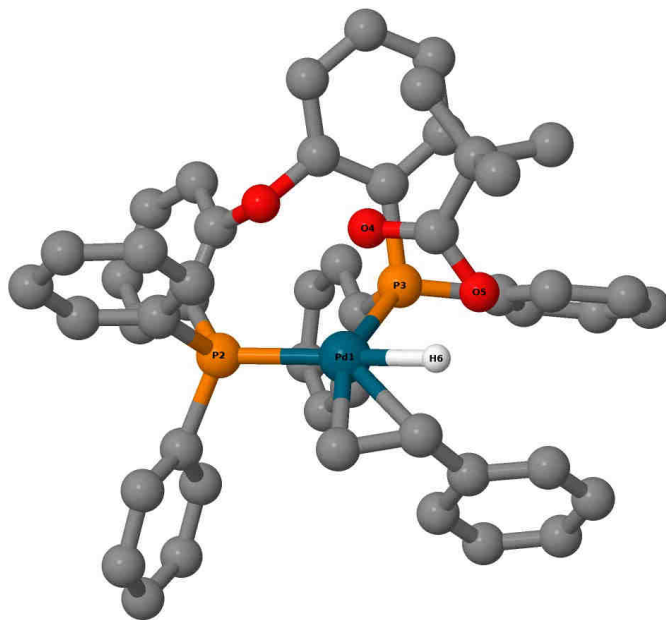


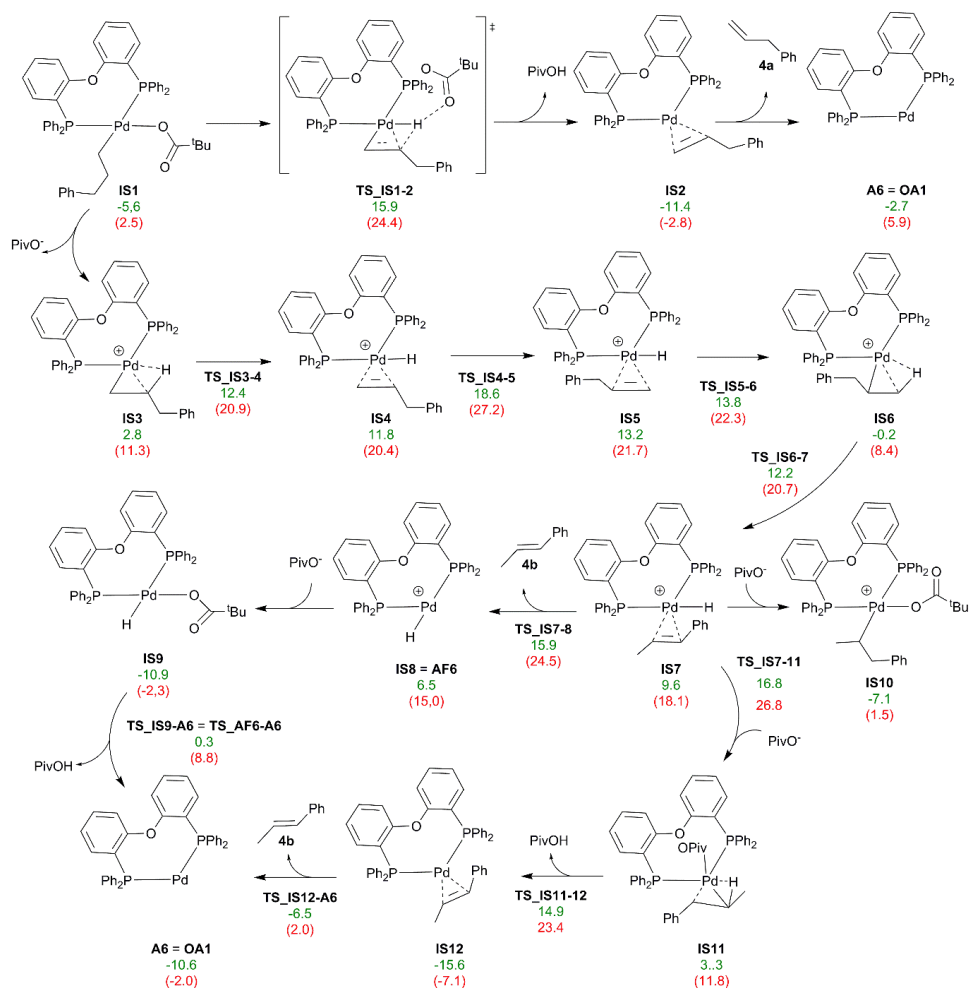
**Figure 3.** The optimized rate-determining transition state, **TS\_AF1-2** (hydrogens, except H6, omitted for clarity). Selected bond lengths. Pd1–P2 2.2928 Å; Pd1–P3 2.4443 Å; Pd1–O4 2.6685 Å; Pd1–H6 2.0327 Å; O5–H6 1.4619 Å. Bite angle P2–Pd1–P3 103.12°.

While the polar solvent does not seem to facilitate the alkene formation, it may instead promote isomerization. As seen, the formation of Pd-hydride species, (**AF5**) which are known to facilitate isomerization, was indeed less demanding than the complete hydrogen transfer and benefitted tremendously from a polar environment. From the hydride, if the carboxylate (anion) is not available, the olefin can rotate to start the isomerization. Note that to investigate the isomerization pathway the model  $\alpha$ -olefin, styrene, that has been used so far but cannot undergo double-bond migration, has been changed to the one methyl unit longer allylbenzene which is susceptible to double-bond migration. The alkyl chain on the starting point **AF1** is thus expanded by one methyl unit to form the rate-determining intermediate **IS1** (Scheme 12). The rate-determining TS from the alkene formation pathway **TS\_AF1-2** is also expanded (called **TS\_IS1-2**) to enable comparison with the isomerization .



The rotation following hydride formation (**TS\_IS3-4**, 12.4 kcal/mol) involves a barrier (*via* **TS\_IS4-5**) of 18.6 kcal/mol. This is already 2.7 more than the rate-determining barrier (*via* **TS\_IS1-2**) to  $\alpha$ -olefin formation, which explains the high 1-alkene selectivity observed for the precatalyst **A1**.<sup>83, 85</sup> Continuing from the rotation, the olefin can reinsert into the Pd-hydride bond (*via* **TS\_IS5-6**) to form a secondary alkyl, with a barrier of 13.8 kcal/mol. From **IS6**, a new hydrogen atom may be reductively eliminated to the metal, again with a low barrier (12.2 kcal/mol, *via* **TS\_IS6-7**). This concludes the internal olefin formation, which can be liberated *via* **TS\_IS7-8** with a barrier lower than the initial olefin rotation. The active catalyst **A6** (=O**A1**) can then be regenerated by transferring the proton to the carboxylate (here pivalate) and dissociation of the carboxylic acid. The proton transfer may start from the olefin-hydride, **IS8**, but in the  $\alpha$ -olefin formation, the proton is transferred before the olefin dissociation. The relatively high stability calculated for intermediates **IS11-12** and for **TS\_IS12-A6** suggest that this natural pathway is also preferred for generating the internal olefin. However, the secondary alkyl is more sterically demanding than the primary one, requiring a substrate rotation from **IS7** to **IS11** ( $\Delta G^\ddagger = 16.8$  kcal/mol, *via* **TS\_IS7-11**) before the transfer of an  $\alpha$ -agostic hydrogen to the pivalate *via* **TS\_IS11-12**. This latter TS is lower in energy than the olefin dissociation TS for the cationic path, **TS\_IS7-8**, but due to the required rotation *via* **TS\_IS7-11**, the cationic pathway has a lower overall barrier. During this part of the reaction, after formation of the internal olefin, the carboxylate may bind to the metal and form a neutral secondary alkyl complex **IS10** (-7.1 kcal/mol). This off-cycle species is even more stable than the primary alkyl analogue **IS1** and increases the subsequent barriers of the cationic and neutral isomerization pathways. Importantly however, regardless of whether the cationic or neutral proton transfer is preferred, rotation *via* **TS\_IS4-5** remains the rate-limiting step in the olefin isomerization. Finally, for longer olefins, the process of rotation, reinsertion, and reductive elimination may continue to migrate the double bond along the chain to generate the further internal olefins. The free energy profile of the isomerization is shown in Scheme 13. The overall reaction free energy for producing the internal olefin is -10.6 kcal/mol (-2.0 kcal/mol without the reduced CO pressure), which reflects the higher thermodynamic

stability of the internal olefin compared to the  $\alpha$ -olefin ( $-2.7$  and  $5.9$  kcal/mol with and without reduced pressure respectively).

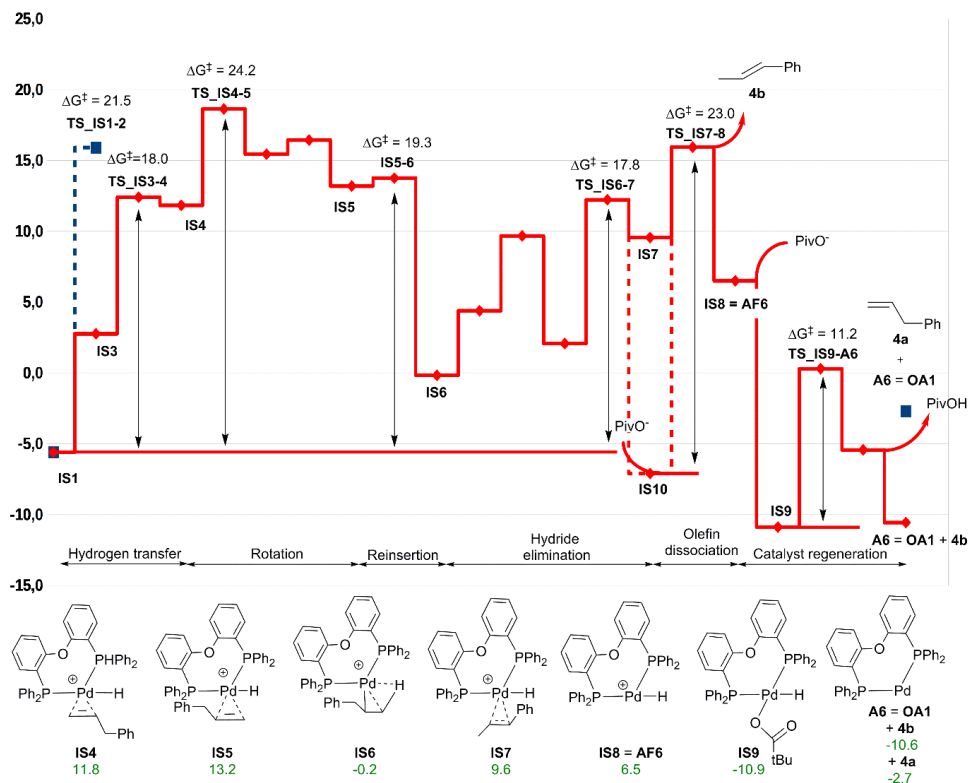


**Scheme 12.** Isomerization pathway leading to the internal olefin **4b**. The starting point IS1 is analogous to AF1 but bears an alkyl ligand with one more methylene group to model the isomerization realistically. Thus, for comparison, the key transition state (**TS\_IS1-2**) and intermediate (**IS2**) leading to  $\alpha$ -olefin **4a** (allylbenzene) instead of **4** (styrene) are also included starting from the same alkyl complex **IS1**. Numbers are calculated free energies (kcal/mol) at 100 °C using DMA as solvent. Thermochemical corrections for CO have been calculated

---

using a reduced ( $10^{-5}$  atm, numbers rendered in green) or standard (1 atm, numbers rendered in red and in parenthesis) pressure. See the Computational details section for more information. Reprinted with permission from ref.[82]. Copyright 2019 Royal Chemistry Society.

The fact that olefin rotation is rate-determining in isomerization is probably due to the steric bulk of the bidentate ligand. For monodentate ligands, either a monodentate coordination, such as that of the NHC, IPr,<sup>66</sup> or a complete dissociation such as  $\text{PPh}_3$ ,<sup>81</sup> has been found to be beneficial in the rate-determining step. This explains why low selectivity is obtained without excess in such *in situ* systems. In contrast bidentate systems (DPEphos, Xantphos) or mixed ligand systems (IPr and Xantphos) show high selectivity due to the steric bulk and strong coordination.<sup>63, 66, 82-83</sup> In fact a partial DPEphos dissociation, as in the formation of 1-alkene, was investigated, but all attempts at stabilizing isomerization-potent Pd-hydride complexes with partially dissociated DPEphos ligands resulted in the rebinding of phosphine and regular, bidentate coordination of DPEphos. Finally, also the carboxylate anion influences the selectivity, as it must dissociate for the olefin rotation to take place instead of the hydrogen transfer to release the  $\alpha$ -olefin. Carboxylate may coordinate in a bidentate fashion and is presumably a better coordinating ligand, and give less isomerization, than alternatives, such as ester groups or chlorides originating from the use of fatty acid ester or acid chloride substrates.<sup>60, 66-67, 173</sup>



**Scheme 13.** The calculated free energies (kcal/mol) of the preferred alkene isomerisation pathway (rendered in red). For comparison, the rate-determining barrier and reaction free energy of  $\alpha$ -olefin formation are also included (rendered in blue and stapled). Temperature: 100 °C. Solvent: DMA via SMD model. CO pressure:  $10^{-5}$  atm to model escaping CO. See the Computational details section for more information. Reprinted with permission from ref.[82]. Copyright 2019 Royal Chemistry Society.

The overall picture coming from the discussion above is that the neutral pathway is favored over the more isomerization-potent cationic complexes by the current DFT/SMD calculations. This is consistent with the fact that the precatalyst **A1** is highly selective for  $\alpha$ -olefins. However, the question remains, what is the role of the polar solvent known to be beneficial in experiments? As seen, the barrier of the neutral alkene formation increases in the polar solvent, while the cationic  $\beta$ -hydride

---

elimination is lowered, indicating a lowering of both activity and selectivity. Caution should be exercised here though as the solvent effects observed here are large and a continuum model like SMD might not be sophisticated enough to properly distinguish between the neutral and cationic pathway. A computational benefit however, as for the Pd(PPh<sub>3</sub>)<sub>2</sub> mechanism, is a lowered stability of the rate-determining intermediates (here, **CD3=AF1** or **IS1**) in a polar solvent compared to a situation without solvent, e.g.  $\Delta G(\mathbf{CD3=AF1}) = -7.7$  kcal/mol in butanoic acid ( $\epsilon_r = 2.9$ ) and  $-6.1$  kcal/mol in DMA ( $\epsilon_r = 37.8$ ). In fact, in butanoic acid the rate-determining intermediate becomes **OA3=DC1** with  $\Delta G(\mathbf{OA3=DC1}) = -12.0$  kcal/mol. This increases the barrier  $\Delta G^\ddagger(G(\mathbf{TS\_AF1-2}) - G(\mathbf{OA3=DC1}))$  to 26.9 kcal/mol (**TS\_AF1-2** is still the rate-determining step) in butanoic acid which is more than the original barrier  $\Delta G^\ddagger(G(\mathbf{TS\_AF1-2}) - G(\mathbf{CD3=AF1})) = 24.2$  in DMA. Thus, there is some benefit of the polar solvent on the overall reaction mechanism. What more, the polar solvent might be important in the activation of the precatalyst, **A1**, here or PdCl<sub>2</sub> typically used in the *in situ* approaches. For example, the cationic complex **A2** (Scheme 5) predicted to partake in the activation, is calculated to be 84.4 kcal/mol less stable than **A1** before solvent effects are included. A more practical benefit of the polar solvent may be that it creates a two-layer system, where the apolar olefins, when dissociated from the catalyst, can form a layer separated from the polar solvent where the catalysis takes place, thus preventing isomerization. Such a separation of layers is reminiscent of CO escaping the reaction mixture and could imply that a similar reduced concentration (or partial pressure) treatment should be applied also here.

### 3.9 Additional Factors Present in Decarbonylative Dehydration Reactions

Due to mainly using the reaction conditions for the **A1** catalyzed reaction as a foundation for the computational investigation, there are certain elements that have not been investigated in this thesis but may serve a role for decarbonylative dehydration. First, many setups have used continuous distillation throughout the reaction to achieve selectivity towards  $\alpha$ -olefins. This has not been required in the setup for **A1** and has therefore not been treated here. However, in computational investigations of systems where distillation has been used, a similar treatment to the reduced pressure to model CO escaping from the reaction should be applied, but with an appropriate choice of the pressure dependent on the solubility. This would give a benefit to the free energy following dissociation of the  $\alpha$ -olefin (Scheme 9) and thus reflect the increased selectivity observed. Indeed, as discussed above, such a treatment should perhaps be employed here if there is experimental evidence that the polar solvent creates a two-phase system which the results hint at.

An additional factor that effects selectivity but has not been investigated here is the build-up of acid. During the reaction two equivalents of acid is formed; in the formation of the mixed anhydride and following hydrogen transfer, and this is detrimental to selectivity presumably due to slower hydrogen transfer.<sup>63</sup> To prevent this, it is standard protocol to add base to the reaction, but we and other have also assumed that this is important for the reduction of the initial Pd<sup>II</sup> specie. Another additive used in different experiments is KI, which may play part in a ligand exchange with chloride for [M]Cl type catalysts.<sup>70-72</sup>

## 4. Suggestions for Future Improvements of the Catalysis

From the results obtained with the optimal conditions for **A1** (pivalic anhydride as activator and pyridine as base) together with GVL as solvent (Table 3) in Paper II, an estimate of the industrial viability can be given. By counting the two pivalic anhydrides (one as excess and one as 2·PivOH) along with the coproduct CO, 10% of the GVL solvent (assuming 90% of the ca. 20 mmol (2 mL) can be recycled), the 9 mol % of pyridine, the 1 mol % of precatalyst **A**, and accounting for 70% yield of 1-heptadecene, the environmental factor, E-factor,<sup>1</sup> is found to be

$$E - \text{factor} = \frac{\text{total waste}}{\text{product}}$$

$$= \frac{(2 * \text{PivOH} + \text{PivO}_2 + \text{CO} + 2 \cdot \text{VL} + 0.09 \cdot \text{Py} + 0.01 \cdot \mathbf{A1})}{0.7 \cdot \text{C}_{17}\text{H}_{34}} = 3.8. \quad (47)$$

This is in the upper end of the range (<1–5) that is typical for bulk chemicals, mainly due to the use of stoichiometric amounts of anhydride. The E-factor also does not take temperature or catalyst stability into account and whereas the temperature used in the experiment (110°C) is the lowest to date and a heterogenous version of the catalyst which allows for recycling has been reported,<sup>161, 174</sup> the obtained TON of 70 is well below those required for industrial uptake. Thus, more stable and active catalysts will still have to be developed to improve the overall sustainability of the reaction. Fortunately, we now have a better understanding of the mechanism and know which factors that are important. These can be targeted for optimization to develop future catalysts.

As seen above the excess of sacrificial anhydride is the main contributor to the E-factor and is thus an area for major improvement. Other types of activation of the fatty acid have been tried but require either a different sacrificial group or a photocatalyst.<sup>66-67, 73, 156-157</sup> In fact, the anhydride in itself is beneficial for the reaction, due to the importance of the resulting carboxylate ligand formed in the oxidative addition. This carboxylate can be modified and improved as a higher basicity and

---

higher Hammett constant ( $\sigma_p$ ) for this group has been found to reduce the barrier for the hydrogen transfer in the rate-determining alkene-formation step.<sup>81</sup> Moreover a bulky group is believed to be beneficial to prevent cleavage of the wrong C-O bond in the mixed anhydride. The requirement for anhydride and cleavage of the wrong bond could both be prevented completely by *in situ* formation of symmetric anhydride by dehydration of two substrate fatty acids as seen for Rh, but this has so far required high temperatures. A dual catalytic system which promotes the formation along with decarbonylative dehydration would be ideal, but the generation of the protic water could hinder the alkene formation as seen from the solvent screening. Indeed, while GVL was found to be the best non-toxic solvent candidate in the screening in Paper III, there may exist other green aprotic solvents with higher polarity. This would further promote separation of a polar catalytic phase and an apolar product (olefin) phase which would thermodynamically drive the reaction forward, prevent isomerization and potentially facilitate catalyst recovery.

A feature of the molecular well-defined precatalyst **A1** is that the effect from varying different parts of the catalyst (metal, ligand, activation) can more easily be examined experimentally and now computationally. While Ni and Fe are interesting from a sustainable point of view, Pd looks to be the best candidate at this point, albeit Rh and Ir, by the simple fact that their reaction mechanism involves more coordinated ligands, have more avenues for optimization. One of the benefits of **A1** was the improved activation by fast dissociation of chloride and reductive elimination of the cinnamyl and a base. This could be further improved by substituting the chloride with an even faster initiating anion. Indeed, by the calculations (Scheme 5), it was found that the pivalate coordinated complex **A3** is even more stable than **A1**, but also facilitates the reduction. Thus, a possibility is to start directly from **A3**, or a similar complex, and potentially eliminate the need for excess base used to generate the pivalate here. The cinnamyl was found in the original screening to be the best  $\eta^3$ -allyl ligand,<sup>85</sup> but in Pd catalyzed cross-coupling bigger and bulkier variations have shown promise due to preventing dimerization, and could perhaps improve activity here as well.<sup>150, 175-176</sup>



---

The most interesting moiety for optimization is the DPEphos ligand as, as seen from the mechanism, it serves multiple purposes. It should both be strongly coordinating and donating to promote oxidative addition and prevent isomerization and decomposition as well as displacing CO but must also provide space for decarbonylation and reductive elimination which favors electron poor complexes. This balance act is fulfilled by the hemilability of DPEphos here, but as this ligand is symmetric it is tempting to envision potential asymmetric variants which parts are optimized for each role. For example, in the decarbonylation of esters it was found that the NHC ligand, IPr, had lower barriers than the bidentate phosphine ligand Xantphos, and thus higher conversion, but suffered from isomerization to internal olefins which was prevented by the bulky Xantphos. However, a mixed system of both ligands seemed to combine the beneficial effect of both, yielding high selectivity and activity.<sup>66</sup> This motivated us to test precatalysts with asymmetric bidentate ligands consisting of an NHC and a more labile group (P, S, N). Unfortunately, the experimental results were underwhelming and probably more confined variations of the DPEphos moiety should be investigated in the future.<sup>177-179</sup> However, there is no doubt a huge potential for improved ligands to be discovered.

Thus, we have identified some parameters that are essential for catalyst activity; the basicity of the carboxylate (or anion), the M-CO bond strength and the donating and hemilabile property of the L ligand. In the future we would like to use these (and other) parameters to predict new catalysts for decarbonylative dehydration. In the group, the computational tool DENOPTIM has been developed for this type of catalyst prediction. This tool identifies potential candidates by optimizing a fitness based on key parameters (descriptors), where the optimization is done by combining molecular fragments through an automated evolutionary algorithm, and has already been used to identify new complexes.<sup>180</sup> Hopefully, with the now deeper understanding of the mechanism of decarbonylative dehydration, an automated catalyst prediction process is not too far away.

## 5. Conclusion

In the work presented in this thesis, the reaction decarbonylative dehydration of fatty acids for sustainable production of  $\alpha$ -olefins has been investigated by DFT-methods. This has given crucial insight to the reaction mechanism and to understand the experimental parameters used during catalysis. Overall it was found that for different metals, solvents, phosphine ligands and CO pressure, the rate-determining step is the alkene-formation, followed by decarbonylation. On the other hand, the oxidative addition is found to be facile, but requires activation of the fatty acid. The CO formed during the reaction binds to the catalyst and forms stable compounds that acts as thermodynamic sinks but can be displaced by phosphine ligands. Isomerization of the 1-alkene to internal olefins as an undesired side-reaction is favored by the formation of cationic complexes, and steric hindrance and olefin removal is key to prevent the olefin rotation which initiates this pathway.

The overall greenness of the decarbonylative dehydration has been improved by the precatalyst **A1** by reducing the operational temperature and the amount of phosphine required. The palladium metal center is beneficial for activity due to the lower barriers compared to other transition metals. This is believed to mainly be due to the relative lower stability of Pd-CO complexes compared to other transition metals like Ni and Rh. By using a molecular precatalyst and combining the strongly coordinating ligand DPEphos and easily displaced chloride and cinnamyl, both the reduction from Pd<sup>2+</sup> to Pd<sup>0</sup> is facilitated, and the Pd(DPEphos) complex is readily available for catalysis without the need for *in situ* coordination of phosphine to the metal. The DPEphos ligand serves multiple purposes as it both is strongly coordinating, preventing dissociation from the metal and catalyst deactivation, and hemilabile due to its flexible backbone, which promotes decarbonylation and CO displacement. The CO is removed from the reaction mixture due to an open system and low solubility which displaces the equilibrium of the reaction towards the product.

A sacrificial anhydride is still required for activation of the fatty acid in this setup as the C-OH in carboxylic acids is difficult to break by oxidative addition. This is

---

unfortunate as it impairs the overall economic and environmental aspect of the reaction. However, the resulting carboxylate formed by oxidative addition of the mixed anhydride also serves a purpose in later stages; it can stabilize intermediates of the catalytic cycle by switching from monodentate to bidentate coordinate and prevent isomerization by fast metal assisted hydrogen transfer. Isomerization is facilitated by the aprotic polar solvents typically used for the reaction which promote carboxylate dissociation and the formation of cationic palladium hydride species, but the steric bulk of DPEphos makes the olefin rotation needed for isomerization more demanding than hydrogen transfer to the carboxylate. A cationic pathway is however not found to be favorable for 1-alkene formation in contrast to other studies using a polar solvent. Instead it is believed that the benefit of the polar solvent stems from faster activation of the precatalyst and possible destabilization of the neutral rate-determining intermediate. Another possibility is that it leads to a better separation of the apolar olefins and the polar catalytic medium, which is implied by the increased selectivity. Finally, GVL was found to be a green alternative to the traditional toxic solvents DMPU and NMP with similar properties and resulting  $\alpha$ -olefin yield.

The work presented in this thesis has thus identified the areas where the reaction is being held back and the major improvements will most likely come in the form of improved catalyst and fatty acid activation and optimization of hemilabile ligands. With the now increased knowledge of the mechanism and the parameters that are important for activity, our hope is that these new catalysts can be realized through intelligent design and automated prediction.

## 6. References

1. Sheldon, R. A., The E factor 25 years on: the rise of green chemistry and sustainability. *Green Chem.* **2017**, *19*, 18-43, 10.1039/C6GC02157C.
2. Sheldon, R. A., Fundamentals of green chemistry: efficiency in reaction design. *Chem. Soc. Rev.* **2012**, *41*, 1437-1451, 10.1039/C1CS15219J.
3. Ragauskas, A. J.; Williams, C. K.; Davison, B. H.; Britovsek, G.; Cairney, J.; Eckert, C. A.; Frederick, W. J.; Hallett, J. P.; Leak, D. J.; Liotta, C. L.; Mielenz, J. R.; Murphy, R.; Templer, R.; Tschaplinski, T., The Path Forward for Biofuels and Biomaterials. *Science* **2006**, *311*, 484-489, 10.1126/science.1114736.
4. Corma, A.; Iborra, S.; Velty, A., Chemical Routes for the Transformation of Biomass into Chemicals. *Chem. Rev.* **2007**, *107*, 2411-2502, 10.1021/cr050989d.
5. Serrano-Ruiz, J. C.; Dumesic, J. A., Catalytic routes for the conversion of biomass into liquid hydrocarbon transportation fuels. *Energ. Environ. Sci.* **2011**, *4*, 83-99, 10.1039/C0EE00436G.
6. Dapsens, P. Y.; Mondelli, C.; Pérez-Ramírez, J., Biobased Chemicals from Conception toward Industrial Reality: Lessons Learned and To Be Learned. *ACS Catal.* **2012**, *2*, 1487-1499, 10.1021/cs300124m.
7. Bomtempo, J.-V.; Chaves Alves, F.; de Almeida Oroski, F., Developing new platform chemicals: what is required for a new bio-based molecule to become a platform chemical in the bioeconomy? *Faraday Discuss.* **2017**, *202*, 213-225, 10.1039/C7FD00052A.
8. Bitter, H.; Clark, J.; Rothenberg, G.; Matharu, A.; Crestini, C.; Argyropoulos, D.; Cabrera-Rodríguez, C. I.; Dale, B. E.; Stevens, C.; Marrocchi, A.; Graca, I.; Luo, H.; Pant, D.; Wilson, K.; Zijlstra, D. S.; Gschwend, F.; Mu, X.; Zhou, L.; Hu, C.; Lapkin, A.; Mascal, M.; Budarin, V.; Hunt, A.; Waldron, K.; Zhang, F.; Zhenova, A.; Samec, J.; Huber, G.; Coma, M.; Huang, X.; Bomtempo, J.-V., Bio-based chemicals: general discussion. *Faraday Discuss.* **2017**, *202*, 227-245, 10.1039/C7FD90048A.
9. Werpy, T.; Petersen, G. *Top Value Added Chemicals from Biomass: Volume I - Results of Screening for Potential Candidates from Sugars and Synthesis Gas*; DOE/GO-102004-1992; TRN: US200427%%671 United States 10.2172/15008859 TRN: US200427%%671 NREL English; ; National Renewable Energy Lab., Golden, CO (US): 2004; p 76 pp. pages.
10. Vennestrøm, P. N. R.; Osmundsen, C. M.; Christensen, C. H.; Taarning, E., Beyond Petrochemicals: The Renewable Chemicals Industry. *Angew. Chem. Int. Ed.* **2011**, *50*, 10502-10509, 10.1002/anie.201102117.
11. Stadler, B. M.; Wulf, C.; Werner, T.; Tin, S.; de Vries, J. G., Catalytic Approaches to Monomers for Polymers Based on Renewables. *ACS Catal.* **2019**, 8012-8067, 10.1021/acscatal.9b01665.
12. Mohan, D.; Pittman, C. U.; Steele, P. H., Pyrolysis of Wood/Biomass for Bio-oil: A Critical Review. *Energy Fuels* **2006**, *20*, 848-889, 10.1021/ef0502397.
13. Franke, R.; Selent, D.; Börner, A., Applied Hydroformylation. *Chem. Rev.* **2012**, *112*, 5675-5732, 10.1021/cr3001803.
14. Skupinska, J., Oligomerization of .alpha.-olefins to higher oligomers. *Chem. Rev.* **1991**, *91*, 613-648, 10.1021/cr00004a007.

15. Ittel, S. D.; Johnson, L. K.; Brookhart, M., Late-Metal Catalysts for Ethylene Homo- and Copolymerization. *Chem. Rev.* **2000**, *100*, 1169-1204, 10.1021/cr9804644.
16. Keim, W., Oligomerization of Ethylene to  $\alpha$ -Olefins: Discovery and Development of the Shell Higher Olefin Process (SHOP). *Angew. Chem. Int. Ed.* **2013**, *52*, 12492-12496, 10.1002/anie.201305308.
17. Belov, G. P.; Matkovsky, P. E., Processes for the production of higher linear  $\alpha$ -olefins. *Pet. Chem.* **2010**, *50*, 283-289, 10.1134/s0965544110040055.
18. Forestière, A.; Olivier-Bourbigou, H.; Saussine, L., Oligomerization of Monoolefins by Homogeneous Catalysts. *Oil Gas Sci. Technol.* **2009**, *64*, 649-667.
19. Kourist, R., A New Class of Enzymes Discovered: A Non-Heme Oxidase Produces Medium-Chain 1-Alkenes. *Angew. Chem. Int. Ed.* **2015**, *54*, 4156-4158, 10.1002/anie.201500466.
20. van Leeuwen, P. W. N. M.; Clément, N. D.; Tschan, M. J. L., New processes for the selective production of 1-octene. *Coord. Chem. Rev.* **2011**, *255*, 1499-1517, 10.1016/j.ccr.2010.10.009.
21. Mol, J. C., Industrial applications of olefin metathesis. *J. Mol. Catal. A: Chem.* **2004**, *213*, 39-45, 10.1016/j.molcata.2003.10.049.
22. Bollmann, A.; Blann, K.; Dixon, J. T.; Hess, F. M.; Killian, E.; Maumela, H.; McGuinness, D. S.; Morgan, D. H.; Neveling, A.; Otto, S.; Overett, M.; Slawin, A. M. Z.; Wasserscheid, P.; Kuhlmann, S., Ethylene Tetramerization: A New Route to Produce 1-Octene in Exceptionally High Selectivities. *J. Am. Chem. Soc.* **2004**, *126*, 14712-14713, 10.1021/ja045602n.
23. McGuinness, D. S., Olefin Oligomerization via Metallocycles: Dimerization, Trimerization, Tetramerization, and Beyond. *Chem. Rev.* **2011**, *111*, 2321-2341, 10.1021/cr100217q.
24. Agapie, T., Selective ethylene oligomerization: Recent advances in chromium catalysis and mechanistic investigations. *Coord. Chem. Rev.* **2011**, *255*, 861-880, 10.1016/j.ccr.2010.11.035.
25. Kumar, A.; Bhatti, T. M.; Goldman, A. S., Dehydrogenation of Alkanes and Aliphatic Groups by Pincer-Ligated Metal Complexes. *Chem. Rev.* **2017**, *117*, 12357-12384, 10.1021/acs.chemrev.7b00247.
26. Liu, F.; Pak, E. B.; Singh, B.; Jensen, C. M.; Goldman, A. S., Dehydrogenation of n-Alkanes Catalyzed by Iridium "Pincer" Complexes: Regioselective Formation of  $\alpha$ -Olefins. *J. Am. Chem. Soc.* **1999**, *121*, 4086-4087, 10.1021/ja983460p.
27. Baudry, D.; Ephritikhine, M.; Felkin, H.; Zakrzewski, J., The selective conversion of n-pentane into pent-1-ene via trihydrido(trans-penta-1,3-diene)bis(triarylphosphine)rhenium. *J. Chem. Soc., Chem. Commun.* **1982**, 1235-1236, 10.1039/C39820001235.
28. Dzik, W. I.; Lange, P. P.; Gooßen, L. J., Carboxylates as sources of carbon nucleophiles and electrophiles: comparison of decarboxylative and decarbonylative pathways. *Chem. Sci.* **2012**, *3*, 2671-2678, 10.1039/c2sc20312j.
29. Rodriguez, N.; Goossen, L. J., Decarboxylative coupling reactions: a modern strategy for C-C bond formation. *Chem. Soc. Rev.* **2011**, *40*, 5030-5048, 10.1039/c1cs15093f.

30. Gooßen, L. J.; Rodríguez, N.; Gooßen, K., Carboxylic Acids as Substrates in Homogeneous Catalysis. *Angew. Chem. Int. Ed.* **2008**, *47*, 3100-3120, 10.1002/anie.200704782.
31. Dawes, G. J. S.; Scott, E. L.; Le Notre, J.; Sanders, J. P. M.; Bitter, J. H., Deoxygenation of biobased molecules by decarboxylation and decarbonylation - a review on the role of heterogeneous, homogeneous and bio-catalysis. *Green Chem.* **2015**, *17*, 3231-3250, 10.1039/C5GC00023H.
32. Santillan-Jimenez, E.; Crocker, M., Catalytic deoxygenation of fatty acids and their derivatives to hydrocarbon fuels via decarboxylation/decarbonylation. *Journal of Chemical Technology & Biotechnology* **2012**, *87*, 1041-1050, 10.1002/jctb.3775.
33. Murray, R. E.; Walter, E. L.; Doll, K. M., Tandem Isomerization-Decarboxylation for Converting Alkenoic Fatty Acids into Alkenes. *ACS Catal.* **2014**, *4*, 3517-3520, 10.1021/cs501019t.
34. Biermann, U.; Friedt, W.; Lang, S.; Lühs, W.; Machmüller, G.; Metzger, J. O.; Rüschen, Klaas, M.; Schäfer, H. J.; Schneider, M. P., New Syntheses with Oils and Fats as Renewable Raw Materials for the Chemical Industry. *Angew. Chem. Int. Ed.* **2000**, *39*, 2206-2224, 10.1002/1521-3773(20000703)39:13<2206::Aid-anie2206>3.0.Co;2-p.
35. Hu, Q.; Sommerfeld, M.; Jarvis, E.; Ghirardi, M.; Posewitz, M.; Seibert, M.; Darzins, A., Microalgal triacylglycerols as feedstocks for biofuel production: perspectives and advances. *Plant J.* **2008**, *54*, 621-639, 10.1111/j.1365-3113x.2008.03492.x.
36. Higman, C. S.; Lummiss, J. A. M.; Fogg, D. E., Olefin Metathesis at the Dawn of Implementation in Pharmaceutical and Specialty-Chemicals Manufacturing. *Angew. Chem. Int. Ed.* **2016**, *55*, 3552-3565, 10.1002/anie.201506846.
37. Chikkali, S.; Mecking, S., Refining of Plant Oils to Chemicals by Olefin Metathesis. *Angew. Chem. Int. Ed.* **2012**, *51*, 5802-5808, 10.1002/anie.201107645.
38. van der Klis, F.; Le Nôtre, J.; Blaauw, R.; van Haveren, J.; van Es, D. S., Renewable linear alpha olefins by selective ethenolysis of decarboxylated unsaturated fatty acids. *Eur. J. Lipid Sci. Technol.* **2012**, *114*, 911-918, 10.1002/ejlt.201200024.
39. Spekrijse, J.; Sanders, J. P. M.; Bitter, J. H.; Scott, E. L., The Future of Ethenolysis in Biobased Chemistry. *ChemSusChem* **2017**, *10*, 470-482, 10.1002/cssc.201601256.
40. Burdett, K. A.; Harris, L. D.; Margl, P.; Maughon, B. R.; Mokhtar-Zadeh, T.; Saucier, P. C.; Wasserman, E. P., Renewable Monomer Feedstocks via Olefin Metathesis: Fundamental Mechanistic Studies of Methyl Oleate Ethenolysis with the First-Generation Grubbs Catalyst. *Organometallics* **2004**, *23*, 2027-2047, 10.1021/om0341799.
41. Thomas, R. M.; Keitz, B. K.; Champagne, T. M.; Grubbs, R. H., Highly Selective Ruthenium Metathesis Catalysts for Ethenolysis. *J. Am. Chem. Soc.* **2011**, *133*, 7490-7496, 10.1021/ja200246e.
42. Forman, G. S.; Bellabarba, R. M.; Tooze, R. P.; Slawin, A. M. Z.; Karch, R.; Winde, R., Metathesis of renewable unsaturated fatty acid esters catalysed by a phoban-indenylidene ruthenium catalyst. *J. Organomet. Chem.* **2006**, *691*, 5513-5516, 10.1016/j.jorganchem.2006.06.021.

- 
43. Schrodi, Y.; Ung, T.; Vargas, A.; Mkrtumyan, G.; Lee, C. W.; Champagne, T. M.; Pederson, R. L.; Hong, S. H., Ruthenium Olefin Metathesis Catalysts for the Ethenolysis of Renewable Feedstocks. *Clean (Weinh)* **2008**, *36*, 669-673, 10.1002/clen.200800088.
44. Nickel, A.; Ung, T.; Mkrtumyan, G.; Uy, J.; Lee, C. W.; Stoianova, D.; Papazian, J.; Wei, W.-H.; Mallari, A.; Schrodi, Y.; Pederson, R. L., A Highly Efficient Olefin Metathesis Process for the Synthesis of Terminal Alkenes from Fatty Acid Esters. *Top. Catal.* **2012**, *55*, 518-523, 10.1007/s11244-012-9830-2.
45. Mol, J. C., Metathesis of unsaturated fatty acid esters and fatty oils. *J. Mol. Catal.* **1994**, *90*, 185-199, 10.1016/0304-5102(94)00009-3.
46. Marx, V. M.; Sullivan, A. H.; Melaimi, M.; Virgil, S. C.; Keitz, B. K.; Weinberger, D. S.; Bertrand, G.; Grubbs, R. H., Cyclic Alkyl Amino Carbene (CAAC) Ruthenium Complexes as Remarkably Active Catalysts for Ethenolysis. *Angew. Chem. Int. Ed.* **2015**, *54*, 1919-1923, 10.1002/anie.201410797.
47. Bidange, J.; Fischmeister, C.; Bruneau, C., Ethenolysis: A Green Catalytic Tool to Cleave Carbon-Carbon Double Bonds. *Chemistry* **2016**, *22*, 12226-44, 10.1002/chem.201601052.
48. Doll, K. M.; Bantchev, G. B.; Walter, E. L.; Murray, R. E.; Appell, M.; Lansing, J. C.; Moser, B. R., Parameters Governing Ruthenium Sawhorse-Based Decarboxylation of Oleic Acid. *Ind. Eng. Chem. Res.* **2017**, *56*, 864-871, 10.1021/acs.iecr.6b04555.
49. Foglia, T. A.; Barr, P. A., Decarbonylation dehydration of fatty acids to alkenes in the presence of transition metal complexes. *J. Am. Oil Chem. Soc.* **1976**, *53*, 737-741, 10.1007/bf02635473.
50. Bacha, J. D.; Kochi, J. K., Alkenes from acids by oxidative decarboxylation. *Tetrahedron* **1968**, *24*, 2215-2226, 10.1016/0040-4020(68)88124-4.
51. Sheldon, R. A.; Kochi, J. K., Oxidative Decarboxylation of Acids by Lead Tetraacetate. In *Organic Reactions*, John Wiley and Sons, Inc.: 2011; pp 279-421, 10.1002/0471264180.or019.04.
52. Kolbe, H., Untersuchungen über die Elektrolyse organischer Verbindungen. *Liebigs Ann. Chem.* **1849**, *69*, 257-294, 10.1002/jlac.18490690302.
53. Anderson, J. M.; Kochi, J. K., Silver(II) complexes in oxidative decarboxylation of acids. *J. Org. Chem.* **1970**, *35*, 986-989, 10.1021/jo00829a026.
54. van der Klis, F.; van den Hoorn, M. H.; Blaauw, R.; van Haveren, J.; van Es, D. S., Oxidative decarboxylation of unsaturated fatty acids. *Eur. J. Lipid Sci. Technol.* **2011**, *113*, 562-571, 10.1002/ejlt.201000126.
55. Chatterjee, A.; Hopen Eliasson, S. H.; Jensen, V. R., Selective production of linear alpha-olefins via catalytic deoxygenation of fatty acids and derivatives. *Catal. Sci. Technol.* **2018**, *8*, 1487-1499, 10.1039/C7CY02580G.
56. Mäki-Arvela, P.; Kubickova, I.; Snåre, M.; Eränen, K.; Murzin, D. Y., Catalytic Deoxygenation of Fatty Acids and Their Derivatives. *Energy Fuels* **2007**, *21*, 30-41, 10.1021/ef060455v.
57. Prince, R. H.; Raspin, K. A., Olefin formation from saturated aldehydes and acids by reaction with ruthenium and rhodium complexes. *Chem. Commun. (London)* **1966**, 156-157, 10.1039/C19660000156.

58. Tsuji, J.; Ohno, K., Organic syntheses by means of noble metal compounds. XXXIV. Carbonylation and decarbonylation reactions catalyzed by palladium. *J. Am. Chem. Soc.* **1968**, *90*, 94-98, 10.1021/ja01003a017.
59. Tsuji, J.; Kiyotaka, O., Decarbonylation reactions using transition metal compounds. *Synthesis* **1969**, *1969*, 157-169.
60. Miller, J. A.; Nelson, J. A.; Byrne, M. P., A Highly Catalytic and Selective Conversion of Carboxylic-Acids to 1-Alkenes of One Less Carbon-Atom. *J. Org. Chem.* **1993**, *58*, 18-20, DOI 10.1021/jo00053a008.
61. Gooßen, L. J.; Rodriguez, N., A mild and efficient protocol for the conversion of carboxylic acids to olefins by a catalytic decarbonylative elimination reaction. *Chem. Commun.* **2004**, *6*, 724-5, 10.1039/b316613a.
62. Kraus, G. A.; Riley, S., A Large-Scale Synthesis of alpha-Olefins and alpha,omega-Dienes. *Synthesis* **2012**, *44*, 3003-3005, 10.1055/s-0031-1290400.
63. Liu, Y.; Kim, K. E.; Herbert, M. B.; Fedorov, A.; Grubbs, R. H.; Stoltz, B. M., Palladium-Catalyzed Decarbonylative Dehydration of Fatty Acids for the Production of Linear Alpha Olefins. *Adv. Synth. Catal.* **2014**, *356*, 130-136, 10.1002/adsc.201301109.
64. Le Nôtre, J.; Scott, E. L.; Franssen, M. C. R.; Sanders, J. P. M., Selective preparation of terminal alkenes from aliphatic carboxylic acids by a palladium-catalysed decarbonylation-elimination reaction. *Tetrahedron Lett.* **2010**, *51*, 3712-3715, 10.1016/j.tetlet.2010.05.018.
65. Liu, Y.; Virgil, S. C.; Grubbs, R. H.; Stoltz, B. M., Palladium-Catalyzed Decarbonylative Dehydration for the Synthesis of  $\alpha$ -Vinyl Carbonyl Compounds and Total Synthesis of (-)-Aspewentins A, B, and C. *Angew. Chem. Int. Ed.* **2015**, *54*, 11800-11803, 10.1002/anie.201505161.
66. John, A.; Dereli, B.; Ortuño, M. A.; Johnson, H. E.; Hillmyer, M. A.; Cramer, C. J.; Tolman, W. B., Selective Decarbonylation of Fatty Acid Esters to Linear  $\alpha$ -Olefins. *Organometallics* **2017**, *36*, 2956-2964, 10.1021/acs.organomet.7b00411.
67. John, A.; Hogan, L. T.; Hillmyer, M. A.; Tolman, W. B., Olefins from biomass feedstocks: catalytic ester decarbonylation and tandem Heck-type coupling. *Chem. Commun.* **2015**, *51*, 2731-2733, 10.1039/C4CC09003A.
68. Miranda, M. O.; Pietrangelo, A.; Hillmyer, M. A.; Tolman, W. B., Catalytic decarbonylation of biomass-derived carboxylic acids as efficient route to commodity monomers. *Green Chem.* **2012**, *14*, 490-494, 10.1039/C2GC16115J.
69. Ternel, J.; Léger, B.; Monflier, E.; Hapiot, F., Amines as effective ligands in iridium-catalyzed decarbonylative dehydration of biosourced substrates. *Catal. Sci. Technol.* **2018**, *8*, 3948-3953, 10.1039/C8CY00621K.
70. Maetani, S.; Fukuyama, T.; Suzuki, N.; Ishihara, D.; Ryu, I., Efficient Iridium-Catalyzed Decarbonylation Reaction of Aliphatic Carboxylic Acids Leading to Internal or Terminal Alkenes. *Organometallics* **2011**, *30*, 1389-1394, 10.1021/om1009268.
71. Ternel, J.; Lebarbé, T.; Monflier, E.; Hapiot, F., Catalytic Decarbonylation of Biosourced Substrates. *ChemSusChem* **2015**, *8*, 1585-1592, 10.1002/cssc.201500214.
72. Maetani, S.; Fukuyama, T.; Suzuki, N.; Ishihara, D.; Ryu, I., Iron-catalyzed decarbonylation reaction of aliphatic carboxylic acids leading to alpha-olefins. *Chem. Commun.* **2012**, *48*, 2552-2554, 10.1039/C2CC18093F.



- 
73. John, A.; Hillmyer, M. A.; Tolman, W. B., Anhydride-Additive-Free Nickel-Catalyzed Deoxygenation of Carboxylic Acids to Olefins. *Organometallics* **2017**, *36*, 506-509, 10.1021/acs.organomet.6b00940.
74. John, A.; Miranda, M. O.; Ding, K.; Dereli, B.; Ortuño, M. A.; LaPointe, A. M.; Coates, G. W.; Cramer, C. J.; Tolman, W. B., Nickel Catalysts for the Dehydrative Decarbonylation of Carboxylic Acids to Alkenes. *Organometallics* **2016**, *35*, 2391-2400, 10.1021/acs.organomet.6b00415.
75. Cataldo, F., Linear olefins from fatty acids with Ni(I) or Rh(I) catalysts. *Eur. Chem. Bull.* **2019**, *8*, 88-95, 10.17628/ecb.2019.8.%25p.
76. Hagen, J., *Industrial catalysis: a practical approach*. John Wiley & Sons: 2015.
77. Miyazaki, H.; Herbert, M. B.; Liu, P.; Dong, X.; Xu, X.; Keitz, B. K.; Ung, T.; Mkrtumyan, G.; Houk, K. N.; Grubbs, R. H., Z-Selective Ethenolysis with a Ruthenium Metathesis Catalyst: Experiment and Theory. *J. Am. Chem. Soc.* **2013**, *135*, 5848-5858, 10.1021/ja4010267.
78. Sanford, M. S.; Love, J. A.; Grubbs, R. H., Mechanism and Activity of Ruthenium Olefin Metathesis Catalysts. *J. Am. Chem. Soc.* **2001**, *123*, 6543-6554, 10.1021/ja010624k.
79. Sanford, M. S.; Ulman, M.; Grubbs, R. H., New Insights into the Mechanism of Ruthenium-Catalyzed Olefin Metathesis Reactions. *J. Am. Chem. Soc.* **2001**, *123*, 749-750, 10.1021/ja003582t.
80. Dias, E. L.; Nguyen, S. T.; Grubbs, R. H., Well-Defined Ruthenium Olefin Metathesis Catalysts: Mechanism and Activity. *J. Am. Chem. Soc.* **1997**, *119*, 3887-3897, 10.1021/ja963136z.
81. Ortuño, M. A.; Dereli, B.; Cramer, C. J., Mechanism of Pd-Catalyzed Decarbonylation of Biomass-Derived Hydrocinnamic Acid to Styrene following Activation as an Anhydride. *Inorg. Chem.* **2016**, *55*, 4124-4131, 10.1021/acs.inorgchem.5b02664.
82. Hopen Eliasson, S. H.; Jensen, V. R., Benefit of a hemilabile ligand in deoxygenation of fatty acids to 1-alkenes. *Faraday Discuss.* **2019**, 10.1039/C9FD00037B.
83. Hopen Eliasson, S. H.; Chatterjee, A.; Occhipinti, G.; Jensen, V. R., Green Solvent for the Synthesis of Linear  $\alpha$ -Olefins from Fatty Acids. *ACS Sustain. Chem. Eng.* **2019**, *7*, 4903-4911, 10.1021/acssuschemeng.8b05523.
84. Eliasson, S.; Chatterjee, A.; Occhipinti, G.; Jensen, V., The Mechanism of Rh-Catalyzed Transformation of Fatty Acids to Linear Alpha olefins. *Inorganics* **2017**, *5*, 87, 10.3390/inorganics5040087.
85. Chatterjee, A.; Hopen Eliasson, S. H.; Törnroos, K. W.; Jensen, V. R., Palladium Precatalysts for Decarbonylative Dehydration of Fatty Acids to Linear Alpha Olefins. *ACS Catal.* **2016**, *6*, 7784-7789, 10.1021/acscatal.6b02460.
86. Vogiatzis, K. D.; Polynski, M. V.; Kirkland, J. K.; Townsend, J.; Hashemi, A.; Liu, C.; Pidko, E. A., Computational Approach to Molecular Catalysis by 3d Transition Metals: Challenges and Opportunities. *Chem. Rev.* **2019**, *119*, 2453-2523, 10.1021/acs.chemrev.8b00361.
87. Ahn, S.; Hong, M.; Sundararajan, M.; Ess, D. H.; Baik, M.-H., Design and Optimization of Catalysts Based on Mechanistic Insights Derived from Quantum

- Chemical Reaction Modeling. *Chem. Rev.* **2019**, *119*, 6509-6560, 10.1021/acs.chemrev.9b00073.
88. Houk, K. N.; Liu, F., Holy Grails for Computational Organic Chemistry and Biochemistry. *Acc. Chem. Res.* **2017**, *50*, 539-543, 10.1021/acs.accounts.6b00532.
89. Jensen, F., *Introduction to computational chemistry*. 2nd ed. ed.; Wiley: Chichester, 2007.
90. Koch, W., *A chemist's guide to density functional theory*. 2nd ed. ed.; Wiley-VCH: Weinheim, 2001.
91. Leach, A. R., *Molecular modelling : principles and applications*. 2nd ed. ed.; Prentice Hall: Harlow, 2001.
92. Szabo, A., *Modern quantum chemistry : introduction to advanced electronic structure theory*. 1st ed., rev. ed.; Dover Publications: Mineola, N.Y, 1996.
93. Minenkov, Y.; Occhipinti, G.; Jensen, V. R., Metal-Phosphine Bond Strengths of the Transition Metals: A Challenge for DFT. *J. Phys. Chem. A* **2009**, *113*, 11833-11844, 10.1021/jp902940c.
94. Zhao, Y.; Truhlar, D. G., Applications and validations of the Minnesota density functionals. *Chem. Phys. Lett.* **2011**, *502*, 1-13, DOI 10.1016/j.cplett.2010.11.060.
95. Zhao, Y.; Truhlar, D. G., Density Functionals with Broad Applicability in Chemistry. *Acc. Chem. Res.* **2008**, *41*, 157-167, DOI 10.1021/ar700111a.
96. Zhao, Y.; Truhlar, D. G., A new local density functional for main-group thermochemistry, transition metal bonding, thermochemical kinetics, and noncovalent interactions. *J. Chem. Phys.* **2006**, *125*, 194101-194118, DOI 10.1063/1.2370993.
97. Grimme, S., Semiempirical GGA-type density functional constructed with a long-range dispersion correction. *J. Comput. Chem.* **2006**, *27*, 1787-1799, 10.1002/jcc.20495.
98. Grimme, S., Accurate description of van der Waals complexes by density functional theory including empirical corrections. *J. Comput. Chem.* **2004**, *25*, 1463-1473, 10.1002/jcc.20078.
99. Wu, Q.; Yang, W., Empirical correction to density functional theory for van der Waals interactions. *J. Chem. Phys.* **2002**, *116*, 515-524, 10.1063/1.1424928.
100. Grimme, S.; Ehrlich, S.; Goerigk, L., Effect of the damping function in dispersion corrected density functional theory. *J. Comput. Chem.* **2011**, *32*, 1456-1465, 10.1002/jcc.21759.
101. Smith, D. G. A.; Burns, L. A.; Patkowski, K.; Sherrill, C. D., Revised Damping Parameters for the D3 Dispersion Correction to Density Functional Theory. *J. Phys. Chem. Lett.* **2016**, *7*, 2197-2203, 10.1021/acs.jpcclett.6b00780.
102. Ribeiro, R. F.; Marenich, A. V.; Cramer, C. J.; Truhlar, D. G., Use of Solution-Phase Vibrational Frequencies in Continuum Models for the Free Energy of Solvation. *J. Phys. Chem. B* **2011**, *115*, 14556-14562, 10.1021/jp205508z.
103. Minenkov, Y.; Occhipinti, G.; Jensen, V. R., Complete Reaction Pathway of Ruthenium-Catalyzed Olefin Metathesis of Ethyl Vinyl Ether: Kinetics and Mechanistic Insight from DFT. *Organometallics* **2013**, *32*, 2099-2111, 10.1021/om301192a.
104. Krogh-Jespersen, K.; Czerw, M.; Summa, N.; Renkema, K. B.; Achord, P. D.; Goldman, A. S., On the Mechanism of (PCP)Ir-Catalyzed Acceptorless

- Dehydrogenation of Alkanes: A Combined Computational and Experimental Study. *J. Am. Chem. Soc.* **2002**, *124*, 11404-11416, 10.1021/ja012460d.
105. Ågren, H.; Mikkelsen, K. V., Theory of solvent effects on electronic spectra. *Comput. Theor. Chem.* **1991**, *234*, 425-467, 10.1016/0166-1280(91)89027-X.
106. Cramer, C. J.; Truhlar, D. G., Implicit Solvation Models: Equilibria, Structure, Spectra, and Dynamics. *Chem. Rev.* **1999**, *99*, 2161, 10.1021/cr960149m.
107. Smith, P.; Pettitt, B. M., MODELING SOLVENT IN BIOMOLECULAR SYSTEMS. *J. Phys. Chem.* **1994**, *98*, 9700-9711, 10.1021/j100090a002.
108. Tomasi, J.; Persico, M., Molecular interactions in solution: An overview of methods based on continuous distributions of the solvent. *Chem. Rev.* **1994**, *94*, 2027, 10.1021/cr00031a013.
109. Tomasi, J., Thirty years of continuum solvation chemistry: a review, and prospects for the near future. *Theor. Chem. Acc* **2004**, *112*, 184-203, 10.1007/s00214-004-0582-3.
110. Tomasi, J.; Mennucci, B.; Cammi, R., Quantum mechanical continuum solvation models. *Chem. Rev.* **2005**, *105*, 2999, 10.1021/cr9904009.
111. Marenich, A. V.; Cramer, C. J.; Truhlar, D. G., Universal solvation model based on solute electron density and on a continuum model of the solvent defined by the bulk dielectric constant and atomic surface tensions. *J. Phys. Chem. B* **2009**, *113*, 6378-6396.
112. Tshipis, A. C.; Orpen, A. G.; Harvey, J. N., Substituent effects and the mechanism of alkene metathesis catalyzed by ruthenium dichloride catalysts. *Dalton Transactions* **2005**, 2849-2858, 10.1039/B506929G.
113. Allen, F. H., The Cambridge Structural Database: a quarter of a million crystal structures and rising. *Acta Cryst. B* **2002**, *58*, 380-388.
114. Frisch, M. J.; Trucks, G. W.; Schlegel, H. B.; Scuseria, G. E.; Robb, M. A.; Cheeseman, J. R.; Scalmani, G.; Barone, V.; Mennucci, B.; Petersson, G. A.; Nakatsuji, H.; Caricato, M.; Li, X.; Hratchian, H. P.; Izmaylov, A. F.; Bloino, J.; Zheng, G.; Sonnenberg, J. L.; Hada, M.; Ehara, M.; Toyota, K.; Fukuda, R.; Hasegawa, J.; Ishida, M.; Nakajima, T.; Honda, Y.; Kitao, O.; Nakai, H.; Vreven, T.; Montgomery Jr., J. A.; Peralta, J. E.; Ogliaro, F.; Bearpark, M. J.; Heyd, J.; Brothers, E. N.; Kudin, K. N.; Staroverov, V. N.; Kobayashi, R.; Normand, J.; Raghavachari, K.; Rendell, A. P.; Burant, J. C.; Iyengar, S. S.; Tomasi, J.; Cossi, M.; Rega, N.; Millam, N. J.; Klene, M.; Knox, J. E.; Cross, J. B.; Bakken, V.; Adamo, C.; Jaramillo, J.; Gomperts, R.; Stratmann, R. E.; Yazyev, O.; Austin, A. J.; Cammi, R.; Pomelli, C.; Ochterski, J. W.; Martin, R. L.; Morokuma, K.; Zakrzewski, V. G.; Voth, G. A.; Salvador, P.; Dannenberg, J. J.; Dapprich, S.; Daniels, A. D.; Farkas, Ö.; Foresman, J. B.; Ortiz, J. V.; Cioslowski, J.; Fox, D. J. *Gaussian 09*, Gaussian, Inc.: Wallingford, CT, USA, 2009.
115. Becke, A. D., Density-functional thermochemistry. V. Systematic optimization of exchange-correlation functionals. *J. Chem. Phys.* **1997**, *107*, 8554-8560, 10.1063/1.475007.
116. Chai, J.-D.; Head-Gordon, M., Long-range corrected hybrid density functionals with damped atom-atom dispersion corrections. *Phys. Chem. Chem. Phys.* **2008**, *10*, 6615-6620, 10.1039/B810189B.

117. Gusev, D. G., Assessing the Accuracy of M06-L Organometallic Thermochemistry. *Organometallics* **2013**, *32*, 4239-4243, 10.1021/om400412p.
118. Sieffert, N.; Bühl, M., Noncovalent Interactions in a Transition-Metal Triphenylphosphine Complex: a Density Functional Case Study. *Inorg. Chem.* **2009**, *48*, 4622-4624, 10.1021/ic900347e.
119. Wavefunction, I. *Spartan '08*, Irvine, CA, 2008.
120. Allen, F. H., The Cambridge Structural Database: a quarter of a million crystal structures and rising. *Acta Cryst. B* **2002**, *58*, 380-8.
121. Halgren, T. A., Merck molecular force field. I. Basis, form, scope, parameterization, and performance of MMFF94. *J. Comput. Chem.* **1996**, *17*, 490-519, 10.1002/(SICI)1096-987X(199604)17:5/6<490::AID-JCC1>3.0.CO;2-P.
122. Stewart, J. J. P., Optimization of parameters for semiempirical methods IV: extension of MNDO, AM1, and PM3 to more main group elements. *J. Mol. Model.* **2004**, *10*, 155-164, 10.1007/s00894-004-0183-z.
123. Stewart, J. J. P., Optimization of parameters for semiempirical methods. III Extension of PM3 to Be, Mg, Zn, Ga, Ge, As, Se, Cd, In, Sn, Sb, Te, Hg, Tl, Pb, and Bi. *J. Comput. Chem.* **1991**, *12*, 320-341, 10.1002/jcc.540120306.
124. Stewart, J. J. P., Optimization of parameters for semiempirical methods II. Applications. *J. Comput. Chem.* **1989**, *10*, 221-264, 10.1002/jcc.540100209.
125. Stewart, J. J. P., Optimization of parameters for semiempirical methods I. Method. *J. Comput. Chem.* **1989**, *10*, 209-220, 10.1002/jcc.540100208.
126. Wheeler, S. E.; Houk, K. N., Integration Grid Errors for Meta-GGA-Predicted Reaction Energies: Origin of Grid Errors for the M06 Suite of Functionals. *J. Chem. Theory Comput.* **2010**, *6*, 395-404, 10.1021/ct900639j.
127. Johnson, E. R.; Mackie, I. D.; DiLabio, G. A., Dispersion interactions in density-functional theory. *J. Phys. Org. Chem.* **2009**, *22*, 1127-1135.
128. Johnson, E. R.; Becke, A. D.; Sherrill, C. D.; DiLabio, G. A., Oscillations in meta-generalized-gradient approximation potential energy surfaces for dispersion-bound complexes. *J. Chem. Phys.* **2009**, *131*, 034111.
129. Peterson, K. A.; Figgen, D.; Dolg, M.; Stoll, H., Energy-consistent relativistic pseudopotentials and correlation consistent basis sets for the 4 d elements Y–Pd. *J. Chem. Phys.* **2007**, *126*, 124101.
130. Woon, D. E.; Dunning, T. H., Gaussian basis sets for use in correlated molecular calculations. III. The atoms aluminum through argon. *J. Chem. Phys.* **1993**, *98*, 1358-1371, 10.1063/1.464303.
131. Dunning, T. H., Gaussian basis sets for use in correlated molecular calculations. I. The atoms boron through neon and hydrogen. *J. Chem. Phys.* **1989**, *90*, 1007-1023, 10.1063/1.456153.
132. Hratchian, H. P.; Schlegel, H. B., Using Hessian Updating To Increase the Efficiency of a Hessian Based Predictor-Corrector Reaction Path Following Method. *J. Chem. Theory Comput.* **2005**, *1*, 61-69, 10.1021/ct0499783.
133. Page, M.; Doubleday, C., Jr., J. W. M., Following steepest descent reaction paths. The use of higher energy derivatives with ab initio electronic structure methods. *J. Chem. Phys.* **1990**, *93*, 5634-5642, 10.1063/1.459634.
134. Fukui, K., The path of chemical reactions - the IRC approach. *Acc. Chem. Res.* **1981**, *14*, 363-368, 10.1021/ar00072a001.

135. Glendening, E. D.; Landis, C. R.; Weinhold, F., NBO 6.0: Natural bond orbital analysis program. *J. Comput. Chem.* **2013**, *34*, 1429-1437.
136. Feller, D., The role of databases in support of computational chemistry calculations. *J. Comput. Chem.* **1996**, *17*, 1571-1586.
137. Kendall, R. A.; Dunning, T. H.; Harrison, R. J., Electron affinities of the first-row atoms revisited. Systematic basis sets and wave functions. *J. Chem. Phys.* **1992**, *96*, 6796-6806.
138. Perdew, J. P.; Burke, K.; Ernzerhof, M., Generalized Gradient Approximation Made Simple [Phys. Rev. Lett. 77, 3865 (1996)]. *Phys. Rev. Lett.* **1997**, *78*, 1396-1396, 10.1103/PhysRevLett.78.1396.
139. Perdew, J. P.; Burke, K.; Ernzerhof, M., Generalized Gradient Approximation Made Simple. *Phys. Rev. Lett.* **1996**, *77*, 3865-3868, 10.1103/PhysRevLett.77.3865.
140. Becke, A. D., Density-functional thermochemistry. III. The role of exact exchange. *J. Chem. Phys.* **1993**, *98*, 5648-5652, 10.1063/1.464913.
141. Marenich, A. V.; Cramer, C. J.; Truhlar, D. G., Universal Solvation Model Based on Solute Electron Density and on a Continuum Model of the Solvent Defined by the Bulk Dielectric Constant and Atomic Surface Tensions. *J. Phys. Chem. B* **2009**, *113*, 6378-6395.
142. Fristrup, P.; Kreis, M.; Palmelund, A.; Norrby, P.-O.; Madsen, R., The mechanism for the rhodium-catalyzed decarbonylation of aldehydes: a combined experimental and theoretical study. *J. Am. Chem. Soc.* **2008**, *130*, 5206-5215.
143. Luo, X.; Bai, R.; Liu, S.; Shan, C.; Chen, C.; Lan, Y., Mechanism of Rhodium-Catalyzed Formyl Activation: A Computational Study. *J. Org. Chem.* **2016**, *81*, 2320-2326, 10.1021/acs.joc.5b02828.
144. Alagona, G.; Ghio, C., Rhodium-Catalyzed Hydroformylation of Ketal-Masked  $\beta$ -Isophorone: Computational Explanation for the Unexpected Reaction Evolution of the Tertiary Rh-Alkyl via an Exocyclic  $\beta$ -Elimination Derivative. *J. Phys. Chem. A* **2015**, *119*, 5117-5133, 10.1021/jp508294z.
145. Murphy, S. K.; Park, J.-W.; Cruz, F. A.; Dong, V. M., Rh-catalyzed C-C bond cleavage by transfer hydroformylation. *Science* **2015**, *347*, 56-60, 10.1126/science.1261232.
146. Miller, J. A.; Nelson, J. A., Oxidative addition of carboxylic acid anhydrides to rhodium (I) phosphine complexes to produce novel rhodium (III) acyl derivatives. *Organometallics* **1991**, *10*, 2958-2961.
147. Gooßen, L. J.; Koley, D.; Hermann, H.; Thiel, W., The mechanism of the oxidative addition of aryl halides to Pd-catalysts: a DFT investigation. *Chem. Commun.* **2004**, 2141-2143, 10.1039/B409144B.
148. Viciu, M. S.; Germaneau, R. F.; Navarro-Fernandez, O.; Stevens, E. D.; Nolan, S. P., Activation and Reactivity of (NHC)Pd(allyl)Cl (NHC = N-Heterocyclic Carbene) Complexes in Cross-Coupling Reactions. *Organometallics* **2002**, *21*, 5470-5472, 10.1021/om020804i.
149. Marion, N.; Navarro, O.; Mei, J.; Stevens, E. D.; Scott, N. M.; Nolan, S. P., Modified (NHC)Pd(allyl)Cl (NHC = N-Heterocyclic Carbene) Complexes for Room-Temperature Suzuki-Miyaura and Buchwald-Hartwig Reactions. *J. Am. Chem. Soc.* **2006**, *128*, 4101-4111, 10.1021/ja057704z.

150. Hruszkewycz, D. P.; Balcells, D.; Guard, L. M.; Hazari, N.; Tilset, M., Insight into the Efficiency of Cinnamyl-Supported Precatalysts for the Suzuki–Miyaura Reaction: Observation of Pd(I) Dimers with Bridging Allyl Ligands During Catalysis. *J. Am. Chem. Soc.* **2014**, *136*, 7300–7316, 10.1021/ja412565c.
151. Johansson Seechurn, C. C. C.; Parisel, S. L.; Colacot, T. J., Air-Stable Pd(R-allyl)Cl (L= Q-Phos, P(t-Bu)<sub>3</sub>, etc.) Systems for C–C/N Couplings: Insight into the Structure–Activity Relationship and Catalyst Activation Pathway. *J. Org. Chem.* **2011**, *76*, 7918–7932, 10.1021/jo2013324.
152. Marion, N.; Nolan, S. P., Well-Defined N-Heterocyclic Carbenes–Palladium(II) Precatalysts for Cross-Coupling Reactions. *Acc. Chem. Res.* **2008**, *41*, 1440–1449, 10.1021/ar800020y.
153. Johns, A. M.; Utsunomiya, M.; Incarvito, C. D.; Hartwig, J. F., A Highly Active Palladium Catalyst for Intermolecular Hydroamination. Factors that Control Reactivity and Additions of Functionalized Anilines to Dienes and Vinylarenes. *J. Am. Chem. Soc.* **2006**, *128*, 1828–1839, 10.1021/ja056003z.
154. Borjian, S.; Baird, M. C., NMR Studies of the Species Present in Cross-Coupling Catalysis Systems Involving Pd( $\eta^3$ -1-Ph-C<sub>3</sub>H<sub>4</sub>)( $\eta^5$ -C<sub>5</sub>H<sub>5</sub>) and [Pd( $\eta^3$ -1-Ph-C<sub>3</sub>H<sub>4</sub>)Cl]<sub>2</sub> Activated by PBut<sub>3</sub>, XPhos, and Mor-Dalpos: Nonexistence of Pd(XPhos)<sub>n</sub> and Pd(Mor-Dalpos)<sub>n</sub> (n = 1, 2) at Moderate Temperatures. *Organometallics* **2014**, *33*, 3936–3940, 10.1021/om500618e.
155. Melvin, P. R.; Balcells, D.; Hazari, N.; Nova, A., Understanding Precatalyst Activation in Cross-Coupling Reactions: Alcohol Facilitated Reduction from Pd(II) to Pd(0) in Precatalysts of the Type ( $\eta^3$ -allyl)Pd(L)(Cl) and ( $\eta^3$ -indenyl)Pd(L)(Cl). *ACS Catal.* **2015**, *5*, 5596–5606, 10.1021/acscatal.5b01291.
156. Sun, X.; Chen, J.; Ritter, T., Catalytic dehydrogenative decarboxyolefination of carboxylic acids. *Nat. Chem.* **2018**, *10*, 1229–1233, 10.1038/s41557-018-0142-4.
157. Tlahuext-Aca, A.; Candish, L.; Garza-Sanchez, R. A.; Glorius, F., Decarboxylative Olefination of Activated Aliphatic Acids Enabled by Dual Organophotoredox/Copper Catalysis. *ACS Catal.* **2018**, *8*, 1715–1719, 10.1021/acscatal.7b04281.
158. Adams, G. M.; Weller, A. S., POP-type ligands: Variable coordination and hemilabile behaviour. *Coord. Chem. Rev.* **2018**, *355*, 150–172, 10.1016/j.ccr.2017.08.004.
159. Venkateswaran, R.; Balakrishna, M. S.; Mobin, S. M.; Tuononen, H. M., Copper(I) Complexes of Bis(2-(diphenylphosphino)phenyl) Ether: Synthesis, Reactivity, and Theoretical Calculations. *Inorg. Chem.* **2007**, *46*, 6535–6541, 10.1021/ic7005474.
160. Ohshima, T.; Miyamoto, Y.; Ipposhi, J.; Nakahara, Y.; Utsunomiya, M.; Mashima, K., Platinum-Catalyzed Direct Amination of Allylic Alcohols under Mild Conditions: Ligand and Microwave Effects, Substrate Scope, and Mechanistic Study. *J. Am. Chem. Soc.* **2009**, *131*, 14317–14328, 10.1021/ja9046075.
161. Ortuño, M. A.; López, N., Creating Cavities at Palladium–Phosphine Interfaces for Enhanced Selectivity in Heterogeneous Biomass Conversion. *ACS Catal.* **2018**, *8*, 6138–6145, 10.1021/acscatal.8b01302.

162. Dimethyl sulfoxide solubility data.  
<https://www.gaylordchemical.com/literature/dmsol-solubility-data/> (accessed 15.11.19).
163. Reichardt, C., *Solvents and solvent effects in organic chemistry*. 3rd., updated and enl. ed. ed.; Wiley-VCH: Weinheim, 2003.
164. George, J.; Sastry, N. V., Densities, Viscosities, Speeds of Sound, and Relative Permittivities for Water + Cyclic Amides (2-Pyrrolidinone, 1-Methyl-2-pyrrolidinone, and 1-Vinyl-2-pyrrolidinone) at Different Temperatures. *J. Chem. Eng. Data* **2004**, *49*, 235-242, 10.1021/je0340809.
165. Ismalaj, E.; Strappaveccia, G.; Ballerini, E.; Elisei, F.; Piermatti, O.; Gelman, D.; Vaccaro, L.,  $\gamma$ -Valerolactone as a Renewable Dipolar Aprotic Solvent Deriving from Biomass Degradation for the Hiyama Reaction. *ACS Sustain. Chem. Eng.* **2014**, *2*, 2461-2464, 10.1021/sc5004727.
166. Horváth, I. T.; Mehdi, H.; Fábos, V.; Boda, L.; Mika, L. T.,  $\gamma$ -Valerolactone— a sustainable liquid for energy and carbon-based chemicals. *Green Chem.* **2008**, *10*, 238-242, 10.1039/B712863K.
167. Feller, M.; Gellrich, U.; Anaby, A.; Diskin-Posner, Y.; Milstein, D., Reductive Cleavage of CO<sub>2</sub> by Metal–Ligand-Cooperation Mediated by an Iridium Pincer Complex. *J. Am. Chem. Soc.* **2016**, *138*, 6445-6454, 10.1021/jacs.6b00202.
168. Langer, J.; Imhof, W.; Fabra, M. J.; García-Orduña, P.; Görls, H.; Lahoz, F. J.; Oro, L. A.; Westerhausen, M., Reversible CO<sub>2</sub> Fixation by Iridium(I) Complexes Containing Me<sub>2</sub>PhP as Ligand. *Organometallics* **2010**, *29*, 1642-1651, 10.1021/om900918t.
169. Anklin, C.; Pregosin, P. S.; Bachechi, F.; Mura, P.; Zambonelli, L., Acyl-platinum(II) and -palladium(II) complexes derived from 2-hydroxybenzaldehyde derivatives. X-ray structure of [Pt(OC<sub>6</sub>H<sub>4</sub>CO)(P(p-CH<sub>3</sub>C<sub>6</sub>H<sub>4</sub>)<sub>3</sub>)<sub>2</sub>]. *J. Organomet. Chem.* **1981**, *222*, 175-185, 10.1016/S0022-328X(00)89025-7.
170. Blake, D. M.; Shields, S.; Wyman, L., Reactions of carboxylic acid anhydrides with nucleophilic iridium(I) and platinum(0) complexes. *Inorg. Chem.* **1974**, *13*, 1595-1600, 10.1021/ic50137a011.
171. Clements, J. H., Reactive Applications of Cyclic Alkylene Carbonates. *Ind. Eng. Chem. Res.* **2003**, *42*, 663-674, 10.1021/ie020678i.
172. Reichardt, C.; Welton, T., *Solvents and solvent effects in organic chemistry*. John Wiley & Sons: 2011.
173. Yeap, J. H.; Héroguel, F.; Shahab, R. L.; Rozmyslowicz, B.; Studer, M. H.; Luterbacher, J. S., Selectivity Control during the Single-Step Conversion of Aliphatic Carboxylic Acids to Linear Olefins. *ACS Catal.* **2018**, *8*, 10769-10773, 10.1021/acscatal.8b03370.
174. Chatterjee, A.; Jensen, V. R., A Heterogeneous Catalyst for Transformation of Fatty Acids to Alpha Olefins. *ACS Catal.* **2017**, *7*, 2543-2547, 10.1021/acscatal.6b03460.
175. DeAngelis, A. J.; Gildner, P. G.; Chow, R.; Colacot, T. J., Generating Active “L-Pd(0)” via Neutral or Cationic  $\pi$ -Allylpalladium Complexes Featuring Biaryl/Bipyrazolylphosphines: Synthetic, Mechanistic, and Structure–Activity Studies in Challenging Cross-Coupling Reactions. *J. Org. Chem.* **2015**, *80*, 6794-6813, 10.1021/acs.joc.5b01005.

- 
176. Melvin, P. R.; Nova, A.; Balcells, D.; Dai, W.; Hazari, N.; Hruszkewycz, D. P.; Shah, H. P.; Tudge, M. T., Design of a Versatile and Improved Precatalyst Scaffold for Palladium-Catalyzed Cross-Coupling: ( $\eta^3$ -1-tBu-indenyl) $_2$ ( $\mu$ -Cl) $_2$ Pd $_2$ . *ACS Catal.* **2015**, *5*, 3680-3688, 10.1021/acscatal.5b00878.
177. Ji, Y.; Plata, R. E.; Regens, C. S.; Hay, M.; Schmidt, M.; Razler, T.; Qiu, Y.; Geng, P.; Hsiao, Y.; Rosner, T.; Eastgate, M. D.; Blackmond, D. G., Mono-Oxidation of Bidentate Bis-phosphines in Catalyst Activation: Kinetic and Mechanistic Studies of a Pd/Xantphos-Catalyzed C–H Functionalization. *J. Am. Chem. Soc.* **2015**, *137*, 13272-13281, 10.1021/jacs.5b01913.
178. Grushin, V. V., Synthesis of Hemilabile Phosphine–Phosphine Oxide Ligands via the Highly Selective Pd-Catalyzed Mono-oxidation of Bidentate Phosphines: Scope, Limitations, and Mechanism. *Organometallics* **2001**, *20*, 3950-3961, 10.1021/om010454k.
179. Grushin, V. V., Mixed Phosphine–Phosphine Oxide Ligands. *Chem. Rev.* **2004**, *104*, 1629-1662, 10.1021/cr030026j.
180. Foscatto, M.; Venkatraman, V.; Jensen, V. R., DENOPTIM: Software for Computational de Novo Design of Organic and Inorganic Molecules. *J. Chem. Inf. Model.* **2019**, *59*, 4077-4082, 10.1021/acs.jcim.9b00516.





IV



## PAPER II

# The Mechanism of Rh-Catalyzed Transformation of Fatty Acids to Linear Alpha olefins.

Hopen Eliasson, S. H. ; Chatterjee, A.; Occhipinti, G.;  
Jensen, V. R.

*Inorganics* 2017, 5, 87

Reprinted with permission from “Eliasson, S.; Chatterjee, A.; Occhipinti, G.; Jensen, V., The Mechanism of Rh-Catalyzed Transformation of Fatty Acids to Linear Alpha olefins. *Inorganics* 2017, 5, 87, 10.3390/inorganics5040087”. Copyright 2017 MDPI



Article

# The Mechanism of Rh-Catalyzed Transformation of Fatty Acids to Linear Alpha olefins

Sondre H. Hopen Eliasson, Anamitra Chatterjee , Giovanni Occhipinti  and Vidar R. Jensen \*

Department of Chemistry, University of Bergen, Allégaten 41, N-5007 Bergen, Norway;

sondre.eliasson@uib.no (S.H.H.E.); anamitra.chatterjee@uib.no (A.C.); giovanni.occhipinti@uib.no (G.O.)

\* Correspondence: Vidar.Jensen@kj.uib.no; Tel.: +47-5558-3489

Received: 15 October 2017; Accepted: 29 November 2017; Published: 4 December 2017

**Abstract:** Linear alpha olefins (LAOs) are key commodity chemicals and petrochemical intermediates that are currently produced from fossil resources. Fatty acids are the obvious renewable starting material for LAOs, which can be obtained via transition-metal-catalyzed decarbonylative dehydration. However, even the best catalysts that have been obtained to date, which are based on palladium, are not active and stable enough for industrial use. To provide insight for design of better catalysts, we here present the first computationally derived mechanism for another attractive transition-metal for this reaction, rhodium. By comparing the calculated mechanisms and free energy profiles for the two metals, Pd and Rh, we single out important factors for a facile, low-barrier reaction and for a stable catalyst. While the olefin formation is rate limiting for both of the metals, the rate-determining intermediate for Rh is, in contrast to Pd, the starting complex,  $(PPh_3)_2Rh(CO)Cl$ . This complex largely draws its stability from the strength of the Rh(I)–CO bond. CO is a much less suitable ligand for the high-oxidation state Rh(III). However, for steric reasons, rhodium dissociates a bulkier triphenylphosphine and keeps the carbonyl during the oxidative addition, which is less favorable than for Pd. When compared to Pd, which dissociates two phosphine ligands at the start of the reaction, the catalytic activity of Rh also appears to be hampered by its preference for high coordination numbers. The remaining ancillary ligands leave less space for the metal to mediate the reaction.

**Keywords:** decarbonylative dehydration; DFT; catalysis; palladium; rhodium; renewable resources

## 1. Introduction

Linear alpha olefins (LAOs) are key commodity chemicals and petrochemical intermediates that are used in applications, such as polyethylene production (where the LAOs are used as co-monomers), synthesis of oxo alcohols to give detergents and plasticizers, and the manufacturing of poly- $\alpha$ -olefins that are used in drilling fluids and synthetic lubricants, to mention but a few [1–3]. LAOs are currently produced via oligomerization of ethylene derived from fossil resources [4,5]. Because of the limited supply of fossil resources and the fact that their use releases carbon dioxide to the atmosphere, research on the utilization of renewable feedstocks has gained extraordinary importance [6–8].  $\alpha$ -Olefins are produced on a scale of tens of millions of tons per year [3]. The development of a viable route from renewable feedstocks to  $\alpha$ -olefins would be a major breakthrough, with a potentially transformative impact on sustainable chemical production.

Fatty acids are attractive as renewable starting materials, and deoxygenation (oxidative decarboxylation or decarbonylative dehydration) of fatty acids and their derivatives is currently being explored as an alternative and more sustainable route to uncommon, odd-numbered LAOs [2,9–11].

LAOs may be obtained from fatty acids using homogenous- [12–17], heterogeneous- [18], and bio-catalysts [19–21]. The highest activities and selectivities have so far been obtained with homogenous catalysts [2,14,22]. Homogeneously catalyzed decarbonylative dehydration has proven

to be a promising reaction in the production of LAOs [12–15,22–30], as well as in the toolbox of the synthetic organic chemist [31].

With this promising outlook, transition-metal catalysts based on palladium [12–15,22,25,29,30,32], rhodium [14,23], iridium [27,33], nickel, [24,34], and iron [28] have been developed. Palladium-based catalysts have so far reached the highest activities [14]. However, even the best catalysts that have been developed to date are insufficiently active for practical purposes. They require high temperatures, normally well above 200 °C, that lead to rapid catalyst decomposition and turnover numbers (TONs) far below the levels (one to ten million) typical of industrial processes [35].

To accelerate development of improved catalysts, researchers have, after decades of trial-and-error, turned to fundamentals for mechanistic and molecular-structural information that should facilitate the rational design of catalysts for decarbonylative dehydration.

Firstly, whereas previous catalysts for decarbonylative dehydration have been formed *in situ*, we recently reported the first well-defined palladium catalyst precursor for this reaction [12]. The availability of a molecular structure facilitates improvement via structure-activity relationships. The well-defined catalyst also requires less phosphine than the *in-situ* recipes. They can also be used at relatively low temperatures (110 °C), give high selectivity (>95% for most substrates), and handle a wide range of substrates.

Secondly, molecular-level computational investigations have finally started to appear, offering valuable insight for rational catalyst redesign. The first molecular-level computational study of the mechanism of the Pd-catalyzed reaction was recently reported [32]. This study, which derived its model system (based on the triphenylphosphine (PPh<sub>3</sub>) ligand) from an earlier experimental investigation [29] using palladium and PPh<sub>3</sub>, found the alkene-forming β-hydrogen transfer step to be rate determining. Prior to this step, the two remaining phosphine ligands dissociate from the complex. This study was followed by a recent report on the Ni-catalyzed mechanism [24] and a study of Pd-based catalysts using combinations of different ligands [30].

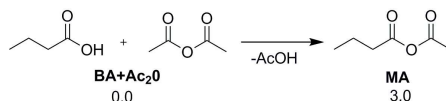
To accelerate the development of improved catalysts for the decarbonylative dehydration reaction, we need all of the options on the table, including variation of the central metal atom. Considering whether there could be alternatives to Pd, we note that the second best activity was reported, in 1993, with Rh [14]. More importantly, Rh, in contrast to Pd, does not need the wasteful stoichiometric additions of acidic anhydride to convert the fatty acids [14,23]. The atom-economy outlook for Rh is further boosted by the fact that this metal also does not need the excess phosphine ligand typical of Pd-based catalysts [14]. In other words, in the search for a greener and more atom-economic conversion of fatty acids to LAOs, Rh seems very promising. Surprisingly, since the 1993 report [14], no-one has further explored this metal for decarbonylative dehydration of fatty acids. In light of the above-mentioned recent mechanistic investigations of the Pd-catalyzed reaction, a corresponding and comparable investigation of Rh could now indicate its potential for this reaction and the extent to which future catalyst development should focus on this metal.

To this end, we have investigated the Rh-catalyzed decarbonylative dehydration of a model carboxylic acid (butanoic acid) using density functional theory (DFT), and have established a possible reaction pathway. Comparison of the thus calculated free energy profile with that of Pd affords insight into the catalytic potential of the two metals.

## 2. Results and Discussion

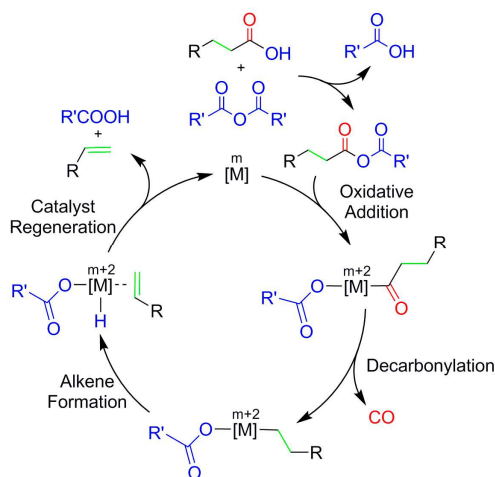
All of the reported relative free energies ( $\Delta G_{BA}$ , [kcal/mol]) correspond to Gibbs energies in butanoic acid (BA) solvent at 523.15 K. Schemes and energies for all of the investigated pathways are given in the Supplementary Materials.

The four-coordinate rhodium(I) complex (PPh<sub>3</sub>)<sub>2</sub>Rh(CO)Cl is known to be the active compound [14,23], and we thus used this complex as the starting point and reference (zero-point) for the calculation of relative free energies. Before the catalytic cycle, the acetic anhydride and the butanoic acid form a mixed anhydride MA (Scheme 1).



**Scheme 1.** Anhydride activation of butanoic acid.

This reaction is calculated to be weakly endergonic (3.0 kcal/mol) and the more reactive mixed anhydride substrate **MA** will be produced by the excess of butanoic acid and acetic anhydride in the reaction mixture. The mixed anhydride **MA** first binds and adds oxidatively to the metal before the cycle continues with decarbonylation; alkene formation; and, catalyst regeneration; see Scheme 2.



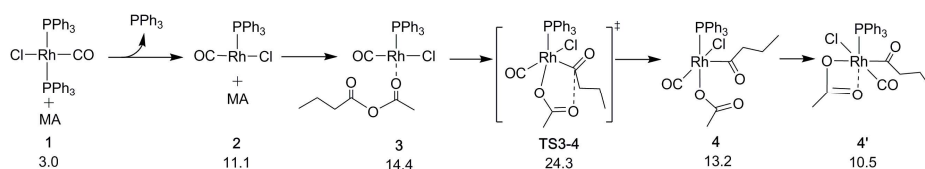
**Scheme 2.** General reaction scheme for decarbonylative dehydration of carboxylic acids, with  $R = R' = \text{CH}_3$  in the present work. The reaction involves four main steps: oxidative addition, decarbonylation, alkene formation and catalyst regeneration. For Pd, CO has been predicted to dissociate in the catalyst regeneration step [32].

### 2.1. Oxidative Addition

The first step of the catalytic cycle leads to the rupture of the C–O bond in the mixed anhydride. In principle, two different C–O bonds may be broken,  $\text{C}(\text{O})\text{--OC}(\text{O})\text{CH}_3$  and  $\text{C}(\text{O})\text{O--C}(\text{O})\text{CH}_3$ . Cleavage of the C–O bond in the anhydride part,  $\text{C}(\text{O})\text{O--C}(\text{O})\text{CH}_3$  (blue in the mixed anhydride in Scheme 2), will not lead to the desired  $\alpha$ -olefin. Cleavage of this C–O bond can be prevented by using symmetric [15] or more sterically demanding anhydrides [13]. In practice, however, such preventive measures are unnecessary. The DFT-calculated barrier to oxidative addition to Pd is in fact lower when cleaving the intended C–O bond [32]. Moreover, experiments have also shown that the unwanted side reaction may be avoided even without strategies, such as the use of sterically demanding anhydride groups [25]. Hence, we will only consider the C–O bond rupture leading to the intended product (Scheme 3). In experiments at a temperature (70 °C), lower than that of typical decarbonylative dehydration reactions, the anhydride did not add oxidatively to the tetracoordinate Rh(I) catalyst [36]. Instead, the reaction could be observed for a less coordinated rhodium and for smaller and more basic phosphine ligands ( $\text{PPhMe}_2$ ). In agreement with these observations, our calculations show that oxidative addition to the tetracoordinate Rh complex is difficult at higher temperatures as well ( $\Delta G_{BA} = 41.3$  kcal/mol, Scheme S1). From the starting point 1 it is more likely that a phosphine ligand dissociates to form the tricoordinate complex 2 before the reaction continues. Together, the calculations



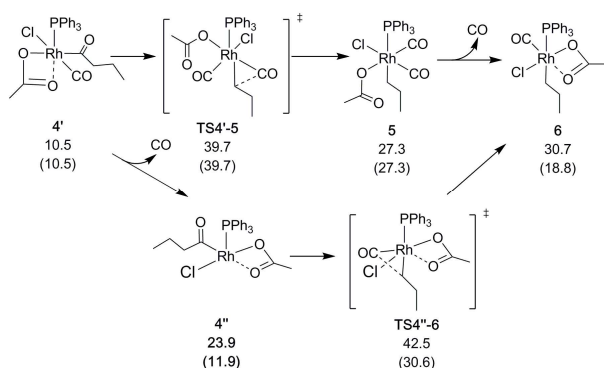
and experimental results suggest that the entropy gain and the steric hindrance from PPh<sub>3</sub> outweigh the benefit of an electron-rich complex that otherwise could be expected to favor oxidative addition followed by dissociation of a neutral donor ligand; see Scheme S1. In general, it is believed that Rh(I) forms a tricoordinate complex before undergoing oxidative addition, the calculated barrier of which is  $\Delta G_{BA}^\ddagger = 24.3$  kcal/mol (via **TS3-4**). This is considerably lower than the corresponding aldehyde reaction [37], illustrating the activating effect of anhydride. A similarity with the aldehyde decarbonylation, however, is that, as here, with Cl as the spectator anionic ligand, CO is preferred over phosphine as the remaining neutral ligand [37]. Finally, following the oxidative addition, the complex rearranges to an essentially octahedral geometry, with the acetate binding in a bidentate ( $\kappa^2$ ) fashion. As we shall see, acetate facilitates the catalytic cycle throughout by switching between  $\kappa^1$  and  $\kappa^2$  coordination to maintain hexacoordination and the octahedral geometry preferred by rhodium(III).



**Scheme 3.** Rh catalyzed oxidative addition of mixed anhydride. Relative free energies  $\Delta G_{BA}$  given in kcal/mol.

## 2.2. Decarbonylation

After the oxidative addition, carbonyl is eliminated from the acyl chain. At this stage of the reaction, a CO molecule will also dissociate from the catalyst. This dissociation may either occur right before or after the decarbonylation, the preference of which depends on the CO pressure that is applied in the calculations, as described in Section 3. As shown in Scheme 4, the decarbonylation at normal pressure involves a barrier of  $\Delta G_{BA}^\ddagger = 39.7$  kcal/mol (via **TS4'-5**, relative to the reference starting point; see above). The alternative route in which CO dissociates before the decarbonylation has a slightly higher decarbonylation barrier ( $\Delta G_{BA}^\ddagger = 42.5$  kcal/mol). In contrast, at low CO pressure ( $10^{-5}$  atm, arbitrarily chosen to model the open system, allowing for CO to escape from the reaction medium) CO dissociation prior to decarbonylation is clearly favorable, with a barrier of only  $\Delta G_{BA}^\ddagger = 30.6$  kcal/mol. With CO having left the complex, acetate once again binds in a bidentate fashion and saturates the rhodium alkyl complex, both electronically and coordinatively.

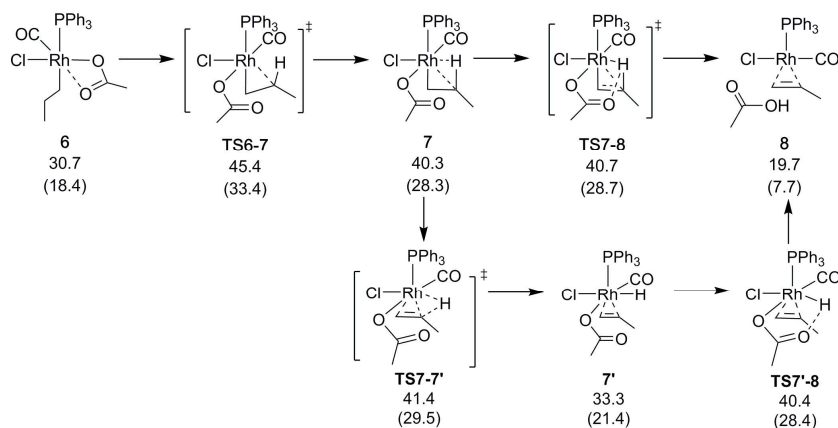


**Scheme 4.** Rh-catalyzed decarbonylation. Relative free energies  $\Delta G_{BA}$  in kcal/mol, with values in parenthesis obtained using reduced CO pressure (see Section 3).

### 2.3. Alkene Formation

To form the  $\alpha$ -olefin, the  $\beta$ -hydrogen atom is transferred from the alkyl chain to the acetate. Our computational exploration shows that the direct, through-space transfer from the alkyl to the acetate is a highly unlikely high-energy process. Rather, the transfer is stabilized by an agostic bond to the metal. To make space for the agostic bond, the acetate may switch to monodentate coordination and/or another ligand must dissociate. A switch to monodentate acetate was found to be energetically favorable, and to give sufficient steric and electronic degrees of freedom to support the formation of the agostic interaction in **7** (Scheme 5 and Scheme S3) prior to the transfer. Complete dissociation of the acetate does not appear to be favorable under the conditions that are modeled here. A highly polar reaction medium ( $\Delta G_{4\text{-Heptanone}} = 41.8$  kcal/mol) might change the situation though, which was found to be a competitive alternative for palladium [30].

The hydrogen may either be transferred directly or sequentially by first being eliminated to form a metal hydride, and next being transferred to the acetate in a second elementary step. We found the direct transfer to be preferred, although with a minimal difference in barrier between the direct and sequential transfer (Scheme 5). In fact, the rate determining step is the formation of the agostic bond in **7**, with a barrier (relative to the reference starting point) of  $\Delta G_{BA}^\ddagger = 45.4$  kcal/mol (Scheme 5). As for the above-mentioned decarbonylation, the alkene-formation barriers are lowered drastically when taking into account the reduced CO pressure to model an open system, to  $\Delta G_{BA}^\ddagger = 33.4$  kcal/mol (**TS6-7**), and  $\Delta G_{BA}^\ddagger = 28.7$  kcal/mol (**TS7-8**).



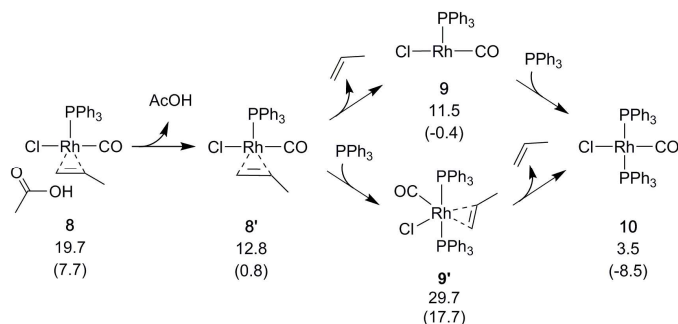
**Scheme 5.** Rh-catalyzed  $\beta$ -hydrogen transfer. Relative free energies  $\Delta G_{BA}$  in kcal/mol, with values in parenthesis obtained using reduced CO pressure (see Section 3).

### 2.4. Catalyst Regeneration

Next, the olefin that was formed by the above-described  $\beta$ -hydrogen transfer dissociates, creating space for reformation of the catalyst by coordination of a phosphine (Scheme 6). The alternative, binding the phosphine first, is disfavored (Scheme 6). The overall reaction is calculated to be slightly endergonic ( $\Delta G_{BA} = 3.5$  kcal/mol) when modeling all of the species in their standard states. However, using a lower pressure (see Section 3) to model that CO is allowed to escape from the reaction mixture drives the equilibrium toward the product side [30] to reflect an exergonic ( $\Delta G_{BA} = -8.5$  kcal/mol) and catalytic process.

The starting complex **1** is clearly the most stable species of the reaction. A new cycle could start from the tricoordinate **9** (**2**), but rebinding a phosphine to form **10** (**1**) is energetically favorable. This may explain the experimentally observed inactivation of the Rh catalyst in phosphine excess. Still,

a low, constant concentration of phosphine is required, even for Rh. Presumably phosphine is needed to prevent loss of both phosphine ligands, which would drive the reaction into the less favorable **d** and **e** pathways (see the Supplementary Materials), and lead to loss of catalytic activity.



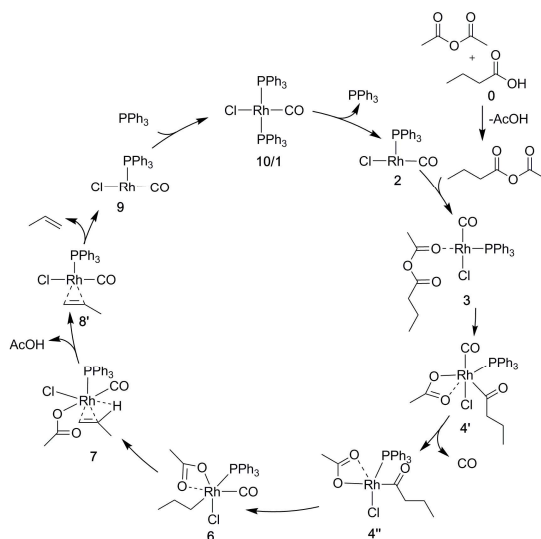
**Scheme 6.** Regeneration of the Rh catalyst. Relative free energies  $\Delta G_{BA}$  in kcal/mol, with values in parenthesis obtained using reduced pressure (see Section 3).

## 2.5. The Overall Reaction Mechanism and Comparison to the Pd-Catalyzed Reaction

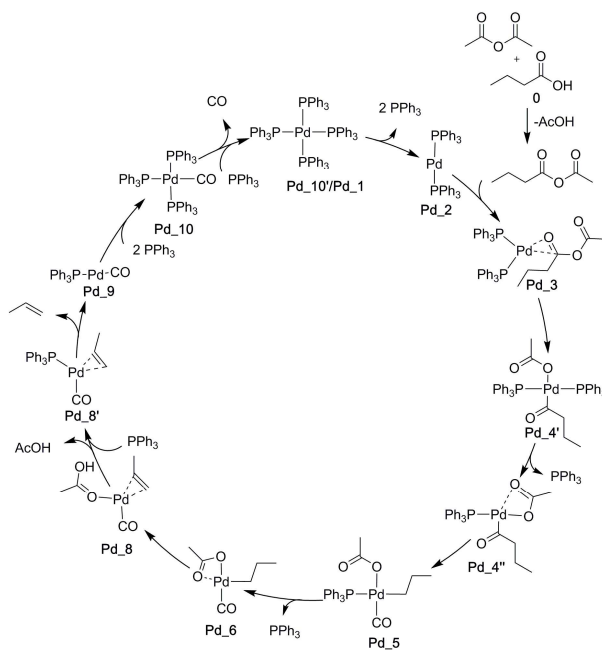
The dominating barriers of the pathways presented above are very high when calculated assuming all of the species in their respective standard states, in particular when compared to the much lower barriers that are calculated for Pd [32]. However, as we have seen above, applying reduced CO pressure to model an open system, from which CO can escape, reduces the barriers subsequent to CO dissociation drastically. For example, the rate-determining barrier is lowered from  $\Delta G_{BA}^\ddagger = 45.4$  kcal/mol to  $\Delta G_{BA}^\ddagger(10^{-5} \text{ atm}) = 33.4$  kcal/mol. This lowering is consistent with experimental observations, as a CO purge is necessary for achieving appreciable reactivity [14]. A corresponding lowering of barriers is not achieved for Pd, because, for this metal, CO dissociates only at the end of the catalytic cycle [32].

Having established the importance of modeling the reduced CO pressure for Rh, we focus on the thus-derived pathways and free energies in the following. The corresponding complete Rh-catalyzed reaction cycle is given in Scheme 7, with less favorable pathways being available in the Supplementary Materials. For example, it is also possible to start from Wilkinson's catalyst  $(\text{PPh}_3)_3\text{RhCl}$  (12.1 kcal/mol less stable than our reference point  $(\text{PPh}_3)_2\text{Rh}(\text{CO})\text{Cl}$ ). With this catalyst, route **b** (see the Supplementary Materials) may be followed. However, after the first decarbonylation and formation of CO, the reaction starting from Wilkinson's catalyst converges with the most favorable mechanism found in this work, termed pathway **a** in the Supplementary Materials. This is also the mechanism shown in Scheme 7 (and other schemes) in the main part of the paper.

As explained in the Introduction, the most active catalysts so far have been obtained for palladium.  $\text{PdCl}_2$ , in combination with an excess of phosphine ligand, is typically used as the catalyst. Pd is then reduced to phosphine-bound Pd(0) before the catalytic cycle. To help to understand the observed differences in the catalytic properties of Rh and Pd, we also calculated the palladium-catalyzed catalytic cycle. Molecular structures corresponding to the lowest-energy profile calculated for decarbonylative dehydration of hydrocinnamic acid and pivalic anhydride [32] were modified to involve our model substrates (butanoic acid and acetic anhydride) before reoptimization and SP calculations using our computational models (defined in Section 3). The thus obtained Pd-catalyzed reaction cycle is shown in Scheme 8.



**Scheme 7.** The reaction cycle of Rh-catalyzed decarbonylative dehydration of butanoic acid.



**Scheme 8.** The calculated reaction cycle of Pd-catalyzed decarbonylative dehydration of butanoic acid. The starting structures were taken from Ref. [32] and modified to the present substrates before reoptimization.

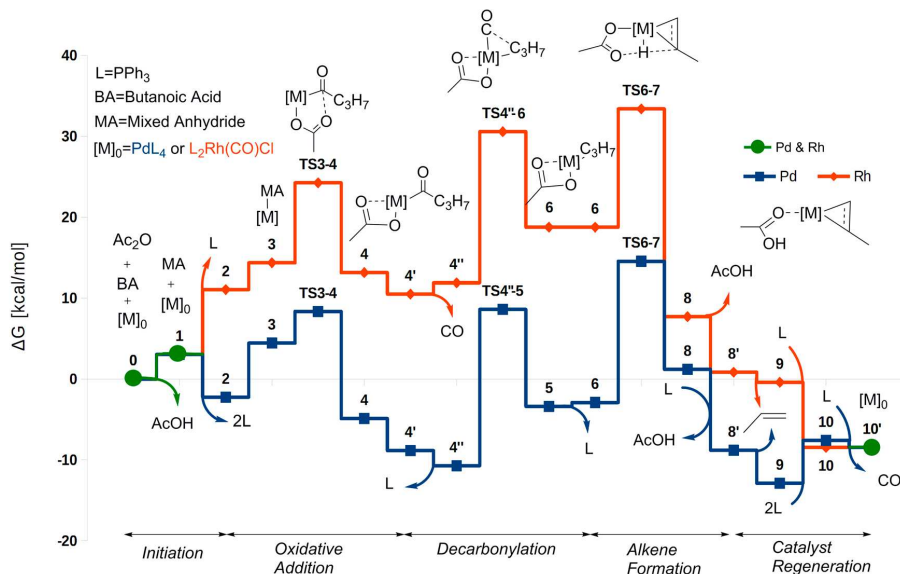
While the coordination number and other properties of the Pd and Rh complexes of the two catalytic cycles (Schemes 7 and 8) differ, the different stages of the reaction can still be recognized and compared between the two catalysts. A comparison of the two free energy profiles is given in

Figure 1. In the Pd cycle, the lowest free energy was calculated for **Pd\_9** (−12.9 kcal/mol), and the highest for **Pd\_TS6-8** (14.6 kcal/mol). Taking the reaction free energy ( $\Delta G_{react} = -8.5$  kcal/mol, due to the above-mentioned reduced pressure of  $10^{-5}$  atm) into account for subsequent cycles, the overall barrier relative to **Pd\_9** is  $\Delta G^{RDB} = (\Delta G^{Pd\_TS6-8} - \Delta G_{Pd\_9}) + \Delta G_{react} = 18.1$  kcal/mol. The overall barrier from **Pd\_4''** (−10.7 kcal/mol) is higher,  $\Delta G^{RDB} = (\Delta G^{Pd\_TS6-8} - \Delta G_{Pd\_4''}) = 25.3$  kcal/mol. Thus, **Pd\_4''** is the rate-determining intermediate (RDI) and also the reference intermediate for the decarbonylation and the alkene formation steps. However, for palladium **Pd\_9** is the reference intermediate against which to calculate the barrier for oxidative addition of a subsequent cycle. For **Pd\_TS3-4** (8.4 kcal/mol), we get that  $\Delta G^{OA\dagger} = (\Delta G^{Pd\_TS3-4} - \Delta G_{Pd\_9}) + \Delta G_{react} = 12.8$  kcal/mol for the barrier relative to **Pd\_9**. The alternative intermediate **Pd\_3**, (−2.2 kcal/mol) gives a lower barrier,  $\Delta G^{OA\dagger} = (\Delta G^{Pd\_TS3-4} - \Delta G_{Pd\_3}) = 10.6$  kcal/mol.

Summarizing, for the Rh-catalyzed cycle, the starting point and zero-level for the free energy, i.e.,  $(PPh_3)_2Rh(CO)Cl$  and the substrates, is also the RDI. For palladium, our RDI (**Pd\_4''**) is 1.8 kcal/mol lower in energy than **Pd\_4'**, the corresponding RDI found in Ref. [32] for decarbonylative dehydration of hydrocinnamic acid and pivalic anhydride. This difference as well as the somewhat lower barriers obtained here in general when compared to those of Ref. [32] can probably be attributed to the difference between the substrate models, the more extended basis sets used here (VQZ as compared to VTZ in Ref. [32]) for the single-point (SP) energy calculations, and the fact that a different functional was used for geometry optimization.

Turning now to the oxidative addition the barrier (via **TS3-4**) for Rh(I) is  $\Delta G_{BA}^\ddagger = 24.3$  kcal/mol (relative to the zero-level starting point), and thus higher than for Pd(0) ( $\Delta G_{BA}^\ddagger = 12.9$  kcal/mol, relative to **Pd\_9**). The oxidative addition is also thermodynamically disfavored for Rh(I) when compared to Pd(0), with the two energy profiles diverging markedly already at this early stage of the catalytic cycle. Part of the explanation for this difference is presumably that the Pd(0) complex is more electron rich compared to Rh(I). Next, rhodium, as opposed to palladium, carries a ligand (CO) that is known to stabilize low oxidation states. CO is much less able to stabilize higher oxidation states than phosphine. Hence, oxidation of Rh(I) in the presence of CO should be less favorable than that of Pd(0) in the presence of phosphine. In addition, palladium increases its coordination number from only two to the preferred square-planar configuration, with little steric hindrance. In comparison, rhodium increases its coordination number from three to six, in a process that could perhaps be hindered by steric repulsion when compared to the low-coordinate palladium case.

Leading up to the decarbonylation, the Pd complex is slightly stabilized by the loss of a phosphine (**Pd\_4' → Pd\_4''**). In contrast, the Rh complex is slightly destabilized by the loss of a CO molecule, probably due to a temporary reduction in coordination number. The decarbonylation barrier is much higher for Rh ( $\Delta G_{BA}^\ddagger = 30.6$  kcal/mol, relative to the starting point) than for the Pd counterpart ( $\Delta G_{BA}^\ddagger = 19.3$  kcal/mol, relative to **Pd\_4''**). High barriers for decarbonylation have also been calculated for Rh-catalyzed decarbonylation of aldehydes [37], where this step is rate determining. Moreover, as for the oxidative addition, the difference in activation barriers between Rh and Pd is paralleled by a marked difference in the thermodynamical stability of the products. This is consistent with the fact that the metal–CO bond formed in the decarbonylation is expected to be stronger for Pd(II) than for Rh(III), since CO prefers low oxidation states (II is better than III). Indeed, in the subsequent step rhodium does not dissociate a ligand, while Pd dissociates a phosphine and keeps the CO. Because CO stabilizes low oxidation states (Rh(I) and Pd(0)), both of the metals need this ligand during the reductive alkene formation.



**Figure 1.** Reaction profile for both decarbonylative dehydration of butanoic acid by Pd (blue) and Rh (red) using reduced CO pressure. The steps that have the same energy along the reaction pathway are indicated by green color. Free energies are given relative to the starting complex for both catalysts.

Broadly speaking, the alkene-formation step is rate determining for both metals. The marked difference in overall barrier between Rh ( $\Delta G_{BA}^{\ddagger} = 33.4$  kcal/mol) and Pd ( $\Delta G_{BA}^{\ddagger} = 25.3$  kcal/mol, relative to **Pd\_4''**) is in agreement with the fact that palladium has proved to give the most active catalysts. A major difference between the palladium and rhodium mechanisms at this stage is that Pd dissociates both of the phosphine ligands before the  $\beta$ -hydrogen transfer. As mentioned above, this is not favorable for the higher-oxidation state Rh complex, which dissociates a CO molecule instead. Alternative dissociation reactions to make room for the agostic bond to rhodium are presented in Scheme S3. The overall more crowded metal center for Rh most likely also causes steric hindrance for the space-requiring transfer reaction and for binding the resulting alkene. Reducing the steric hindrance is probably part of the reason why, for Pd, the  $\beta$ -hydrogen is transferred in a Pd complex with no (bulky) phosphines. Indeed, the mono-phosphine-coordinated Pd complex has a much higher barrier for the  $\beta$ -hydrogen transfer. A second reason for keeping a CO at this stage, as do both Rh and Pd, is that this ligand stabilizes the reduced metal oxidation state that is resulting from the transfer.

The above-described complete phosphine dissociation comes at cost for Pd. For this metal, as opposed to Rh, an excess of phosphine is needed to ensure catalytic activity, which is consistent with the fact that two phosphines must bind again before a new catalytic cycle can start. A lack of phosphine will lead to olefin isomerization at the phosphine-free and coordinatively available Pd sites [30], and probably also to catalyst decomposition via formation of Pd(0) clusters.

The rate-determining intermediates for Rh ( $(PPh_3)_2Rh(CO)Cl$ ) and Pd ( $Pd(CO)PPh_3$ , **Pd\_9**) are similar, with CO still bonded. However for Pd, while **Pd\_9** is able to mediate the oxidative addition [32], this intermediate dissociates the carbonyl to give the subsequent, preferred pathway. In contrast,  $(PPh_3)_2Rh(CO)Cl$  is a very stable intermediate of the catalytic cycle for Rh. This stability is due to the strong Rh(I)–CO bond, which thus stands out as one of the most important contrasts to the Pd-based catalyst. CO is much less favorable for the Rh(III) oxidation state.

### 3. Computational Method

All of the calculations have been performed at the DFT level using the Gaussian 09 program [38].

#### 3.1. Geometry Optimization

All of the geometry optimizations were done assuming gas phase using the hybrid range-separated functional  $\omega$ B97XD [39–41], which includes empirical atom-atom dispersion terms. The  $\omega$ B97XD functional has been shown to reproduce X-ray geometries of transition-metal-based homogeneous catalysts with high accuracy when compared to other density functionals [42]. Input geometries for the Rh complexes were constructed using the Spartan 08 software [43] by modifying available X-ray structures [44] or previously DFT optimized geometries. Conformational searches were performed using the MMFF force-field [45]. The input geometries for the Pd complexes were all taken from Ref. [32]. The substrate (hydrocinnamic acid) used in Ref. [32] was changed to butanoic acid before reoptimization of the geometry. Tight convergence criteria (keyword opt=tight), corresponding to a maximum force of  $1.5 \times 10^{-5}$  a.u., were used for the geometry optimizations. Numerical integrations were performed with the ultrafine grid of Gaussian (Int=Ultrafine). The SCF density-based convergence criterion was tightened to  $10^{-10}$  (SCF=(Conver=10)). The located stationary points were characterized by the eigenvalues of the analytically calculated Hessian matrices. The most important transition states of the Rh-catalyzed reaction were connected to the corresponding reactants and products by using the intrinsic reaction coordinate (IRC) [46] method that was implemented in Gaussian. For Rh and Pd, the Stuttgart 28-electron relativistic effective core potential (ECP28MDF) was used in conjunction with the accompanying correlation-consistent valence double- $\zeta$  plus polarization (cc-pVDZ-PP) basis sets [47]. All of the other atoms were described by standard correlation-consistent valence double- $\zeta$  plus polarization (cc-pVDZ) basis sets [48,49].

#### 3.2. Thermochemistry

Translational, rotational, and vibrational partition functions for thermal corrections to give total Gibbs free energies were computed within the ideal gas, rigid-rotor, and harmonic oscillator approximations. To reduce the problems that are caused by soft, harmonic modes, all of the frequencies below  $100 \text{ cm}^{-1}$  were shifted to  $100 \text{ cm}^{-1}$  when calculating entropies [50]. The temperature used in the calculation of thermochemical corrections was set to 523.15 K, which is the temperature that is used in experiments [14].

#### 3.3. Single-Point Calculations (SP)

The reported energies were obtained in SP calculations on optimized geometries using the M06L local density functional [51–53], which has been applied to decarbonylative dehydration and has proved to correlate well in benchmark studies of this reaction [32]. To monitor the degree to which the results are dependent on the functional, several other functionals were tested: (i) the gradient-corrected Perdew–Burke–Ernzerhof (PBE) functional [54,55] in combination with Grimme’s empirical dispersion term D3 and the original Becke–Johnson damping [56] (together termed D3-BJ) and the recently modified damping parameters [57] (to give D3-M(BJ)), and, (ii) the hybrid B3LYP functional [58] combined with the modified dispersion correction (to give B3LYP-D3M(BJ)). These additional SP results are available in the Supplementary Materials. Numerical integrations were performed using the ultrafine grid and the SP SCF convergence criterion was set to  $10^{-5}$ . The Stuttgart 28-electron relativistic effective core potential (ECP28MDF) in conjunction with the accompanying correlation consistent valence quadruple- $\zeta$  (cc-pVQZ-PP) basis set was used for the Rh and Pd atom. The C and H atoms were treated with the correlation consistent valence quadruple- $\zeta$  plus polarization (cc-pVQZ) basis sets obtained from the ESML basis set exchange website [59]. All of the other atoms were treated with an extended cc-pVQZ basis set with diffuse functions added from the “aug-cc-pVQZ Diffuse” set [60]. The model reaction is solvent free, but in experiments reflecting the present modeling,

butanoic acid (the model substrate) and acetic anhydride would be present in excess to drive the equilibrium toward the product. No continuum solvent model parameters are available in Gaussian 09 for the corresponding mixed anhydride (butyric anhydride,  $\epsilon = 12.00$ ). In addition, two molecules of acetic acid (AA,  $\epsilon = 6.25$ ) would be produced by the reaction. To mimic this environment, we used butanoic acid (BA,  $\epsilon = 2.85$ ) and 4-Heptanone (4-Hep,  $\epsilon = 12.26$ ), respectively, in our calculations. The electrostatic and non-electrostatic solvent effects were taken into account, with default settings, using the SMD [61] solvation model, as implemented in Gaussian 09. All the relative energies ( $\Delta G_{BA}$ , [kcal/mol]) reported for the most favorable and alternative reaction pathways in the main part of the paper and in Schemes S1–S3 (Supplementary Materials) are Gibbs free energies in butanoic acid (BA) solvent at 523.15 K. Scheme S4 illustrates the relatively minor effect of modifying the continuum solvent in the SMD calculations.

### 3.4. Free Energies

Free energies were obtained using a standard state corresponding to a 1 M infinitely diluted solution and a temperature of 523.15 K. Accordingly, for all species but CO (gas),  $3.9 \text{ kcal}\cdot\text{mol}^{-1}$  ( $RT \ln 42.9$ ) was added to account for the change from 1 atm to 1 M [62]. Experimentally, CO is purged from the reaction mixture. We model this by using reduced pressure ( $10^{-5}$  atm, arbitrarily chosen [32]) when calculating the thermal corrections of CO.

With the above-described energies and corrections, the total free energy becomes  $G_{Tot} = G_{Gas} + \Delta G_{Solv} + \Delta G^{1 \text{ atm} \rightarrow 1M}$ , where  $G_{Gas}$  is the gas phase Gibbs free energy resulting from the SCF SP energy and the added thermal correction ( $G_{corr}$ ),  $\Delta G_{Solv}$  is the solvation free energy obtained as the difference between the SMD and the gas phase SCF energies, and  $\Delta G^{1 \text{ atm} \rightarrow 1M}$  is the standard-state correction. All of the energies reported are in kcal/mol, unless otherwise stated. Where relevant, we report both of the the energies obtained using normal (1 atm) and reduced ( $10^{-5}$  atm) CO pressure.

## 4. Conclusions

Based on molecular-level calculations, we have presented the first reaction mechanism of Rh-catalyzed decarbonylative dehydration of anhydride-activated carboxylic acid. The results for rhodium are compared to those of the corresponding Pd-catalyzed reaction. Firstly, we conclude that the calculated activation barriers are consistent with the observation that Pd gives the most active catalyst. Still, for both of the metals, alkene formation is rate determining. Specifically, for Rh, the rate-limiting elementary step is the formation of the initial agostic interaction leading up to the  $\beta$ -hydrogen transfer from the alkyl, while for Pd, the transfer itself is the bottleneck. The rate-determining intermediate for rhodium is the starting complex  $(\text{PPh}_3)_2\text{Rh}(\text{CO})\text{Cl}$  with two phosphines, while the overall cycle only requires a single bonded phosphine. This is consistent with the experimental observation that phosphine excess inhibits the activity of the Rh-based catalyst. Furthermore, this also underlines the contrast to palladium. For the latter metal, all of the phosphine ligands dissociate from the complex during the reaction, but excess phosphine is still required to ensure catalyst regeneration and to prevent olefin isomerization via double-bond migration. A second important difference between the two metals, partly explaining the higher overall barrier for Rh, originates from their difference in oxidation states and differential binding to CO. The Rh(I)–CO bond is much stronger than Rh(III)–CO. Still rhodium keeps the carbonyl ligand during the oxidative addition. Rhodium prefers higher coordination numbers than palladium and dissociates only a single ligand at the start of the reaction, the bulkier triphenylphosphine. This phosphine could otherwise have stabilized the Rh(III) state more than CO does.

**Supplementary Materials:** The following are available online at [www.mdpi.com/2304-6740/5/4/87/s1](http://www.mdpi.com/2304-6740/5/4/87/s1), Scheme S1: All pathways investigated for oxidative addition, Scheme S2: All pathways investigated for decarbonylation, Scheme S3: All pathways investigated for alkene formation by  $\beta$ -hydrogen transfer, Scheme S4: The free energy profile for Rh-catalyzed decarbonylative dehydration as calculated in gas phase, butanoic acid (SMD model) and 4-heptanone solvent (SMD model) using the M06L functional and QZ basis sets, Table S1: Gibbs free energies for the main pathway calculated using different DFT-functionals, Table S2: Electronic energies



and Gibbs free energies for all species in gas phase, and with the solvents butanoic acid and 4-heptanone. Optimized Cartesian coordinates (XYZ) of all examined compounds.

**Acknowledgments:** The authors gratefully acknowledge the Research Council of Norway for financial support via the Idélab initiative and the BIOTEK2021 program (grant number 238851), the ENERGIX program (255373), and for CPU and storage resources granted through the NOTUR (NN2506K) and NORSTORE (NS2506K) supercomputing programs. Sondre H. Hopen Eliasson acknowledges the University of Bergen for a doctoral fellowship.

**Author Contributions:** Sondre H. Hopen Eliasson, Giovanni Occhipinti and Vidar R. Jensen conceived the calculations; Sondre H. Hopen Eliasson performed all the calculations; Sondre H. Hopen Eliasson analyzed the data, with contributions and discussion from Giovanni Occhipinti, Anamitra Chatterjee and Vidar R. Jensen; Sondre H. Hopen Eliasson and Vidar R. Jensen wrote the paper, with contributions from Anamitra Chatterjee and Giovanni Occhipinti.

**Conflicts of Interest:** The authors declare no conflict of interest.

## References

1. Franke, R.; Selent, D.; Börner, A. Applied hydroformylation. *Chem. Rev.* **2012**, *112*, 5675–5732. [[CrossRef](#)] [[PubMed](#)]
2. Dawes, G.J.S.; Scott, E.L.; Le Notre, J.; Sanders, J.P.M.; Bitter, J.H. Deoxygenation of biobased molecules by decarboxylation and decarbonylation—A review on the role of heterogeneous, homogeneous and bio-catalysis. *Green Chem.* **2015**, *17*, 3231–3250. [[CrossRef](#)]
3. Arpe, H.J.; Hawkins, S. *Industrial Organic Chemistry*, 5th ed.; Wiley-VCH Verlag GmbH: Weinheim, Germany, 2010; ISBN 978-3-527-32002-8.
4. Agapie, T. Selective ethylene oligomerization: Recent advances in chromium catalysis and mechanistic investigations. *Coord. Chem. Rev.* **2011**, *255*, 861–880. [[CrossRef](#)]
5. Skupinska, J. Oligomerization of  $\alpha$ -olefins to higher oligomers. *Chem. Rev.* **1991**, *91*, 613–648. [[CrossRef](#)]
6. Dodds, D.R.; Gross, R.A. Chemicals from biomass. *Science* **2007**, *318*, 1250–1251. [[CrossRef](#)] [[PubMed](#)]
7. Dapsens, P.Y.; Mondelli, C.; Pérez-Ramírez, J. Biobased chemicals from conception toward industrial reality: Lessons learned and to be learned. *ACS Catal.* **2012**, *2*, 1487–1499. [[CrossRef](#)]
8. Vennestrøm, P.N.R.; Osmundsen, C.M.; Christensen, C.H.; Taarning, E. Beyond petrochemicals: The renewable chemicals industry. *Angew. Chem. Int. Ed.* **2011**, *50*, 10502–10509. [[CrossRef](#)] [[PubMed](#)]
9. Santillan-Jimenez, E.; Crocker, M. Catalytic deoxygenation of fatty acids and their derivatives to hydrocarbon fuels via decarboxylation/decarbonylation. *J. Chem. Technol. Biotechnol.* **2012**, *87*, 1041–1050. [[CrossRef](#)]
10. Gosselink, R.W.; Hollak, S.A.W.; Chang, S.-W.; van Haveren, J.; de Jong, K.P.; Bitter, J.H.; van Es, D.S. Reaction pathways for the deoxygenation of vegetable oils and related model compounds. *ChemSusChem* **2013**, *6*, 1576–1594. [[CrossRef](#)] [[PubMed](#)]
11. Goossen, L.J.; Rodriguez, N.; Goossen, K. Carboxylic acids as substrates in homogeneous catalysis. *Angew. Chem. Int. Ed.* **2008**, *47*, 3100–3120. [[CrossRef](#)] [[PubMed](#)]
12. Chatterjee, A.; Hopen Eliasson, S.H.; Törnroos, K.W.; Jensen, V.R. Palladium precatalysts for decarbonylative dehydration of fatty acids to linear alpha olefins. *ACS Catal.* **2016**, *6*, 7784–7789. [[CrossRef](#)]
13. Goossen, L.J.; Rodriguez, N. A mild and efficient protocol for the conversion of carboxylic acids to olefins by a catalytic decarbonylative elimination reaction. *Chem. Commun.* **2004**, 724–725. [[CrossRef](#)] [[PubMed](#)]
14. Miller, J.A.; Nelson, J.A.; Byrne, M.P. A highly catalytic and selective conversion of carboxylic-acids to 1-alkenes of one less carbon-atom. *J. Org. Chem.* **1993**, *58*, 18–20. [[CrossRef](#)]
15. Liu, Y.; Kim, K.E.; Herbert, M.B.; Fedorov, A.; Grubbs, R.H.; Stoltz, B.M. Palladium-catalyzed decarbonylative dehydration of fatty acids for the production of linear alpha olefins. *Adv. Synth. Catal.* **2014**, *356*, 130–136. [[CrossRef](#)] [[PubMed](#)]
16. John, A.; Hogan, L.T.; Hillmyer, M.A.; Tolman, W.B. Olefins from biomass feedstocks: Catalytic ester decarbonylation and tandem heck-type coupling. *Chem. Commun.* **2015**, *51*, 2731–2733. [[CrossRef](#)] [[PubMed](#)]
17. Murray, R.E.; Walter, E.L.; Doll, K.M. Tandem isomerization-decarboxylation for converting alkenoic fatty acids into alkenes. *ACS Catal.* **2014**, *4*, 3517–3520. [[CrossRef](#)]
18. Chatterjee, A.; Jensen, V.R. A heterogeneous catalyst for the transformation of fatty acids to  $\alpha$ -olefins. *ACS Catal.* **2017**, *7*, 2543–2547. [[CrossRef](#)]

19. Dennig, A.; Kuhn, M.; Tassoti, S.; Thiessenhusen, A.; Gilch, S.; Bülter, T.; Haas, T.; Hall, M.; Faber, K. Oxidative decarboxylation of short-chain fatty acids to 1-alkenes. *Angew. Chem. Int. Ed.* **2015**, *54*, 8819–8822. [[CrossRef](#)] [[PubMed](#)]
20. Wang, J.-B.; Lonsdale, R.; Reetz, M.T. Exploring substrate scope and stereoselectivity of p450 peroxygenase OleT<sub>JE</sub> in olefin-forming oxidative decarboxylation. *Chem. Commun.* **2016**, *52*, 8131–8133. [[CrossRef](#)] [[PubMed](#)]
21. Herman, N.A.; Zhang, W. Enzymes for fatty acid-based hydrocarbon biosynthesis. *Curr. Opin. Chem. Biol.* **2016**, *35*, 22–28. [[CrossRef](#)] [[PubMed](#)]
22. Kraus, G.A.; Riley, S. A large-scale synthesis of  $\alpha$ -olefins and  $\alpha,\omega$ -dienes. *Synthesis* **2012**, *44*, 3003–3005. [[CrossRef](#)]
23. Foglia, T.A.; Barr, P.A. Decarbonylation dehydration of fatty acids to alkenes in the presence of transition metal complexes. *J. Am. Oil Chem. Soc.* **1976**, *53*, 737–741. [[CrossRef](#)]
24. John, A.; Miranda, M.O.; Ding, K.; Dereli, B.; Ortuño, M.A.; LaPointe, A.M.; Coates, G.W.; Cramer, C.J.; Tolman, W.B. Nickel catalysts for the dehydrative decarbonylation of carboxylic acids to alkenes. *Organometallics* **2016**, *35*, 2391–2400. [[CrossRef](#)]
25. Le Nôtre, J.; Scott, E.L.; Franssen, M.C.R.; Sanders, J.P.M. Selective preparation of terminal alkenes from aliphatic carboxylic acids by a palladium-catalysed decarbonylation–Elimination reaction. *Tetrahedron Lett.* **2010**, *51*, 3712–3715. [[CrossRef](#)]
26. Le Notre, J.; Scott, E.L.; Franssen, M.C.R.; Sanders, J.P.M. Biobased synthesis of acrylonitrile from glutamic acid. *Green Chem.* **2011**, *13*, 807–809. [[CrossRef](#)]
27. Maetani, S.; Fukuyama, T.; Suzuki, N.; Ishihara, D.; Ryu, I. Efficient iridium-catalyzed decarbonylation reaction of aliphatic carboxylic acids leading to internal or terminal alkenes. *Organometallics* **2011**, *30*, 1389–1394. [[CrossRef](#)]
28. Maetani, S.; Fukuyama, T.; Suzuki, N.; Ishihara, D.; Ryu, I. Iron-catalyzed decarbonylation reaction of aliphatic carboxylic acids leading to  $\alpha$ -olefins. *Chem. Commun.* **2012**, *48*, 2552–2554. [[CrossRef](#)] [[PubMed](#)]
29. Miranda, M.O.; Pietrangelo, A.; Hillmyer, M.A.; Tolman, W.B. Catalytic decarbonylation of biomass-derived carboxylic acids as efficient route to commodity monomers. *Green Chem.* **2012**, *14*, 490–494. [[CrossRef](#)]
30. John, A.; Dereli, B.; Ortuño, M.A.; Johnson, H.E.; Hillmyer, M.A.; Cramer, C.J.; Tolman, W.B. Selective decarbonylation of fatty acid esters to linear  $\alpha$ -olefins. *Organometallics* **2017**, *36*, 2956–2964. [[CrossRef](#)]
31. Liu, Y.; Virgil, S.C.; Grubbs, R.H.; Stoltz, B.M. Palladium-catalyzed decarbonylative dehydration for the synthesis of  $\alpha$ -vinyl carbonyl compounds and total synthesis of (–)-aspewintins A, B, and C. *Angew. Chem. Int. Ed.* **2015**, *54*, 11800–11803. [[CrossRef](#)] [[PubMed](#)]
32. Ortuño, M.A.; Dereli, B.; Cramer, C.J. Mechanism of Pd-catalyzed decarbonylation of biomass-derived hydrocinnamic acid to styrene following activation as an anhydride. *Inorg. Chem.* **2016**, *55*, 4124–4131. [[CrossRef](#)] [[PubMed](#)]
33. Ternel, J.; Lebarbé, T.; Monflier, E.; Hapiot, F. Catalytic decarbonylation of biosourced substrates. *ChemSusChem* **2015**, *8*, 1585–1592. [[CrossRef](#)] [[PubMed](#)]
34. John, A.; Hillmyer, M.A.; Tolman, W.B. Anhydride-additive-free nickel-catalyzed deoxygenation of carboxylic acids to olefins. *Organometallics* **2017**, *36*, 506–509. [[CrossRef](#)]
35. Hagen, J. *Industrial Catalysis: A Practical Approach*, 2nd ed.; Wiley-VCH Verlag GmbH: Weinheim, Germany, 2006; ISBN 978-3-527-31144-6.
36. Miller, J.A.; Nelson, J.A. Oxidative addition of carboxylic acid anhydrides to rhodium(I) phosphine complexes to produce novel rhodium(III) acyl derivatives. *Organometallics* **1991**, *10*, 2958–2961. [[CrossRef](#)]
37. Fristrup, P.; Kreis, M.; Palmelund, A.; Norrby, P.-O.; Madsen, R. The mechanism for the rhodium-catalyzed decarbonylation of aldehydes: A combined experimental and theoretical study. *J. Am. Chem. Soc.* **2008**, *130*, 5206–5215. [[CrossRef](#)] [[PubMed](#)]
38. Frisch, M.J.; Trucks, G.W.; Schlegel, H.B.; Scuseria, G.E.; Robb, M.A.; Cheeseman, J.R.; Scalmani, G.; Barone, V.; Mennucci, B.; Petersson, G.A.; et al. *Gaussian 09*; Gaussian, Inc.: Wallingford, CT, USA, 2009.
39. Becke, A.D. Density-functional thermochemistry. V. Systematic optimization of exchange-correlation functionals. *J. Chem. Phys.* **1997**, *107*, 8554–8560. [[CrossRef](#)]
40. Chai, J.D.; Head-Gordon, M. Long-range corrected hybrid density functionals with damped atom-atom dispersion corrections. *Phys. Chem. Chem. Phys.* **2008**, *10*, 6615–6620. [[CrossRef](#)] [[PubMed](#)]

41. Wu, Q.; Yang, W. Empirical correction to density functional theory for van der Waals interactions. *J. Chem. Phys.* **2002**, *116*, 515–524. [[CrossRef](#)]
42. Minenkov, Y.; Singstad, A.; Occhipinti, G.; Jensen, V.R. The accuracy of DFT-optimized geometries of functional transition metal compounds: A validation study of catalysts for olefin metathesis and other reactions in the homogeneous phase. *Dalton Trans.* **2012**, *41*, 5526–5541. [[CrossRef](#)] [[PubMed](#)]
43. *Spartan '08*, Wavefunction Inc.: Irvine, CA, USA, 2008.
44. Allen, F.H. The Cambridge structural database: A quarter of a million crystal structures and rising. *Acta Crystallogr. Sect. B Struct. Sci.* **2002**, *58*, 380–388. [[CrossRef](#)]
45. Halgren, T.A. Merck molecular force field. I. Basis, form, scope, parameterization, and performance of MMFF94. *J. Comput. Chem.* **1996**, *17*, 490–519. [[CrossRef](#)]
46. Fukui, K. The path of chemical reactions—the IRC approach. *Acc. Chem. Res.* **1981**, *14*, 363–368. [[CrossRef](#)]
47. Peterson, K.A.; Figgen, D.; Dolg, M.; Stoll, H. Energy-consistent relativistic pseudopotentials and correlation consistent basis sets for the 4d elements Y–Pd. *J. Chem. Phys.* **2007**, *126*, 124101. [[CrossRef](#)] [[PubMed](#)]
48. Woon, D.E.; Dunning, T.H. Gaussian basis sets for use in correlated molecular calculations. III. The atoms aluminum through argon. *J. Chem. Phys.* **1993**, *98*, 1358–1371. [[CrossRef](#)]
49. Dunning, T.H. Gaussian basis sets for use in correlated molecular calculations. I. The atoms boron through neon and hydrogen. *J. Chem. Phys.* **1989**, *90*, 1007–1023. [[CrossRef](#)]
50. Ribeiro, R.F.; Marenich, A.V.; Cramer, C.J.; Truhlar, D.G. Use of solution-phase vibrational frequencies in continuum models for the free energy of solvation. *J. Phys. Chem. B* **2011**, *115*, 14556–14562. [[CrossRef](#)] [[PubMed](#)]
51. Zhao, Y.; Truhlar, D.G. Density functionals with broad applicability in chemistry. *Acc. Chem. Res.* **2008**, *41*, 157–167. [[CrossRef](#)] [[PubMed](#)]
52. Zhao, Y.; Truhlar, D.G. A new local density functional for main-group thermochemistry, transition metal bonding, thermochemical kinetics, and noncovalent interactions. *J. Chem. Phys.* **2006**, *125*, 194101. [[CrossRef](#)] [[PubMed](#)]
53. Zhao, Y.; Truhlar, D.G. Applications and validations of the Minnesota density functionals. *Chem. Phys. Lett.* **2011**, *502*, 1–13. [[CrossRef](#)]
54. Perdew, J.P.; Burke, K.; Ernzerhof, M. Generalized gradient approximation made simple. *Phys. Rev. Lett.* **1996**, *77*, 3865–3868. [[CrossRef](#)] [[PubMed](#)]
55. Perdew, J.P.; Burke, K.; Ernzerhof, M. Generalized Gradient Approximation Made Simple [Phys. Rev. Lett. *77*, 3865 (1996)]. *Phys. Rev. Lett.* **1997**, *78*, 1396. [[CrossRef](#)]
56. Grimme, S.; Ehrlich, S.; Goerigk, L. Effect of the damping function in dispersion corrected density functional theory. *J. Comput. Chem.* **2011**, *32*, 1456–1465. [[CrossRef](#)] [[PubMed](#)]
57. Smith, D.G.; Burns, L.A.; Patkowski, K.; Sherrill, C.D. Revised damping parameters for the D3 dispersion correction to density functional theory. *J. Phys. Chem. Lett.* **2016**, *7*, 2197–2203. [[CrossRef](#)] [[PubMed](#)]
58. Becke, A.D. Density-functional thermochemistry. III. The role of exact exchange. *J. Chem. Phys.* **1993**, *98*, 5648–5652. [[CrossRef](#)]
59. Feller, D. The role of databases in support of computational chemistry calculations. *J. Comput. Chem.* **1996**, *17*, 1571–1586. [[CrossRef](#)]
60. Kendall, R.A.; Dunning, T.H.; Harrison, R.J. Electron affinities of the first-row atoms revisited. Systematic basis sets and wave functions. *J. Chem. Phys.* **1992**, *96*, 6796. [[CrossRef](#)]
61. Marenich, A.V.; Cramer, C.J.; Truhlar, D.G. Universal solvation model based on solute electron density and on a continuum model of the solvent defined by the bulk dielectric constant and atomic surface tensions. *J. Phys. Chem. B* **2009**, *113*, 6378–6396. [[CrossRef](#)] [[PubMed](#)]
62. Minenkov, Y.; Occhipinti, G.; Jensen, V.R. Complete reaction pathway of ruthenium-catalyzed olefin metathesis of ethyl vinyl ether: Kinetics and mechanistic insight from DFT. *Organometallics* **2013**, *32*, 2099–2111. [[CrossRef](#)]



V



## **PAPER II - SUPPORTING INFORMATION**

# The Mechanism of Rh-Catalyzed Transformation of Fatty Acids to Linear Alpha olefins.

Hopen Eliasson, S. H. ; Chatterjee, A.; Occhipinti, G.;  
Jensen, V. R.

*Inorganics* 2017, 5, 87

Optimized structures (.xyz) not included. Available at <https://www.mdpi.com/2304-6740/5/4/87#supplementary>.



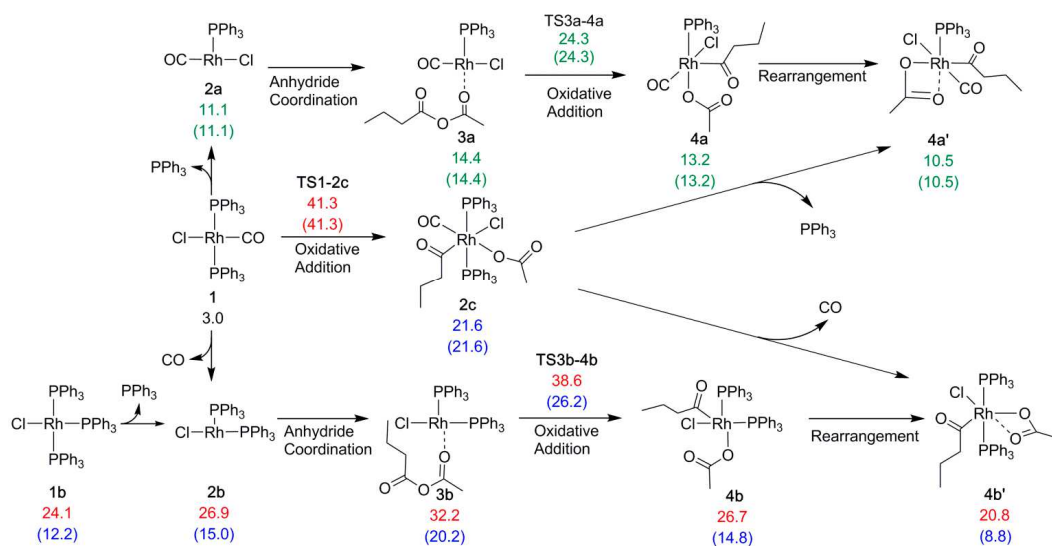
# Supplementary Materials: The Mechanism of Rh-catalyzed Transformation of Fatty Acids to Linear Alpha Olefins.

Sondre H. Hopen Eliasson, Anamitra Chatterjee, Giovanni Occhipinti and Vidar R. Jensen

## 1. Rh reaction pathways

To find the most favored pathway for the Rh catalyzed decarbonylative dehydration many different possibilities, presented in the following, were explored. The free energy of the most favorable route(s) is colored in green, while energies of highly unfavorable species and pathways are colored in red. Other energies have been given a blue tint. The pathway reported in the manuscript corresponds to the pathway labeled “a” in the following. Except where otherwise indicated, all reported energies are Gibbs free energies calculated at 523 K, with butanoic acid as continuum solvent (termed  $\Delta G_{BA}$ ). The values in parentheses are the energies calculated using a CO pressure of  $10^{-5}$  atm as described in the Computational Method section.

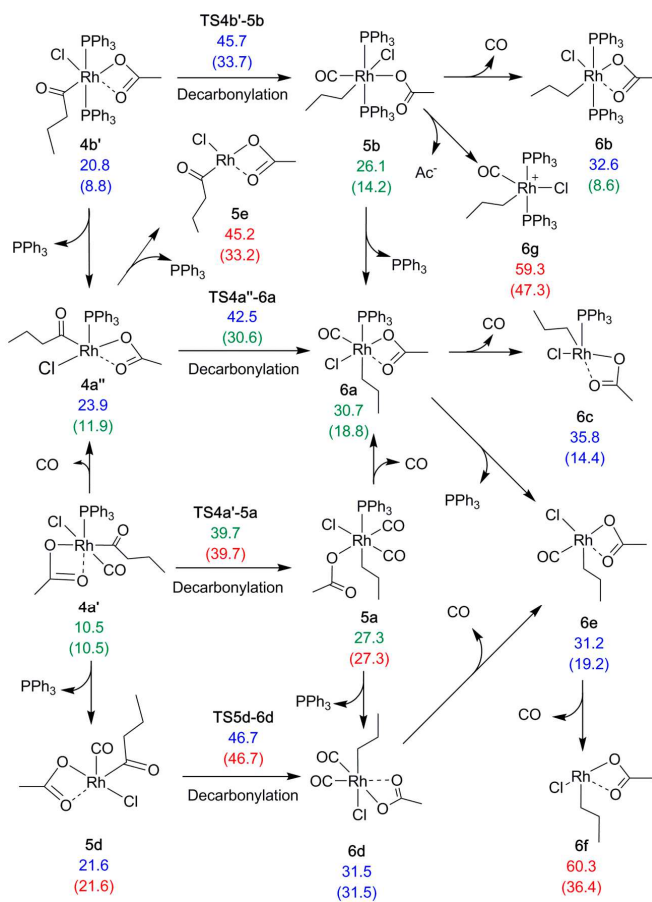
### a) Oxidative addition.



Scheme S1. The investigated pathways for oxidative addition of mixed anhydride.

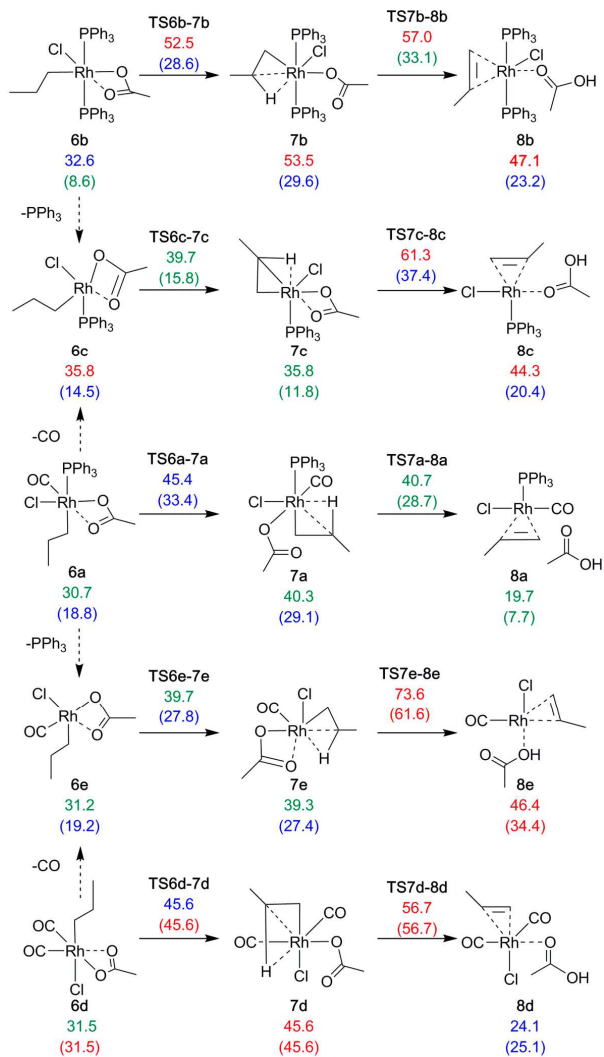


b) Decarbonylation.



Scheme S2. The investigated pathways for decarbonylation.

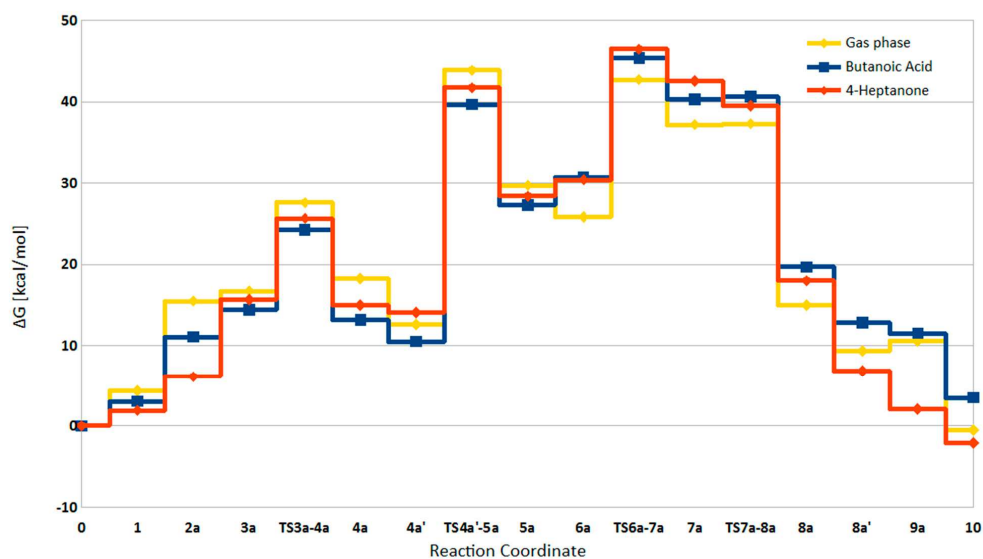
c) Alkene formation.



**Scheme S3.** The investigated pathways for  $\beta$ -hydrogen transfer to form alkene.

## 2. The energy profile for the Rh-Mechanism in gas phase and butanoic acid and 4-heptanone solvent.

The decarbonylative dehydration reactions are typically carried out in neat substrates and anhydride additives, i.e., without solvent. In other words, the reaction environment is dominated by the substrate and the additive (here: butanoic acid and acetic anhydride, respectively) and the acetic acid produced by the reaction. We have modeled this environment by using two solvents with different dielectric constants, butanoic acid (BA,  $\epsilon = 2.85$ ) and 4-heptanone (4-Hep,  $\epsilon = 12.26$ ), respectively, for which parameters are available in Gaussian 09. The corresponding free energy profiles of Rh-catalyzed decarbonylative dehydration in Scheme S4 are quite similar, with slightly higher barriers in general for the reaction modeled in 4-heptanone.



**Scheme S4.** The free energy profile for Rh-catalyzed decarbonylative dehydration as calculated in gas phase, butanoic acid (SMD model) and 4-heptanone solvent (SMD model) using the M06L functional and QZ basis sets.

### 3. The free energies for the reaction using different functionals and modified BJ-dampening.

SP calculations were performed using different DFT functionals (see the Computational Method section) to investigate the influence on the  $\Delta G_{BA}$  for species of pathway **a**. The functionals investigated were PBE [1,2], B3LYP [3] and M06L [4-6]. PBE was used in combination Grimme's empirical dispersion term D3 in combination with Becke-Johnson damping [7], using both the original (termed D3-BJ) and the modified [8] (termed D3-(M)BJ) parameters. B3LYP was used in combination with D3-(M)BJ. The functionals were found to reproduce similar trends, but with some differences. M06L gave the overall lowest barrier for the rate-determining step, but gave, together with B3LYP, a higher decarbonylation barrier compared to the PBE functional. For the oxidative addition, B3LYP was the outlier. The effect of the modified damping parameters was limited as PBE-D3(M)BJ and PBE-D3BJ in general gave energies in close agreement.

**Table S1.** The Gibbs free energies (kcal/mol) of the main species in butanoic acid solvent (SMD-model) at 523 K, calculated using different DFT functionals.

Species	PBE-D3BJ	B3LYP-D3(M)BJ	M06L	PBE-D3(M)BJ
<b>0</b>	0.0	0.0	0.0	0.0
<b>1</b>	2.8	2.7	3.0	2.8
<b>2</b>	16.6	19.7	11.1	21.1
<b>3</b>	21.4	21.5	14.4	24.1
<b>TS3-4</b>	22.2	28.5	24.3	23.4
<b>4'</b>	9.9	14.6	10.5	10.3
<b>TS4'-5</b>	34.3	41.6	39.7	34.8
<b>5</b>	22.9	28.1	27.3	20.9
<b>6</b>	34.4	33.6	30.7	36.7
<b>TS6-7</b>	49.5	47.5	45.4	51.4
<b>7</b>	43.4	42.1	40.3	45.0
<b>TS7-8</b>	39.3	41.3	40.7	40.3
<b>8</b>	24.6	21.8	19.7	27.0
<b>8'</b>	18.9	16.9	12.8	21.7
<b>9</b>	21.5	17.6	11.5	26.6
<b>10</b>	7.6	0.6	3.5	8.3

#### 4. Energies of all species

**Table S2.** The electronic energy and free energy in a.u. calculated for the solvents (SMD-model), butanoic acid (BA) and 4-heptanone (4-Hep), and in gas phase. Calculations were performed with the M06L functional with QZ basis sets. Free energy calculated at 523 K.

Species	E(Gas Phase)	E(BA)	E(4-Hep)	G(Gas Phase)	G(BA)	G(4-Hep)
MA	-460.5042843	-460.5029881	-460.5176	-460.4172857	-460.4159896	-460.4306015
PPh <sub>3</sub>	-1036.501858	-1036.507937	-1036.519006	-1036.312966	-1036.319045	-1036.330114
CO	-113.3485452	-113.3359949	-113.3444143	-113.3802592	-113.3677089	-113.3761283
BA	-307.8115738	-307.8135656	-307.8222835	-307.7485168	-307.7505086	-307.7592264
Propene	-117.9395724	-117.9397813	-117.942485	-117.9030978	-117.9033067	-117.9060103
AcOH	-229.1567229	-229.1592332	-229.169882	-229.141733	-229.1442433	-229.1548921
Ac <sub>2</sub> O	-381.856609	-381.8537243	-381.8684754	-381.817451	-381.8145662	-381.8293174
AcO <sup>-</sup>	-228.5923073	-228.6589378	-228.6798309	-228.5906698	-228.65733003	-228.6781934
1	-2757.071683	-2757.082413	-2757.111887	-2756.660443	-2756.671173	-2756.700647
2a	-1720.511493	-1720.521085	-1720.545596	-1720.329746	-1720.339338	-1720.36385
3a	-2181.051202	-2181.056167	-2181.085301	-2180.745081	-2180.750046	-2180.779180
TS3a-4a	-2181.035992	-2181.042545	-2181.071544	-2180.727743	-2180.734296	-2180.763295
4a	-2181.0467	-2181.05611	-2181.084476	-2180.742573	-2180.751982	-2180.780348
4a'	-2181.056956	-2181.061485	-2181.087053	-2180.751684	-2180.756212	-2180.781781
TS4'a-5a	-2181.007812	-2181.015746	-2181.043721	-2180.7018	-2180.709733	-2180.737709
5a	-2181.028852	-2181.033958	-2181.063446	-2180.724359	-2180.729466	-2180.758954
4a''	-2067.651966	-2067.668488	-2067.688056	-2067.350697	-2067.367219	-2067.386787
TS4a''-6a	-2067.630565	-2067.639393	-2067.661559	-2067.328615	-2067.337444	-2067.35961
6a	-2067.651191	-2067.657121	-2067.680477	-2067.350328	-2067.356258	-2067.379614
TS6a-7a	-2067.624228	-2067.633807	-2067.654854	-2067.323375	-2067.332955	-2067.354001
7a	-2067.632795	-2067.641596	-2067.66078	-2067.332211	-2067.341012	-2067.360196
TS7a-7a'	-2067.628549	-2067.637953	-2067.66078	-2067.329807	-2067.339211	-2067.362038
7a'	-2067.64211	-2067.650802	-2067.673704	-2067.343445	-2067.352138	-2067.375039
TS7a'-8a	-2067.630298	-2067.6386	-2067.663347	-2067.3326	-2067.340902	-2067.365648
TS7a-8a	-2067.630312	-2067.638721	-2067.663364	-2067.332023	-2067.340432	-2067.365075
8a	-2067.664733	-2067.671059	-2067.696565	-2067.367568	-2067.373894	-2067.3994
8a'	-1838.487015	-1838.492787	-1838.514414	-1838.234822	-1838.240593	-1838.26222
1b	-3680.210544	-3680.231629	-3680.260911	-3679.56783	-3679.588915	-3679.618197
2b	-2643.652908	-2643.675346	-2643.700997	-2643.242964	-2643.265402	-2643.291053
3b	-3104.191897	-3104.208899	-3104.235654	-3103.656039	-3103.673040	-3103.699795
TS3b-4b	-3104.181405	-3104.199876	-3104.225731	-3103.644238	-3103.662710	-3103.688564
4b	-3104.197519	-3104.217673	-3104.225731	-3103.661546	-3103.681701	-3103.689758
4b'	-3104.209859	-3104.227847	-3104.252933	-3103.673211	-3103.691199	-3103.716285
TS4b'-5b	-3104.171401	-3104.18635	-3104.212954	-3103.636575	-3103.651524	-3103.678128
5b	-3104.202875	-3104.216915	-3104.245808	-3103.668608	-3103.682648	-3103.711542
6b	-2990.818793	-2990.835085	-2990.858024	-2990.288407	-2990.304699	-2990.327638
TS6b-7b	-2990.786422	-2990.80381	-2990.82531	-2990.255508	-2990.272896	-2990.294396

<b>7b</b>	-2990.785804	-2990.80204	-2990.825816	-2990.255024	-2990.271261	-2990.295037
<b>TS7b-8b</b>	-2990.776621	-2990.792344	-2990.817661	-2990.25005	-2990.265772	-2990.291089
<b>8b</b>	-2990.797756	-2990.813345	-2990.839146	-2990.265912	-2990.281501	-2990.307302
<b>9b</b>	-2875.004799	-2875.016633	-2875.045464	-2874.520934	-2874.532767	-2874.561598
<b>TS1-2c</b>	-3217.546511	-3217.561455	-3217.592786	-3217.006406	-3217.02135	-3217.052681
<b>2c</b>	-3217.580027	-3217.595966	-3217.627642	-3217.041577	-3217.057515	-3217.089191
<b>6c</b>	-1954.263658	-1954.27902	-1954.298064	-1953.965185	-1953.980548	-1953.999591
<b>TS6c-7c</b>	-1954.257063	-1954.272673	-1954.288554	-1953.958636	-1953.974246	-1953.990127
<b>7c</b>	-1954.265317	-1954.279304	-1954.295065	-1953.966547	-1953.980533	-1953.996295
<b>TS7c-8c</b>	-1954.221037	-1954.233994	-1954.252739	-1953.926914	-1953.939871	-1953.958616
<b>8c</b>	-1954.253601	-1954.264741	-1954.284376	-1953.955749	-1953.966888	-1953.986524
<b>5d</b>	-1144.493223	-1144.4953	-1144.518011	-1144.417425	-1144.419502	-1144.442213
<b>TS5d-6d</b>	-1144.457923	-1144.455237	-1144.477712	-1144.382108	-1144.379421	-1144.401897
<b>6d</b>	-1144.484509	-1144.479322	-1144.503139	-1144.408836	-1144.403649	-1144.427465
<b>TS6d-7d</b>	-1144.458205	-1144.455539	-1144.479186	-1144.383941	-1144.381276	-1144.404923
<b>7d</b>	-1144.456751	-1144.454427	-1144.478924	-1144.383623	-1144.381299	-1144.405796
<b>TS7d-8d</b>	-1144.440722	-1144.435487	-1144.460199	-1144.368755	-1144.36352	-1144.388232
<b>8d</b>	-1144.497263	-1144.487408	-1144.511462	-1144.425295	-1144.415441	-1144.439495
<b>5e</b>	-1031.074686	-1031.087539	-1031.103391	-1031.001381	-1031.014234	-1031.030086
<b>6e</b>	-1031.105227	-1031.108686	-1031.125937	-1031.0326	-1031.036059	-1031.05331
<b>TS6e-7e</b>	-1031.09436	-1031.096622	-1031.110664	-1031.020633	-1031.022896	-1031.036938
<b>7e</b>	-1031.095099	-1031.096172	-1031.111883	-1031.022478	-1031.023552	-1031.039263
<b>TS7e-8e</b>	-1031.036847	-1031.036349	-1031.05242	-1031.010244	-1030.968975	-1030.985046
<b>8e</b>	-1031.077618	-1031.081148	-1031.099458	-1031.008709	-1031.012239	-1031.030549
<b>6f</b>	-917.6774244	-917.6924607	-917.6924607	-917.6073244	-917.6223607	-917.6223607
<b>6g</b>	-2875.423143	-2875.46786	-2875.508578	-2874.927857	-2874.972574	-2875.013291
<b>Pd_1</b>	-4273.754605	-4273.771938	-4273.804088	-4272.880946	-4272.898279	-4272.930429
<b>Pd_2</b>	-2200.668712	-2200.678967	-2200.700648	-2200.258349	-2200.268604	-2200.290285
<b>Pd_3</b>	-2661.198721	-2661.212059	-2661.235511	-2660.660606	-2660.673944	-2660.697396
<b>Pd_TS3-4</b>	-2661.188138	-2661.203815	-2661.228114	-2660.652024	-2660.667702	-2660.692
<b>Pd_4</b>	-2661.208432	-2661.224667	-2661.24845	-2660.672576	-2660.688811	-2660.712594
<b>Pd_4'</b>	-2661.214252	-2661.229675	-2661.253548	-2660.679711	-2660.695134	-2660.719008
<b>Pd_4''</b>	-1624.676916	-1624.684073	-1624.705069	-1624.371904	-1624.379061	-1624.400057
<b>Pd_TS4''-5</b>	-1624.643861	-1624.650293	-1624.670313	-1624.341832	-1624.348264	-1624.368284
<b>Pd_5</b>	-1624.664978	-1624.66907	-1624.689664	-1624.363269	-1624.36736	-1624.387954
<b>Pd_6</b>	-588.1290868	-588.1228221	-588.1383892	-588.0538157	-588.047551	-588.0631181
<b>Pd_TS6-8</b>	-588.0980855	-588.0908256	-588.1066388	-588.0269829	-588.0197229	-588.0355362
<b>Pd_8</b>	-588.1221798	-588.1130032	-588.1301152	-588.0502063	-588.0410297	-588.0581417
<b>Pd_8'</b>	-1395.485308	-1395.483547	-1395.503128	-1395.233532	-1395.231771	-1395.251352
<b>Pd_9</b>	-1277.520941	-1277.517252	-1277.536379	-1277.338645	-1277.334957	-1277.354084
<b>Pd_10</b>	-3350.596519	-3350.606511	-3350.639653	-3349.954637	-3349.964629	-3349.997771

## 5. References

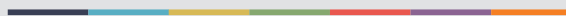
1. Perdew, J.P.; Burke, K.; Ernzerhof, M. Generalized gradient approximation made simple. *Phys. Rev. Lett.* **1996**, *77*, 3865.
2. Perdew, J.P.; Burke, K.; Ernzerhof, M. Generalized gradient approximation made simple [phys. Rev. Lett. *77*, 3865 (1996)]. *Phys. Rev. Lett.* **1997**, *78*, 1396-1396.
3. Becke, A.D. Density-functional thermochemistry. III. The role of exact exchange. *J. Chem. Phys.* **1993**, *98*, 5648-5652.
4. Zhao, Y.; Truhlar, D.G. Density functionals with broad applicability in chemistry. *Acc. Chem. Res.* **2008**, *41*, 157-167.
5. Zhao, Y.; Truhlar, D.G. A new local density functional for main-group thermochemistry, transition metal bonding, thermochemical kinetics, and noncovalent interactions. *J. Chem. Phys.* **2006**, *125*, 194101.
6. Zhao, Y.; Truhlar, D.G. Applications and validations of the Minnesota density functionals. *Chem. Phys. Lett.* **2011**, *502*, 1-13.
7. Grimme, S.; Ehrlich, S.; Goerigk, L. Effect of the damping function in dispersion corrected density functional theory. *J. Comput. Chem.* **2011**, *32*, 1456-1465.
8. Smith, D.G.; Burns, L.A.; Patkowski, K.; Sherrill, C.D. Revised damping parameters for the D3 dispersion correction to density functional theory. *J. Phys. Chem. Lett.* **2016**, *7*, 2197-2203.







Graphic design: Communication Division, UIB / Print: Skjipes Kommunikasjon AS



[uib.no](http://uib.no)

ISBN: 9788230862971 (print)  
9788230846155 (PDF)